INVESTIGATION OF HIGH STRENGTH STAINLESS STEEL PRESTRESSING STRANDS

A Thesis
Presented to
The Academic Faculty

by

Daniel P. Schuetz

In Partial Fulfillment
of the Requirements for the Degree
Master of Science in the
School of Civil & Environmental Engineering

Georgia Institute of Technology
May 2013

INVESTIGATION OF HIGH STRENGTH STAINLESS STEEL PRESTRESSING STRANDS

Approved by:

Dr. Lawrence Kahn, Advisor
School of Civil & Environmental Engineering
Georgia Institute of Technology

Dr. Kimberly Kurtis
School of Civil & Environmental Engineering
Georgia Institute of Technology

Dr. Preet Singh
School of Materials Science Engineering
Georgia Institute of Technology

Date Approved: January 2nd, 2013

ACKNOWLEDGEMENTS

I would first like to thank my advisor, Dr. Lawrence Kahn, as well as my other committee members, Dr. Kimberly Kurtis and Dr. Preet Singh. I am lucky to have had the opportunity to work on this project with such phenomenally talented people. I attribute the success of this project as well as my growth as an engineer to their guidance and support.

Next, I would like to personally thank my predecessors in this project, Robert Moser and Brett Holland. Their help has been instrumental, and I owe my opportunity to work on this project to their excellent work.

My fellow graduate researchers have always been more than willing to help with anything I needed, and I sincerely thank them for their aid. Falak Shah, Mitchell McKay, Tim Wright, Nick Reynolds, Amal Jayapalan, Bradley Dolphyn, Lorintz Gleich, and Alvaro Paul, among others, have helped with a number of things—from material testing to data recovery.

I was also lucky enough to have had the help of a group of wonderful undergraduate research assistants in Kyle Manweiler, Jack Schenker, Ted Trent, and Brandon Webster. There are many things I could have not done without their help.

The support staff at Georgia Tech has also been extremely helpful over the course of this project. Jeremy Mitchell, Andy Udell, and Mike Sorenson have each made themselves available to teach and help me with various technical aspects of the project.

Lastly, I'd like to thank my family for their support. I am certain that I would not be where I am without the support of my father, Jeff, my mother, Phyllis and my brothers, Greg and Tyler. Thank you for everything.

TABLE OF CONTENTS

Page

ACKNOWLEDGEMENTS iii

LIST OF TABLES ix

LIST OF FIGURES xi

LIST OF SYMBOLS AND ABBREVIATIONS xv

CHAPTER 1 INTRODUCTION 1

1.1 Research Purpose, Objectives, and Scope 1

1.2 Motivation 2

1.3 Thesis Organization 4

CHAPTER 2 BACKGROUND 5

2.1 High Carbon Prestressing Strands 5

2.1.1 Metallurgy 6

2.1.2 Production of Prestressing Strands 7

2.1.2.1 Cold Drawing 7

2.1.2.2 Thermomechanical Treatment 9

2.2 Stainless Steels: Metallurgy and Mechanical Properties 10

2.2.1 Identification of Stainless Steels 10

2.2.2 Duplex Stainless Steels 11

2.2.3 Mechanical Properties of Duplex Stainless Steels 14

2.2.4 Previous Studies on HSSS Prestressing Strand 15

CHAPTER 3 STRAND PRODUCTION 17

3.1 Alloys Selected for Strand Production 17

3.2 Strand Production 18

CHAPTER 4 STRESS-STRAIN BEHAVIOR 24
4.1 Stress-Strain Behavior of Strand Samples 24
4.1.1 Experimental Methods 24
4.1.2 Results and Discussion 26
4.1.2.1 Stress-Strain Behavior 26
4.1.2.2 Failure Modes 29
4.2 Stress-Strain Behavior of Wire Samples 31
4.2.1 Experimental Methods 31
4.2.2 Results and Discussion 32
CHAPTER 5 STRESS RELAXATION BEHAVIOR 36
5.1 Stress Relaxation Behavior of Strand Samples 36
5.1.1 Experimental Methods 36
5.1.2 Results and Discussion 38
5.2 Stress Relaxation Behavior of Wire Samples 43
5.2.1 Experimental Methods 43
5.2.2 Results and Discussion 46
CHAPTER 6 PILE SPECIMEN EXPERIMENT DESIGN 53
6.1 Fabrication of Pile Specimens 53
6.1.1 Design of Steel Reinforcement 53
6.1.2 Lengths of Pile Specimens 55
6.1.3 Mix Designs 56
6.2 Pile Driving 57
6.3 Flexural Behavior 58
6.3.1 Experimental Methods 58
6.3.2 Moment-Curvature and Force-Displacement Curves 59

6.4 Shear Behavior 63
6.4.1 Experimental Methods 63
6.4.2 Shear Capacity 64
6.5 Transfer and Development Length 65
6.5.1 Introduction 65
6.5.2 Elements of Bond 67
6.5.2.1 Adhesion 67
6.5.2.2 Hoyer's Effect 67
6.5.2.3 Mechanical Interlocking 68
6.5.3 Transfer Length: Experimental Methods 68
6.5.3.1 Concrete Surface Strain Measurements 68
6.5.3.2 End-Slip Measurements 72
6.5.4 Development Length Experimental Methods 72
6.6 Long-Term Prestressing Losses 75
6.7 Durability 75
CHAPTER 7 CONCLUSIONS, RECOMMENDATIONS, AND FUTURE RESEARCH 77
7.1 Conclusions 77
7.1.1 Stress vs. Strain Behavior 77
7.1.2 Stress Relaxation Behavior 78
7.1.3 General Conclusions 79
7.2 Recommendations 80
7.2.1 Implementation in Coastal Bridges 80
7.2.2 Standards for HSSS Prestressing Strand 81
7.3 Future Research 81

APPENDIX A: Strand Grip Methods 84
A.1 Wet Sand Grips 84
A.2 Expansive Cement Grips 85
APPENDIX B: Stress-Strain Curve Formulation 91
APPENDIX C: Stress-Strain Results 97
C.1 Strand Testing 97
C.2 Wire Testing 99
APPENDIX D: Stress Relaxation Results 109
D.1 Strand Results 109
D.2 Wire Results 112
APPENDIX E: Moment-Curvature and Load Deflection Calculations 116
E.1 Moment-Curvature Calculations 116
E.2 Load-Deflection Calculations 137
APPENDIX F: Development Length Testing Calculations 146
REFERENCES 154

LIST OF TABLES

Page

Table 3.1: Composition of alloys selected for strand production 18

Table 3.2: Die schedule for outer and center wires 20

Table 3.3: Temperature of wire during drawing 20

Table 3.4: Ultimate tensile strength of drawn wire samples 21

Table 4.1: Mechanical properties of strand specimens 27

Table 4.2: Comparison of methods to estimate yield stress 29

Table 4.3: Mechanical properties of 2205 wire samples 33

Table 4.4: Mechanical properties of 2304 wire samples 34

Table 5.1: Mean stress relaxation losses of strand specimens at 1000 hours 41

Table 5.2: Comparison of 1000 hr stress relaxation losses—2205 strand at 70% UTS .. 42

Table 5.3: Comparison of 1000 hr stress relaxation values—2304 strand at 40% UTS . 42

Table 5.4: Wire relaxation measurement increments 45

Table 5.5: Mean stress relaxation losses of wire specimens stressed to 70% UTS at 1000 hours 47

Table 6.1: Mix designs for both girder types 57

Table 6.2: Shear strength of pile specimens 65

Table 6.3: Estimated transfer lengths of each strand 70

Table C.1: Mechanical properties of 2205 strand 97

Table C.2: Mechanical properties of 2304 strand 98

Table C.3: Mechanical properties of 2205 rod 99

Table C.4: Mechanical properties of 2205 #3 wire 100

Table C.5: Mechanical properties of 2205 #5 wire 101

Table C.6: Mechanical properties of 2205 #7 UW wire 102

Table C.7: Mechanical properties of 2205 #7 HW wire 103

Table C.8: Mechanical properties of 2304 rod 104

Table C.9: Mechanical properties of 2304 #3 wire 105

Table C.10: Mechanical properties of 2304 #5 wire 106

Table C.11: Mechanical properties of 2304 #7 UW wire 107

Table C.12: Mechanical properties of 2304 #7 HW wire 108

Table D.1: Stress relaxation losses at 1000 hr for 2205 tests 110

Table D.2: Stress relaxation losses at 1000 hr for 2304 strand tests 111

Table D.3: Stress relaxation losses at 1000 hr for 2205 UW wire tests 112

Table D.4: Stress relaxation losses at 1000 hr for 2205 HW wire tests 113

Table D.5: Stress relaxation losses at 1000 hr for 2304 UW wire tests 114

Table D.6: Stress relaxation losses at 1000 hr for 2304 HW wire tests 115

Table E.1: Load-deflection calculations for 12-in. sq. piles with 1080 strand, f_c' = 5 ksi 142

Table E.2: Load-deflection calculations for 12-in. sq. piles with 1080 strand, f_c' = 10 ksi 142

Table E.3: Load-deflection calculations for 12-in. sq. piles with 2304 strand, f_c' = 5 ksi 143

Table E.4: Load-deflection calculations for 12-in. sq. piles with 2304 strand, f_c' = 10 ksi 143

Table E.5: Load-deflection calculations for 18-in. sq. piles with 1080 strand, f_c' = 5 ksi 144

Table E.6: Load-deflection calculations for 18-in. sq. piles with 1080 strand, f_c' = 10 ksi 144

Table E.7: Load-deflection calculations for 18-in. sq. piles with 2205 strand, f_c' = 5 ksi 145

Table E.8: Load-deflection calculations for 18-in. sq. piles with 2205 strand, f_c' = 10 ksi 145

LIST OF FIGURES

Page

Figure 1.1: Bridge substructure deterioration in Georgia's coastal counties 3

Figure 2.1: Pearlitic microstructure of 1080 prestressing steel in (a) longitudinal and (b) transverse directions 6

Figure 2.2: Influence of cold work on stress vs. strain behavior 8

Figure 2.3: Residual stresses in 1080 prestressing steel vs. relative depth, or normalized depth from the outer face to a point in the cross section, 1-r/R 9

Figure 2.4: Microstructure of 2205 duplex stainless steel 12

Figure 2.5: Schaeffler constitution diagram for stainless steels 13

Figure 2.6: Comparison between the stress-strain behavior of stainless steel and carbon steel 15

Figure 3.1: Production of HSSS strand 19

Figure 4.1: Strand tension testing apparatus 25

Figure 4.2: Stress-strain curves of strand specimens 27

Figure 4.3: Typical failure modes from (a) notching of 2304 strand, (b) uniform failure of 2205 and 2304 strand 30

Figure 4.4: Wire tension testing apparatus 31

Figure 4.5: Stress-strain curves of 2205 wire samples 32

Figure 4.6: Stress-strain curves of 2304 wire samples 33

Figure 5.1: (a) Relaxation frame, (b) dead end of frame, (c) jacked end of frame during loading 37

Figure 5.2: Stress relaxation of strand specimens 39

Figure 5.3: Average stress relaxation of 2304 strand at an initial stress of 40% UTS 39

Figure 5.4: Stress relaxation of 2205 strand at an initial stress of 50% UTS 40

Figure 5.5: Average stress relaxation of 2205 strand at an initial stress of 70% UTS 40

Figure 5.6: Stress relaxation of 2205 strand at an initial stress of 80% UTS 41

Figure 5.7: Wire relaxation test setup 46

Figure 5.8: Stress relaxation of wire specimens 47

Figure 5.9: Stress relaxation of 2205 untreated wire at an initial stress of 70% UTS 48

Figure 5.10: Stress relaxation of 2205 thermomechanically treated wire at an initial stress of 70% UTS 48

Figure 5.11: Stress relaxation of 2304 untreated wire at an initial stress of 70% UTS ... 49

Figure 5.12: Stress relaxation of 2304 thermomechanically treated wire at an initial stress of 70% UTS 49

Figure 6.1: Cross sections of (a) 18-in. (46 cm) 2205, (b) 18-in. (46 cm) 1080, (c) 12-in. (30 cm) 2304, and (d) 12-in. (30 cm) 1080 piles 54

Figure 6.2: Typical wire spiral layout 55

Figure 6.3: Construction layouts for (a) 12-in. (30 cm) sq. and (b) 18-in. (46 cm) sq. ... 56

Figure 6.4: Flexural test apparatus 59

Figure 6.5: Moment-curvature relationships for 18-in. (46 cm) sq. piles 60

Figure 6.6: Moment-curvature relationships for 12-in. (30 cm) sq. piles 60

Figure 6.7: Load-displacement relationships for 18-in. (46 cm) sq. piles 61

Figure 6.8: Load-displacement relationships for 12-in. (30 cm) sq. piles 61

Figure 6.9: Shear test apparatus 63

Figure 6.10: Idealized strand stress profile in a pretensioned element under applied load 66

Figure 6.11: Sample idealized concrete surface strain profile for transfer length 69

Figure 6.12: DEMEC gage and CSS gage point 71

Figure 6.13: Embedment connection details for (a) embedment to embedment plate and (b) embedment plate to formwork 71

Figure 6.14: Concrete topping for development length testing 74

Figure 6.15: Development length test apparatus 74

Figure 6.16: Vibrating wire strain gage placement 75

Figure 6.17: Material durability sample design 76

Figure A.1: Wet sand grip in universal testing machine 84

Figure A.2: Wet sand grip 85

Figure A.3: Placement of expansive cement grips 86

Figure A.4: Expansive cement grip in universal testing machine 87

Figure B.1: Adjusted Extensometer Data 92

Figure B.2: Corrected crosshead position data for tests conducted using expansive cement grips 96

Figure B.3: Corrected crosshead position data for tests conducted using wet sand grips 96

Figure C.1: 2205 strand stress-strain curves for a) test 1, b) test 2, c) test 3, and d) average 97

Figure C.2: 2304 strand stress-strain curves for a) test 1, b) test 2, c) test 3, and d) average 98

Figure C.3: 2205 rod stress-strain curves for a) test 1, b) test 2, c) test 3, and d) average 99

Figure C.4: 2205 #3 wire stress-strain curves for a) test 1, b) test 2, and c) average 100

Figure C.5: 2205 #5 wire stress-strain curve 101

Figure C.6: 2205 #7 UW wire stress-strain curves for a) test 1, b) test 2, c) test 3, and d) average 102

Figure C.7: 2205 #7 HW wire stress-strain curves for a) test 1, b) test 2, c) test 3, and d) average 103

Figure C.8: 2304 rod stress-strain curves for a) test 1, b) test 2, c) test 3, and d) average 104

Figure C.9: 2304 #3 wire stress-strain curves for a) test 1, b) test 2, c) test 3, and d) average 105

Figure C.10: 2304 #5 wire stress-strain curve 106

Figure C.11: 2304 #7 UW wire stress-strain curves for a) test 1, b) test 2, and c) average 107

Figure C.12: 2304 #7 HW wire stress-strain curves for a) test 1, b) test 2, and c) average 108

Figure D.1: 2205 strand stress relaxation, 70% UTS initial Stress, 1000 hr duration, a) test 1, b) test 2, c) test 3, and d) average 109

Figure D.2: 2205 strand stress relaxation, 200 hr duration, a) 50% initial stress, and b) 80% initial stress 110

Figure D.3: 2304 strand stress relaxation, 40% UTS initial stress, 1000 hr duration, a) test 1, b) test 2, c) test 3, and d) average 111

Figure D.4: 2205 UW wire relaxation results for a) test 1, b) test 2, c) test 3, and d) average 112

Figure D.5: 2205 HW wire relaxation results for a) test 1, b) test 2, c) test 3, and d) average 113

Figure D.6: 2304 UW wire relaxation results for a) test 1, b) test 2, c) test 3, and d) average 114

Figure D.7: 2304 HW wire relaxation results for a) test 1, b) test 2, c) test 3, and d) average 115

Figure E.1: Load-deflection calculation methodology for ultimate condition with yield point 138

Figure E.2: Load-deflection calculation methodology for ultimate condition without yield point 139

Figure E.3: Load-deflection calculation methodology for yield condition 140

Figure E.4: Load-deflection calculation methodology for cracking condition 141

LIST OF SYMBOLS AND ABBREVIATIONS

AASHTO	American Association of State Highway and Transportation Officials
ACI	American Concrete Institute
AISI	American Iron and Steel Institute
ASTM	American Society for Testing and Materials
DEMEC	Detachable Mechanical Strain Gage
DSS	Duplex Stainless Steel
E	Young's Modulus
f_c'	Compressive Strength of concrete
f_y	Yield Strength
GDOT	Georgia Department of Transportation
HPC	High Performance Concrete
HPMC	High Performance Marine Concrete
HSSS	High-Strength Stainless Steel
HW	Thermomechanically Treated Wire
l_d	Development Length
l_t	Transfer Length
LVDT	Linear Variable Displacement Transformer
PREN	Pitting Resistance Equivalency Number
PSC	Prestressed Concrete
RA	Reduction of Area by Cold Drawing
RC	Reinforced Concrete
RH	Relative Humidity

SAE	Society of Automotive Engineers
SWPC	Sumiden Wire Products Corporation
UNS	Unified Numbering System
UTS	Ultimate Tensile Strength
UW	Untreated Wire
V_{ci}	Flexure-Shear Capacity
V_{cw}	Web Shear Capacity
V_n	Nominal Shear Capacity
V_s	Steel Shear Capacity
α	Ferrite Phase of Steel
γ	Austenite Phase of Steel

CHAPTER 1

INTRODUCTION

1.1 Research Purpose, Objectives, and Scope

The purpose of this research was to assess the feasibility of implementing corrosion resistant high-strength stainless steel (HSSS) prestressing strand in prestressed concrete (PSC) bridge substructures, with the overall goal of developing a corrosion-free bridge pile, capable of a service life of longer than 100 years. The scope of this experimental study was limited to testing the mechanical behavior and performance of candidate HSSS prestressing strands, and further attention is paid to assessing the remaining issues involved with their design and large scale implementation. The key objectives associated with this research were:

1. To characterize the mechanical properties of the HSSS strand, including stress-strain and stress relaxation behavior, and to differentiate the types of HSSS strand tested.
2. To design a test program to assess the performance of bridge piles reinforced with HSSS strand based on pile driving performance, flexural and shear behavior, strand transfer and development length, long-term prestressing force losses, and material durability.
3. To provide recommendations for the design of PSC piles with HSSS strand reinforcement.

1.2 Motivation

Bridges and other coastal structures in Georgia and throughout the Southeast are deteriorating prematurely due to corrosion of reinforcement (Griggs, 1987; Hamilton III, 2007). Numerous corrosion initiated failures have occurred in precast prestressed concrete piles and reinforced concrete (RC) pile caps, leading to the costly repair and replacement of either the entire bridge or the affected members (Griggs, 1987). Figure 1 shows the results of a study of Georgia Department of Transportation (GDOT) bridge inspection records for bridges with concrete pile substructures along Georgia's coastal counties. Approximately 30%, or 85 out of 290, of the bridges showed substructure ratings of 6 or less (shown by red dots in Figure 1), indicating that piles exhibited visible damage. Reported damage included cracking, rust staining, spalling, biological growth, and physical abrasion. While other examples of reinforcement corrosion can be found elsewhere, it is believed that numerous corrosion-related failures go undocumented and are settled through litigation before any investigation or research is conducted (Hope and Nmai, 2001).

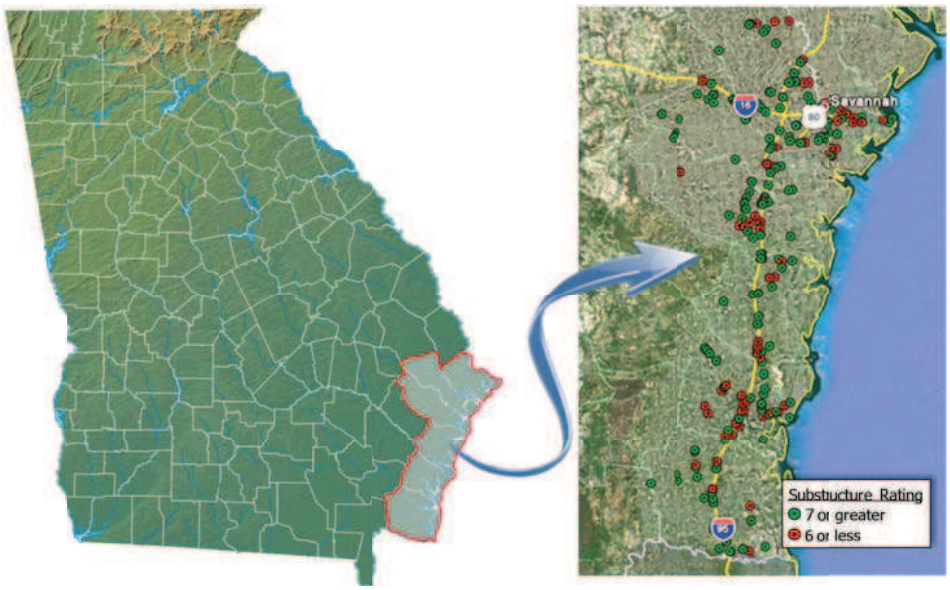

Figure 1.1 Bridge substructure deterioration in Georgia's coastal counties

With the Federal Highway Administration's goal of a 100-year bridge service life and recent legislative action such as the Bridge Life Extension Act, new emphasis has been placed on the development and implementation of new corrosion mitigation techniques (Koch et al, 2008; NACE, 2008). Traditional methods of corrosion mitigation in PSC structures include the use of lower permeability high-performance concrete, larger cover thicknesses, and proper design and construction to limit cracking. However, each of these methods only reduces the amount of time needed to reach a sufficient chloride concentration at the surface of the steel to initiate pitting corrosion. In order to raise this threshold, corrosion resistant prestressing steel is being investigated. Moser conducted a preliminary investigation into high strength stainless steel (HSSS) alloys were found to be viable options for the production of strand samples for further investigation (Moser, 2011). Cold drawn wires were created from six different stainless steels, including austenitic, duplex (austenite and ferrite), and martensitic alloys. The wires were evaluated

based on their strength, corrosion resistance, stress relaxation behavior, cost, and availability. While each alloy exhibited sufficient tensile strength and similar relaxation, duplex grades 2205 and 2304 were proven the most corrosion resistance in seawater, chloride rich environments, and they were selected for production of ½-in. diameter, 7-wire prestressing strand conforming to ASTM A416 (ASTM, 2006).

1.3 Thesis Organization

- Chapter 2 provides a background of the properties of the materials tested and information about the current standards for prestressing strand.
- Chapter 3 summarizes the production process of the HSSS strand.
- Chapter 4 presents the stress-strain behavior of the HSSS strand and wire samples taken from production.
- Chapter 5 presents the stress relaxation behavior of the HSSS strand and selected wire samples.
- Chapter 6 outlines the proposed testing program on piles reinforced with HSSS and typical prestressing strand.
- Chapter 7 provides a summary of the research and presents its key conclusions. Recommendations for further testing and the implementation of HSSS strand in PSC structures are addressed.
- Appendices are included to provide all information not included in the body of the thesis, including individual test results, sample calculations, and other relevant data.

CHAPTER 2

BACKGROUND

2.1 High Carbon Prestressing Strands

The most common prestressing strand used in PSC structures is a 7-wire uncoated strand, designated by the American Society for Testing and Materials (ASTM) A416 (ASTM A416, 2006). The standard allows for strands of nominal diameters between 0.25-in (6.8mm) and 0.7-in (17.8mm), but restricts the geometry of the strands. A416 strand consists of 7 wires: a straight center wire and six wires coiled around the center wire. The center wire is required to be larger than the outer wires to facilitate contact between the outer wires. Outer wires are helically wound around the center wire at a pitch between 12 and 16 times the nominal diameter of the strand.

Although A416 does not specify a specific metallurgy other than the designation "carbon steel", strands must meet certain mechanical property requirements to comply with the standard. A416 strand can be divided into Grades 250 (1725) and 270 (1680), which specifies the minimum ultimate tensile strength (UTS) of the strand—250 ksi (1725 MPa) and 270 ksi (1680 MPa), respectively. A minimum total elongation under load (ultimate strain) of 3.5% is also specified for both grades of strand.

Strands may also be designated by the method used to reduce stress relaxation losses. Low relaxation strand, the standard type, accomplishes reduction in stress relaxation loss by thermomechanical treatment; normal relaxation (stress relieved) strand undergoes a mechanical treatment that allows losses occur prior to use in construction

and is less commonly used. Over 1000 hours of test time, low relaxation strand may not relax more than 2.5% when initially stressed to 70% of its UTS, and 3.5% when stressed to 80% UTS per ASTM A416.

2.1.1 Metallurgy

Pearlitic AISI 1080 steel is typically used in prestressing strand due to its high strength after cold drawing. Pearlite is a two phase eutectic alloy of body-centered cubic ferrite (denoted as α) and iron carbide, also referred to as cementite (Fe_3C). The two phases form as austenite, which is stable at high temperatures, is cooled below the eutectoid temperature, leaving interlocking lamellar crystals of each phase. Figure 2.1 shows the typical ferrite (white) and cementite (black) lamellar microstructure of a cold drawn 1080 prestressing strand.

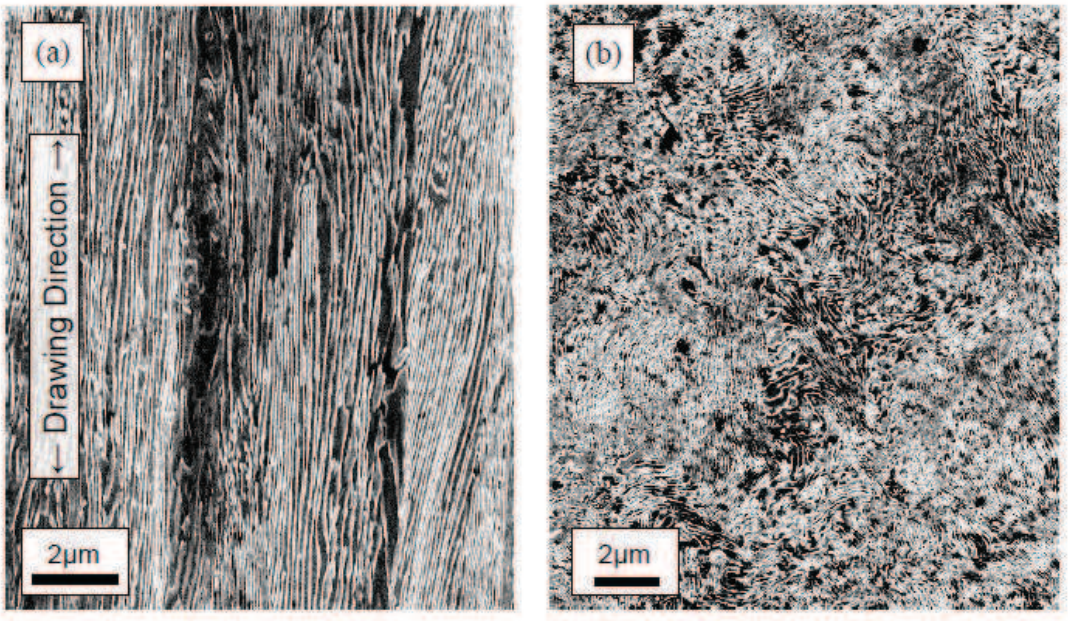

Figure 2.1 Pearlitic microstructure of 1080 prestressing steel in (a) longitudinal and (b) transverse directions (Moser, 2011)

The designation 1080 is given by the American Iron and Steel Institute (AISI), which identifies steels by using 3- or 4-digit numbers; each digit typically corresponds to the class and different components of the composition of the steel. Carbon steels are included in the 1000 series. 1080 is given its designation digit-by-digit as such: 1xxx refers to carbon steel, 10xx refers to mild carbon steel with less than 1.0 wt% Mn content, and 1080 refers to such steel with 0.80 wt% carbon.

2.1.2 Production of Prestressing Strand

2.1.2.1 Cold Drawing

The primary strengthening mechanism for prestressing strand is cold drawing. Cold formed wire rod is reduced in area by a series of dies of sequentially smaller diameters. To achieve the desired strength, wire rod is typically cold drawn for a reduction of area around 80%. Cold drawing serves to strengthen steels primarily by the mechanism of work hardening.

Work hardening is an important strengthening process in steel, particularly in obtaining high strength levels in rod and wire, both in plain carbon and alloy steels. Without the addition of special alloying elements, plain carbon steels can be raised to strength levels above 200 ksi simply by the phenomenon of work hardening. Work hardening in conventional materials is largely due to the creation of crystal defects, primarily dislocations, during plastic deformation. High dislocation density creates "forest" dislocations, areas of high concentrations of dislocations that hinder further dislocation, therefore increases the stress for plastic deformation. (LeMay, 1981)

Work hardening has an important consequence on ductility. During tensile testing, the sample will inevitably contain features which cause the stress to concentrate and hence to initiate necking. The reduced cross-sectional area at the neck increases the stress in the necked region. In the absence of work hardening to help resist local deformation, the neck becomes unstable and the sample fractures with poor overall ductility. To encourage uniform elongation, the work hardening rate must raise the yield strength at a rate greater than the increase in stress due to the reduced area at the neck (Moser, 2011).

In the annealed condition, most metals exhibit negligible residual stresses, resulting in linear stress vs. strain behavior prior to yielding. When cold drawn, significant residual stresses can form inside of the metal and produce low-strain nonlinearity, as shown in Figure 2.2. In high-strength cold drawn wire, residual stresses are typically tensile at the surface of the wire and compressive at the center of the wire (Atienza and Elices, 2007). Therefore, upon tensile loading, the surface of the wire will begin to yield prior to the center, resulting in observed nonlinearity. Figure 2.3 shows the typical residual stress distribution in cold drawn 1080 prestressing steel.

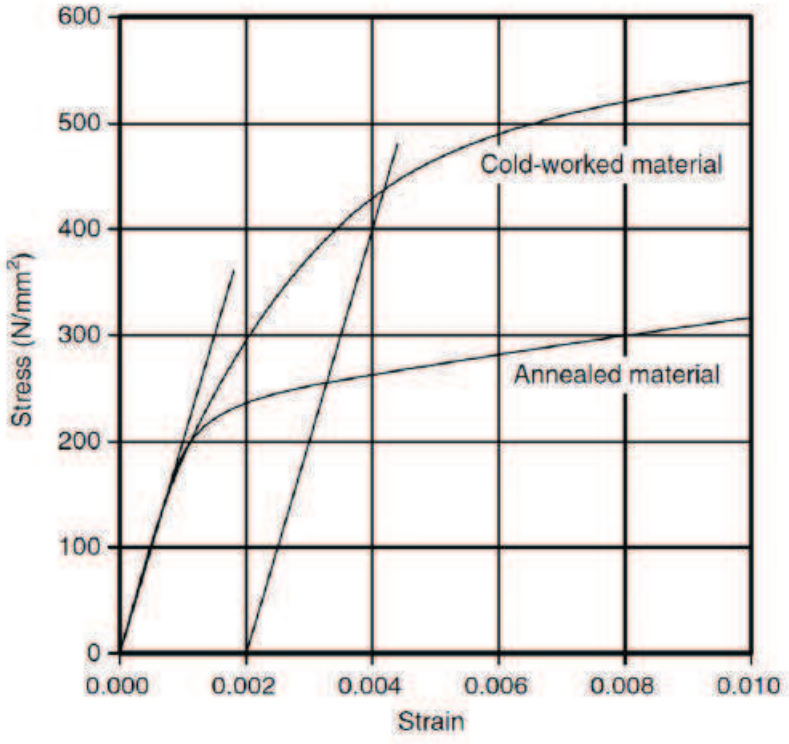

Figure 2.2 Influence of cold work on stress vs. strain behavior (from Gardner, 2005)

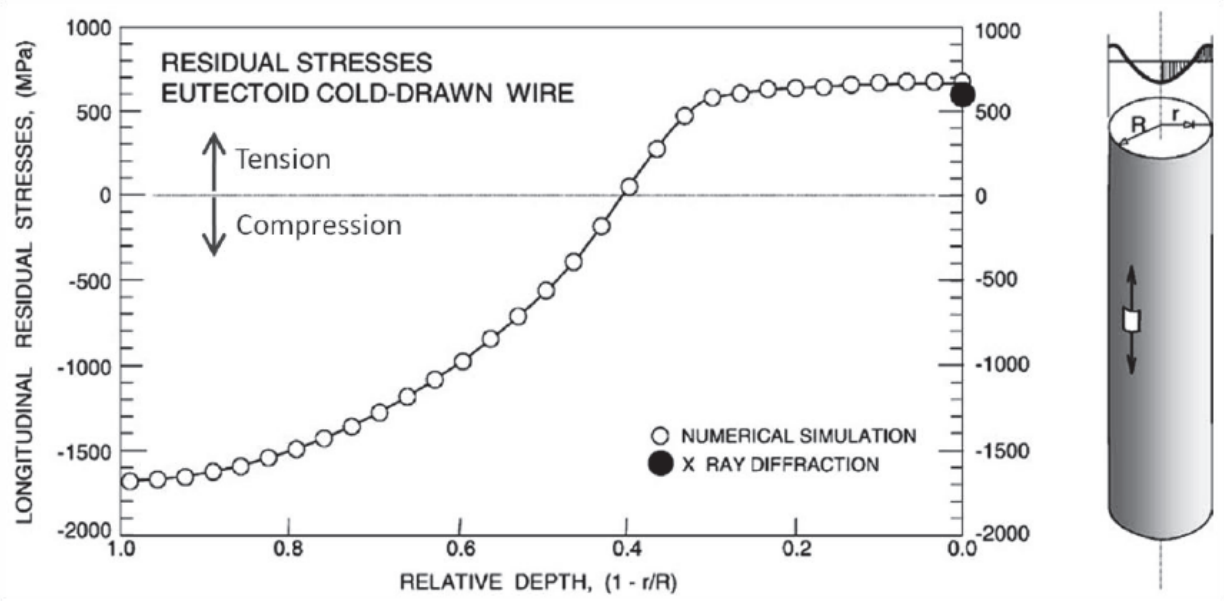

Figure 2.3 Residual stresses in 1080 prestressing steel vs. relative depth, or normalized depth from the outer face to a point in the cross section, 1-r/R (from Elices, 2004)

2.1.2.2 Thermomechanical Treatment

Low relaxation strands are subjected to thermomechanical treatment, which serves to reduce residual stresses and to accelerate dislocation creep, resulting in improved stress vs. strain linearity, increased yield strength, and reduced stress relaxation Reductions in ultimate strain may also occur due to the decrease in compressive residual strains in the center of the wire which would normally have to be overcome prior to failure (Atienza and Elices, 2007). The low-relaxation thermomechanical heat treatment used for the production of A416 prestressing strands consists of heating the strands to 716 to 752 ˚F (380 to 400 ˚C) while the strand is stressed in tension at 40% of UTS (ACI 222.2, 2001).

2.2 Stainless Steels: Metallurgy and Mechanical Properties

Stainless steels are alloys containing a minimum of approximately 11 wt% chromium. This amount of chromium prevents the formation of rust in unpolluted atmospheres; it is from this characteristic that their popular designation “stainless” is derived. Their corrosion resistance is provided by a very thin surface film known as the “passive film,” which is self-healing in a wide variety of environments.

Today, hundreds of different alloys can be recognized as belonging to the stainless steel group, and each year new ones and modifications of existing ones appear. Many elements are added to provide specific properties, such as Ni, N, and Mo for

corrosion resistance; C, Mo, N, Ti, Al, and Cu for strength; S and Se for machinability; and Ni for formability and toughness.

It is customary to divide the more common stainless steels into three groups according to metallurgical structure: austenitic (face-centered cubic, denoted as γ), ferritic (body-centered cubic, denoted as α), and martensitic (body-centered tetragonal or cubic). Stainless steels containing both austenite and ferrite, usually in roughly equal amounts, are known as "duplex" (Sedriks, 1996). Austenite is a non-magnetic phase, while ferrite and martensite are both ferromagnetic.

2.2.1 Identification of Stainless Steels

Stainless steels produced in the United States can be identified in three general ways: (a) by the Unified Numbering System (UNS) numbers developed by the American Society for Testing and Materials (ASTM) and the Society of Automotive Engineers (SAE), (b) by the American Iron and Steel Institute (AISI) numbering system, and (c) by names based on compositional abbreviations, proprietary designations, and trademarks (Sedriks, 2006). AISI designations and compositional abbreviations will be discussed briefly, as they are the numbering systems used for the stainless steels discussed in this thesis.

AISI designates steels using three- or four-digit numbers. Each digit corresponds to a component of the metallurgy of a class of steel. For example, wrought standard grades of stainless steels are identified in the 200 to 400 series. Austenitic grades fall into the 200-300 series; high-manganese austenitic stainless steels are in the 200 series, while other austenitic grades are classified in the 300 series, including common grades 304 and 316. Ferritic and martensitic stainless steels fall into the 400 series. Carbon steels are

included in the 1000 series. These designations do not explicitly give the chemical compositions of the different steels. 304, for example, may also be referred to as 18-8, or 18 wt% Cr and 8 wt% Ni. 316 has similar Cr and Ni contents, but added Mo for pitting resistance.

Compositional abbreviations typically refer to the content of the most significant alloying elements in the steel. Duplex stainless steels typically do not have AISI designations and are often identified using compositional abbreviations. For example, the designations for duplex stainless steels 2205 and 2304 each refer to the Cr and Ni contents of the steel—2205 steel is composed of 22 wt% Cr and 5 wt% Ni, while 2304 steel contains 23 wt% Cr and 4 wt% Ni.

2.2.2 Duplex Stainless Steels

A duplex alloy is one which possesses a two phase microstructure. This term is generally reserved for alloys in which the phases are present in substantial volume fractions and are present in the form of relatively large separate volumes (in contrast to the situation where one phase is present as a fine precipitate within a major phase). A duplex stainless steel (DSS) is an alloy where the two phases are each stainless steels. The most common stainless phases are face centered cubic austenite, denoted as γ, and body centered cubic ferrite, denoted as α when it is formed via a high temperature diffusion controlled reaction and martensite when it forms martensitically at low temperatures (i.e., via a diffusionless shear transformation). The predominant phases in most duplex stainless steels are α and γ, although austenite-martensite and ferrite-martensite duplex stainless steels are also possible, as are ferrite-austenite-martensite triplex stainless steels (Solomon and Devine, 1983). The transverse microstructure of a

cold drawn α + γ Grade 2205 duplex stainless steel is shown in Figure 2.4. Dark areas represent grains of ferrite, while the brighter areas are austenite (Moser, 2011).

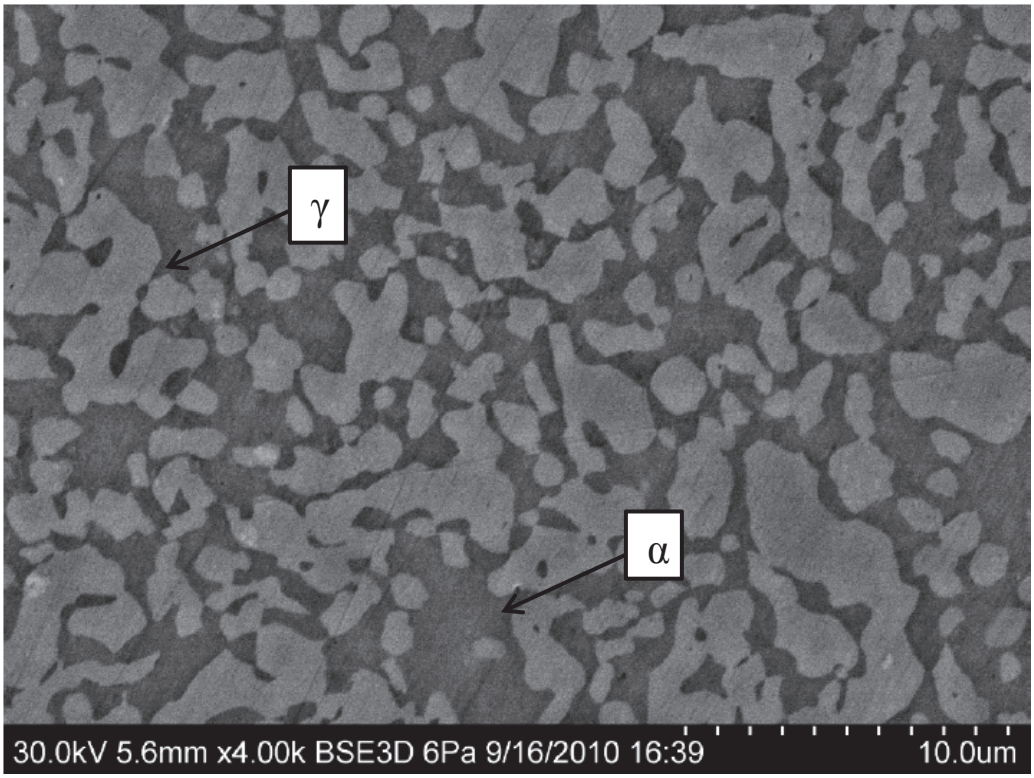

Figure 2.4 Microstructure of 2205 duplex stainless steel (from Moser, 2011)

All duplex stainless steels (as well as single phase stainless steels) contain alloying elements such as C, N, Mn, and Si which influence the amount of α and γ which forms. The relative effectiveness of elements of stabilizing α is compared to the effectiveness of Cr and expressed in terms of their Cr equivalents. A Cr equivalent of 1 means that an element (in a wt% basis) is as strong as Cr in stabilizing α. α stabilizing elements include Cr, Si, Mo, V, Al, Nb, Ti, and W. Elements which stabilize γ, including Ni, Co, C, N, Mn, and Cu, are similarly expressed in terms of their Ni equivalent. Experimental observations of the amount of ferrite present are then correlated with the composition of the steel. The result is a diagram which displays the structure as a

function of Cr and Ni equivalents, or a Schaeffler diagram, shown in Figure 2.5. Since the Schaeffler diagram was developed for rapidly cast and cooled alloys, is not strictly applicable to castings, but may provide a good indication of the phases likely to be present as well as information regarding the relative influence of different alloying elements (Solomon and Devine, 1983).

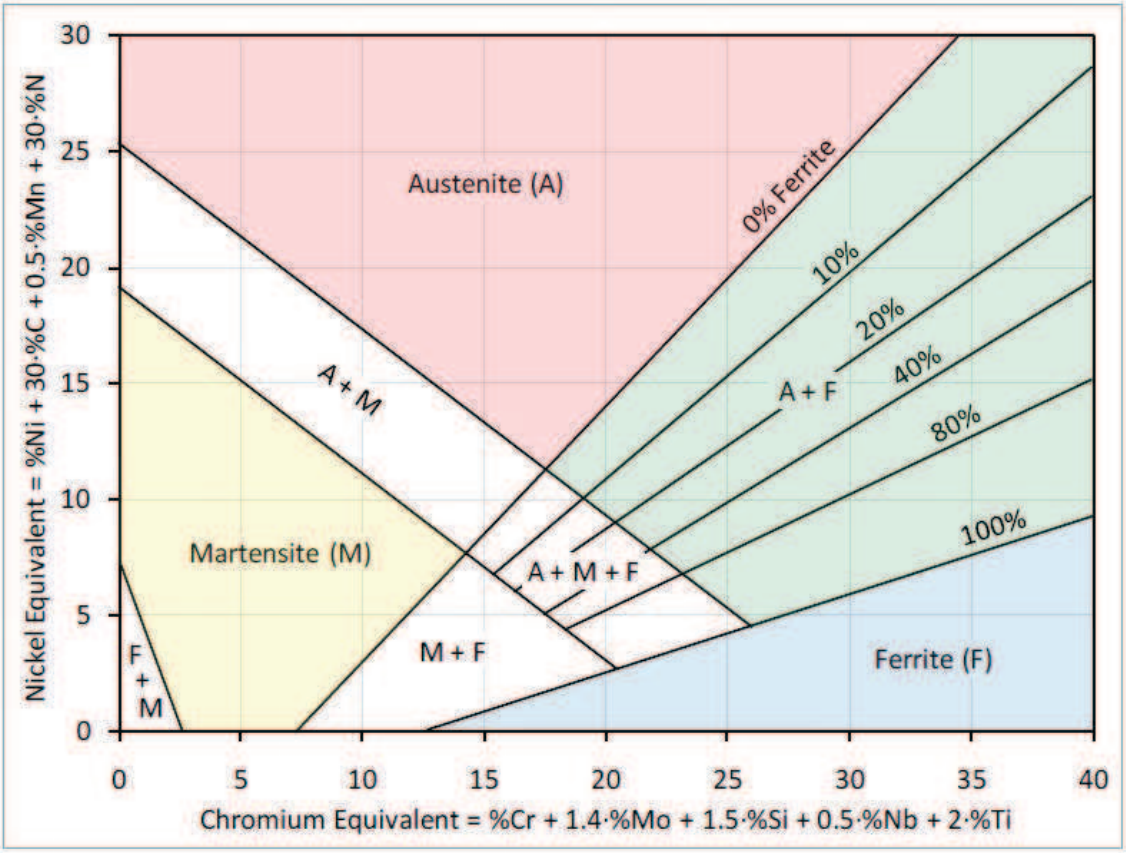

Figure 2.5 Schaeffler constitution diagram for stainless steels (from Moser, 2011, adapted from DeLong, et al., 1956; Schaeffler, 1949)

2.2.3 Mechanical Properties of Duplex Stainless Steels

The mechanical properties of α + γ duplex stainless steel reflect the mechanical properties of the individual α and γ phases, particularly the α phase (Solomon and Devine, 1983). Austenitic stainless steels typically exhibit high ductility, toughness, and

workability when compared with other stainless steels, while ferritic stainless steels exhibit properties similar to carbon steels and have higher yield and ultimate strengths but lower ductility and toughness (Moser, 2011). Ferrite, therefore, has the effect of increasing the yield strength when it is added to austenite to make up a duplex stainless steel. Duplex stainless steels also exhibit a finer grain structure as compared to the coarser grained, single phase ferrite and austenite; the finer structure leads to higher strengths. Duplex stainless steels also typically have a higher ultimate tensile strength than austenitic stainless steels, but reduced ultimate strain (Solomon and Devine, 1983).

Stainless steels typically exhibit non-linear stress strain behavior. Figure 2.6 shows the typical difference in stress vs. strain behavior between stainless and carbon steel, with stainless steels generally exhibiting a poorly defined yield point when compared with carbon steels (Gardner, 2005). As a result, stainless steels do not adhere to bilinear design curve assumptions, and other methods must be used in the design of structures with stainless steel.

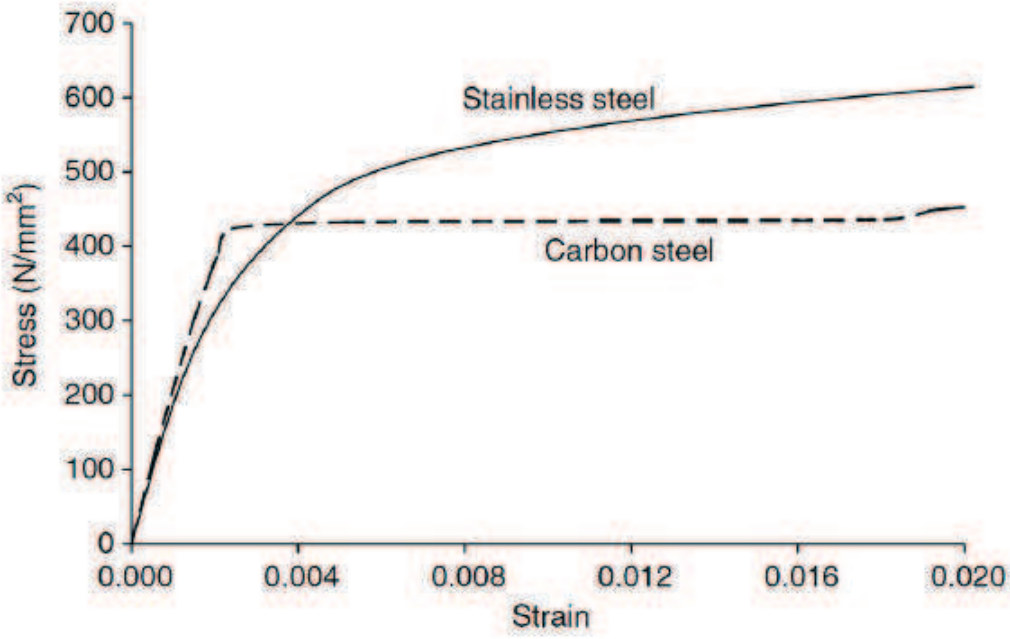

Figure 2.6 Comparison between the stress-strain behavior of stainless steel and carbon steel (from (Gardner, 2005))

2.2.4 Previous Studies on HSSS Prestressing Strand

One of the first studies investigating the use of HSSS for PSC applications was led by the Naval Facilities Engineering Command (Jenkins, 1987). The primary goal of this study was to develop a high-strength non-magnetic prestressing steel for use in concrete piling to be placed in a military deperming facility where ships and submarines are serviced to reduce their magnetic signature. Consequently, an austenitic stainless steel with high resistance to the formation of ferromagnetic-martensite was desired in order to preserve paramagnetic properties even under excessive cold drawing. A nitrogen-strengthened high Mn proprietary alloy known as Nitronic® 33 (ASTM XM-29) was cold drawn and produced as 7-wire prestressing strand. The resulting strand exhibited a UTS of 938MPa (136 ksi), and ultimate strain of 33.3 %. No stress relaxation values were

reported. Mechanical properties were far below those required for most prestressing systems, although strengths as high as 1650 MPa (240 ksi) have been achieved using the same alloy in more recent unpublished studies (Insteel Industries, 2002).

CHAPTER 3

STRAND PRODUCTION

3.1 Alloys Selected for Strand Production

Duplex grades 2205 and 2304 were chosen for strand production based on their low corrosion susceptibility as described by Moser (2011). While 2205 was shown to be more resistant to corrosion, 2304, a "lean duplex" stainless steel, was also selected as a lower cost option due to its lower Mo and Ni contents. It is estimated that the cost of these HSSS strands is 6 to 8 times the cost of ordinary strand. The composition and pitting resistance equivalency number (PREN) of these steels and standard of practice high carbon 1080 prestressing steel is shown in Table 3.1. PREN is calculated by an empirical equation that is based on the compositions of Chromium, Molybdenum and Nitrogen; pitting resistance increases with the addition of each, according to Equation 3.1. Depending on the environment, stainless steels typically offer mild pitting resistance from PREN values of around 10 and up; for steel embedded in concrete in a seawater environment, mild pitting resistance is offered around a PREN of 20-25, and good pitting resistance may occur above a PREN of 30-35 (Moser, 2011).

$$PREN = \%Cr + 3.3 \times \%Mo + \beta \times \%N \tag{3.1}$$

Where:
β=30 for duplex grades
β=16 for other grades

Table 3.1: Composition of alloys selected for strand production

Alloy	Structure	Composition (%) – Balance Fe				PREN
		Cr	Ni	Mo	Other	
1080	Pearlitic	-	-	-	0.8C	<0.1*
2205	Duplex	22	5.5	3	0.17N	37.0
2304	Duplex	23	4.8	0.3	0.10N	27.0

*Contains trace Cr, Mo, N.

3.2 Strand Production

Stainless steel strand was produced at Sumiden Wire Products Corporation (SWPC) in Dickson, TN, USA using equipment and production methods typically used for the manufacture of high carbon (i.e. 1080), low relaxation prestressing strand, as illustrated in Figure 3.1. The strands were produced from 2205 and 2304 wire rod coil supplied from Fagersta Stainless in Fagersta, Sweden. The wire rod (9.50-mm diameter) was cleaned, drawn, stranded, and subjected to a low relaxation heat treatment to produce ½-in. (13 mm) diameter 7-wire prestressing strand sized in accordance with ASTM A416. This process is outlined in Figure 3.1. The strands were manufactured using standard practices for conventional low relaxation prestressing strands which satisfy ASTM A416. The production was documented to assess the problems associated with the substitution of DSS wire rod in the process and to optimize future stainless steel strand production.

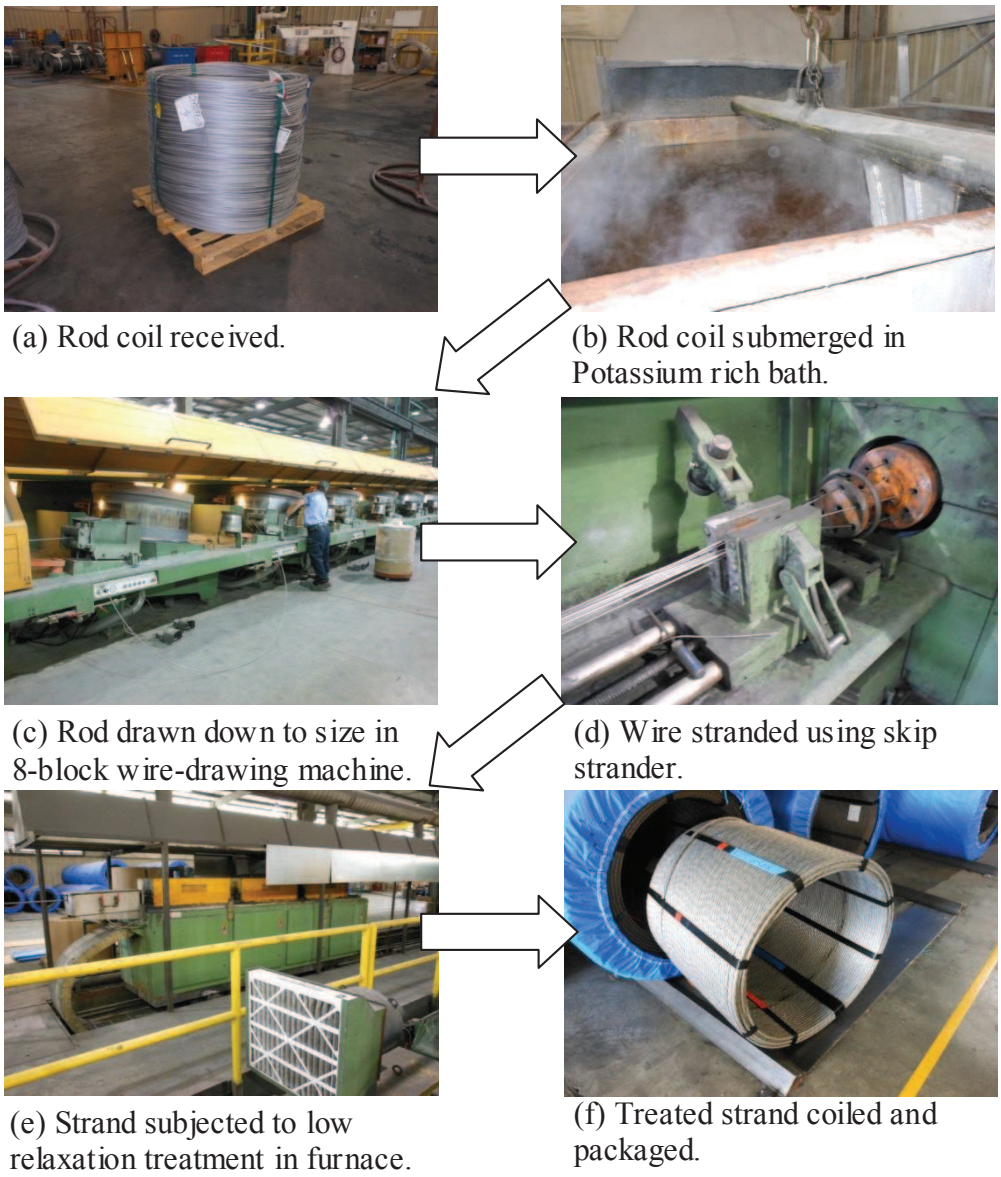

(a) Rod coil received.

(b) Rod coil submerged in Potassium rich bath.

(c) Rod drawn down to size in 8-block wire-drawing machine.

(d) Wire stranded using skip strander.

(e) Strand subjected to low relaxation treatment in furnace.

(f) Treated strand coiled and packaged.

Figure 3.1 Production of HSSS strand

Rod coils were dipped in an 11-13% potassium salt solution for 15 minutes to clean prior to cold drawing that was performed at a rate of 9.8 ft/s (3.0 m/s). The wires were drawn through seven carbide dies, sequentially reducing the area of the wire down to sizes corresponding to ASTM A416 ½-in. diameter prestressing strand and a 78%

reduction of cross-sectional area. The die schedules for outer and center wires are shown in Table 3.2. During the drawing of the wires, temperature was measured with a rolling thermocouple at each die, summarized in Table 3.3. Outer and center wires samples taken from the #7 die were tested to determine the tensile strength after drawing, summarized in Table 3.4 These values were later used to determine the force on the strand during low-relaxation thermomechanical treatment.

Table 3.2 Die schedule for outer and center wires

	Outer Wire				Center Wire			
Die #	Die Size		R.A. (%)	Approach Angle (°)	Die Size		R.A. (%)	Approach Angle (°)
	in	mm			in	mm		
Rod	0.374	9.50	-	-	0.374	9.50	-	-
1	0.323	8.20	25.50	12	0.323	8.20	25.50	12
2	0.283	7.20	22.90	10	0.283	7.20	22.90	10
3	0.254	6.44	20.00	10	0.254	6.44	20.00	10
4	0.226	5.75	20.28	10	0.226	5.75	20.28	10
5	0.202	5.14	20.09	8	0.207	5.26	16.32	8
6	0.181	4.60	19.91	8	0.190	4.82	16.03	8
7	0.165	4.20	16.64	8	0.173	4.40	16.67	8

Table 3.3 Temperature of wires during drawing

Die	2205 Temperature ° F / ° C	2304 Temperature ° F / ° C
#1	246 / 119	223 / 106
#2	284 / 140	275 / 135
#3	271 / 133	262 / 128
#4	298 / 148	297 / 147
#5	302 / 150	302 / 150
#6	318 / 159	309 / 154
#7	273 / 134	271 / 133

Table 3.4 Ultimate tensile strength of drawn wire samples

Sample		Diameter in / mm	UTS ksi / MPa
2205	Center Wire	0.173 / 4.40	236.5 / 1631
	Outer Wire	0.165 / 4.20	237.9 / 1640
2304	Center Wire	0.173 / 4.40	247.0 / 1703
	Outer Wire	0.165 / 4.20	252.2 / 1739

Samples for measuring the mechanical properties of cold drawn 2205 and 2304 were taken at different points in the production of the strand. In addition to the strand end product, approximately 5-ft. (1.5 m) of wire was taken from each of dies #3 (0.254-in., 6.44 mm diameter), #5 (0.202-in., 5.26 mm diameter), and the wire rod. Over 100-ft. (30 m) of wire was sampled from the #7 (0.173-in., 4.40 mm diameter) die. These samples were taken from the strand center wire and their sizes correspond to the center wire die schedule. Samples were only taken at these intervals to minimize the number of times the wire-drawing machine needed to be shut down during production. Wire samples are designated by their metallurgy and die number. Since tests were also performed on the center wire of the heat treated strand, an additional designation is used to differentiate between the two #7 wires—HW for heat treated wire and UW for untreated wire.

The main issue encountered during the stainless steel wire drawing was the “blow out” failure of the dies during drawing. Six dies failed in the first attempt to draw the wire. The majority of blow out failures occurred at dies #5, 6, and 7, primarily with the 2304 wire. These failures are potentially due to strain-induced martensite formation, in which austenite transforms to a stronger martensite phase under high plastic strain. 2304, a lean duplex, is more susceptible to strain–induced martensite formation than 2205 since

2304 contains a lower proportion of austenite stabilizing elements. The stronger martensite phase stressed the die more than expected and led to die failure.

Also contributing to blow out failure was the poor quality of the wire's roll points—the points of contact between the wire and the die. The roll points were observed to have large deformations and scrapes that seemed to damage the dies as the rod was drawn. Sumiden technicians were able to work the roll point area to be smooth to the touch, which resulted in better drawing. Only one more die blew out during the remainder of the strand production.

Seven wire prestressing strand was produced from the drawn wire using a skip strander, and then subjected to a low relaxation thermomechanical treatment using an induction furnace. Due to the presence of the paramagnetic austenite phase in DSS, the induction heating efficiency of the stainless steels was initially assumed to be lower than that of 1080 steel, and the induction heater was set to lower efficiency and adjusted to meet the desired temperature while monitored by infrared camera and rolling thermocouple. Although previous studies by Moser (2011) suggested that the two DSS materials exhibited similar induction heating behavior, the optimal heating efficiency for 2205 strand was 55%, while the heating efficiency of 2304 was considerably higher. This was likely due to the presence of ferromagnetic strain induced martensite in 2304 drawn wires.

The 2205 strand was subjected to 716° F (380° C) and a pull force of 40% UTS of the cold drawn wires, a common thermomechanical treatment for 1080 prestressing strand. The first length (around 300 feet, 90 m) of 2304 strand was subjected to the same treatment. A second length (around 2200 feet, 670 m) was treated with 716° F (380° C)

and a pull force of 45% UTS of the first length of treated strand. This treatment was chosen to test the hypothesis that a higher pull force would increase the rate of microstructural slippage during the treatment, resulting in strand that would exhibit lower relaxation. 2304 strand results in this study correspond to the second treatment.

CHAPTER 4

STRESS-STRAIN BEHAVIOR

4.1 Stress-Strain Behavior of Strand Samples

4.1.1 Experimental Methods

Triplicate direct tension tests were performed in accordance with ASTM A370 on both 2205 and 2304 strand. 5-ft. (1.5 m) long segments were placed in a Baldwin hydraulic universal testing machine, which resulted in a length between grips of approximately 3-ft. (1 m), the longest practical gage length supported by the testing machine. As outlined in Appendix A, wet sand grips were used on 2205 strand while expansive cement grips were necessary for 2304 strand due to its notch sensitivity. The wet sand or expansive cement grips were placed on each end of the specimen, then fit into the wedge grips in the testing machine and clamped tight.

The apparatus and specimen were instrumented as shown in Figure 4.1 to record load and displacements for generation of stress-strain curves. The strand was instrumented with a 24-in. (60 cm) gage length extensometer to measure strain. To avoid damage to the extensometer, it was removed prior to strand rupture. To calculate strain near failure, crosshead displacement data were recorded using a string potentiometer. The force in the strand was measured using the force transducer integral to the testing machine. The force gage mechanism was completely mechanical, but an LVDT was fit to the mechanism for the dial readout and calibrated against an external load cell. This

allowed for simultaneous analog signal readings of force and displacement data throughout the test. These data were recorded at an interval of 2 seconds.

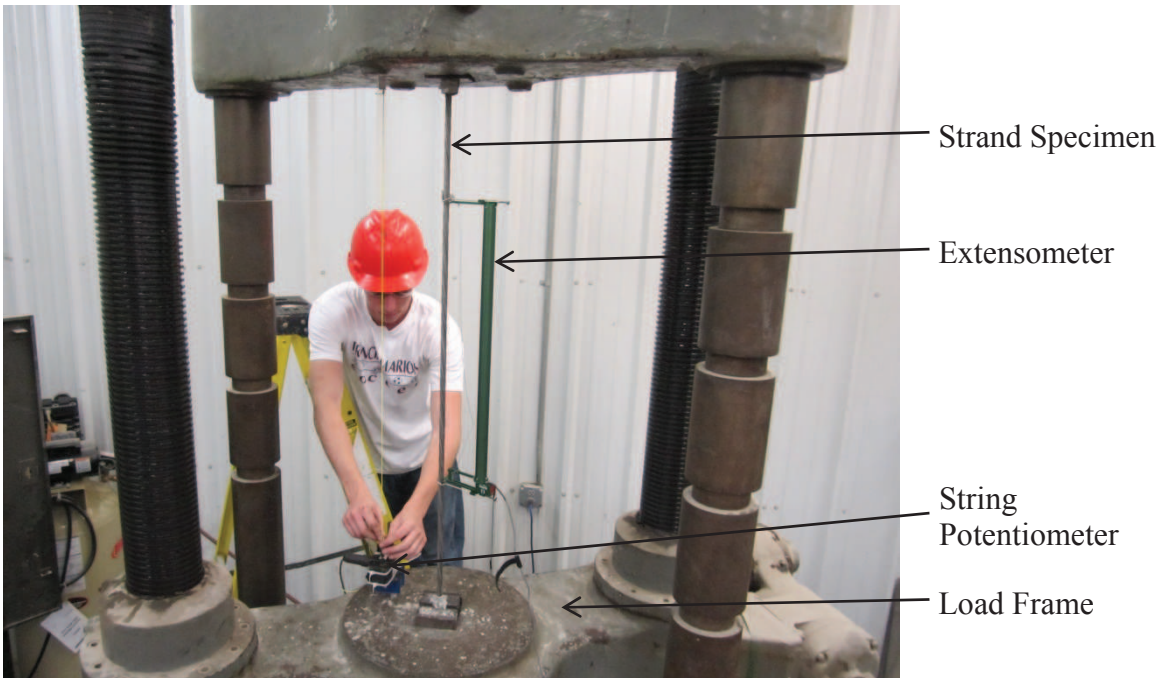

Figure 4.1: Strand tension testing apparatus

Prior to testing with any displacement instrumentation, each strand type was tested once to provide an estimate of the breaking strength. This value was used as a reference for when the strain instrumentation needed to be removed. Before the start of each test, the extensometer was placed on the strand, away from the grips, and secured in place. Load was applied at a rate of 150 lb/s (676 N/s, or strain rate of approximately 0.0025 in/in/min) until the force read 10% of the breaking strength. At this point, the load was held constant and the string potentiometer was secured at the lower crosshead and attached by a string to a bracket on the upper crosshead. The string potentiometer was placed with load on the specimen to reduce the travel required of the string

potentiometer, which had a maximum travel of 2.5-in. (64 mm). After the string potentiometer was secured, the load rate was returned to its initial rate until 80% of the breaking strength was reached. The strand was unloaded at a rate no more than twice the loading rate down to a strand force of 50% of the breaking strength. This was done for safety reasons, as well as to provide a match point for corrections in the crosshead displacement data. The extensometer was then removed, and the specimen was loaded through the elastic range at the initial load rate. The head displacement rate was not changed when the specimen began to exhibit inelastic behavior, though the load rate was not maintained. At this setting, the strand was loaded to failure.

Stress-strain plots were constructed from these data as discussed in Appendix B. From these plots, 0.2% offset and 1% yield strengths, ultimate tensile strength (UTS), elastic modulus (E), and ultimate strain were determined, and average stress-strain curves were created. Three tests were performed on each strand type.

4.1.2 Results and Discussion

4.1.2.1 Stress-Strain Behavior

Figure 4.2 gives stress-strain relations for strands composed of 2205, 2304 and 1080 steels, and Table 4.1 shows the corresponding mechanical properties. Three tests were performed on each strand and used to compute average stress-strain curves and mechanical properties. Individual results are given in Appendix C.

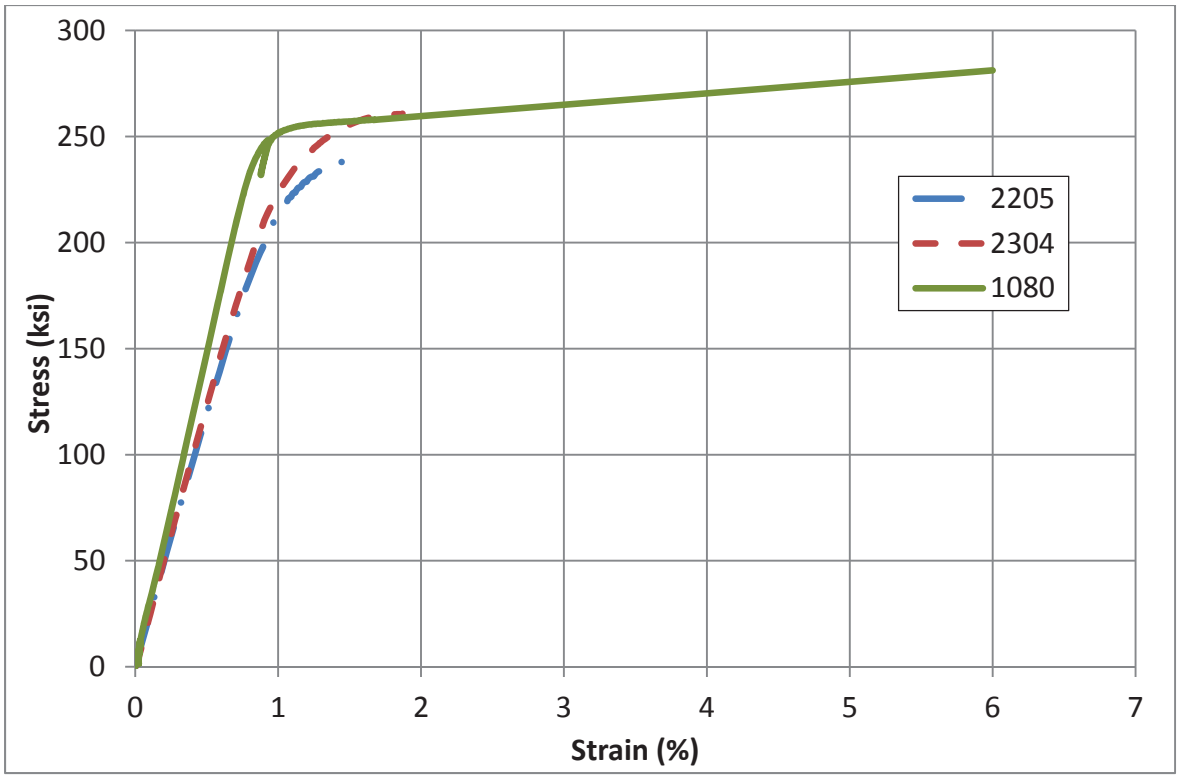

Figure 4.2: Stress-strain curves of strand specimens

Table 4.1: Mechanical properties of strand specimens*

Alloy	f_y -0.2% Offset ksi / MPa	UTS ksi / MPa	Ultimate Strain (%)	E ksi / GPa
1080	254.7 [0.64] / 1756 [4.4]	281.8 [2.00] / 1943 [13.8]	5.89 [0.59]	29400 [130] / 202 [9.0]
2205	228.7 [2.35] / 1577 [16.2]	241.5 [1.6] / 1665 [11.0]	1.60 [0.07]	23500 [190] / 162 [1.3]
2304	242.0 [0.25] / 1669 [1.7]	260.5 [0.25] / 1796 [1.7]	1.87 [0.07]	24100 [290] / 166 [20]

* Standard deviation shown in brackets

Although ASTM A416 does not require a specific metallurgy, it prescribes minimum mechanical properties—specifically, 270 ksi (1860 MPa) minimum ultimate strength and 3.5% minimum ultimate strain. Neither 2205 nor 2304 strands met these qualifications.

While the HSSS strands exhibited less tensile capacity than 1080 strand, their ultimate strengths are within 8 to 15% of the 1080 strand, meaning that approximately 8 to 15% more area of strand would be necessary to construct a similar structure to one made with 1080 strand. This could easily be achieved by using the same strand configuration but by using strands with a slightly larger diameter than the strands currently in use. Many standard pile designs use $^{7}/_{16}$-in. diameter prestressing strand, with an area of 0.115 square inches. ½-in. diameter strand has a cross sectional area of 0.153 square inches, an increase of 33%. The use of ½-in. stainless steel strand in place of $^{7}/_{16}$-in. 1080 strand would easily make up for the difference in UTS and provide comparable, or even allow for higher, overall prestressing forces. Further study is warranted to optimize the size and configuration of the strands for the most efficient pile design.

The main concern for design with these HSSS strands is their lower ductility—approximately 30% that of 1080 strand. Strain localization immediately followed yielding, as seen in preliminary tests of drawn HSSS wires, and failure was categorized by necking of the wires. For bridge piles, this lower ductility is not a major concern since the primary purpose of the strand in piles is to provide a uniform compression force on the concrete and since there is little demand on the strands for elongation compared to the elongation demand for flexural members. Further studies are required to investigate methods of improving the ductility and inducing strain hardening in the drawn HSSS strand.

Per ASTM A416, the yield strength of 1080 prestressing strand is allowed to be determined as the stress corresponding to 1% strain on the stress vs. strain diagram; this

1% strain typically provides approximately the same value of the yield strength calculated by the 0.2% offset method. However, due to a decrease in Young's modulus in the HSSS strand, the yield point calculated by the 0.2% offset method was seen to be near 1.2% strain, and the 1% strain method underestimated the yield strength by 5 to 8%. As shown in Table 4.2, the 1.2% strain method estimated the 0.2% offset yield stress within 2% difference for the stainless steels. Table 4.2 also gives the average strain corresponding to the intersect of the 0.2% offset curve with the stress-strain curve, which is typically near 1.2% for the stainless steel strands.

Table 4.2: Comparison of methods to estimate yield stress

Alloy	f_y -0.2% Offset	0.2% Offset Strain	f_y -1.0% Strain		f_y -1.2% Strain	
	ksi / MPa	%	ksi / MPa	% diff	ksi / MPa	% diff
1080	254.7 / 1756	1.13	281.8 / 1734	-1.3	255.5 / 1762	+0.3
2205	228.7 / 1577	1.18	214.8 / 1481	-7.6	230.0 / 1586	+1.6
2304	242.0 / 1669	1.21	223.5 / 1541	-5.8	241.4 / 1664	-0.2

4.1.2.2 Failure Modes

Despite its higher strength, the 2304 strand was very notch sensitive. This behavior was first noticed when the strand was tested in tension using wet sand grips. Typical failure consisted of a single outer wire failure within the grips. Further tensile testing utilizing chucks as grips was conducted to determine the extent of the notch sensitivity of the 2304 strand and showed that the stress at which this failure occurred was approximately 161 ksi, or 62% UTS. Since the chucks used in testing are similar to the ones used in prestressing operations, it was estimated that a maximum allowable stress of 40% UTS would need to be implemented in practice. While the 2304 strand is

cheaper than 2205 strand by around 30%, these savings would be negated by the increased amount of strand that would be required to achieve the same prestressing force; of the two HSSS strand types, the 2205 strand is both the more corrosion resistant and cheaper per unit of prestressing force.

Failure of 2205 strand was characterized by breaking of all or most of the wires at the face of the grip. Some necking was observed at the failure point. Similar failure was observed in tests of 2304 strand using expansive cement grips. Representative failures of 2205 and 2304 are shown in Figure 4.3.

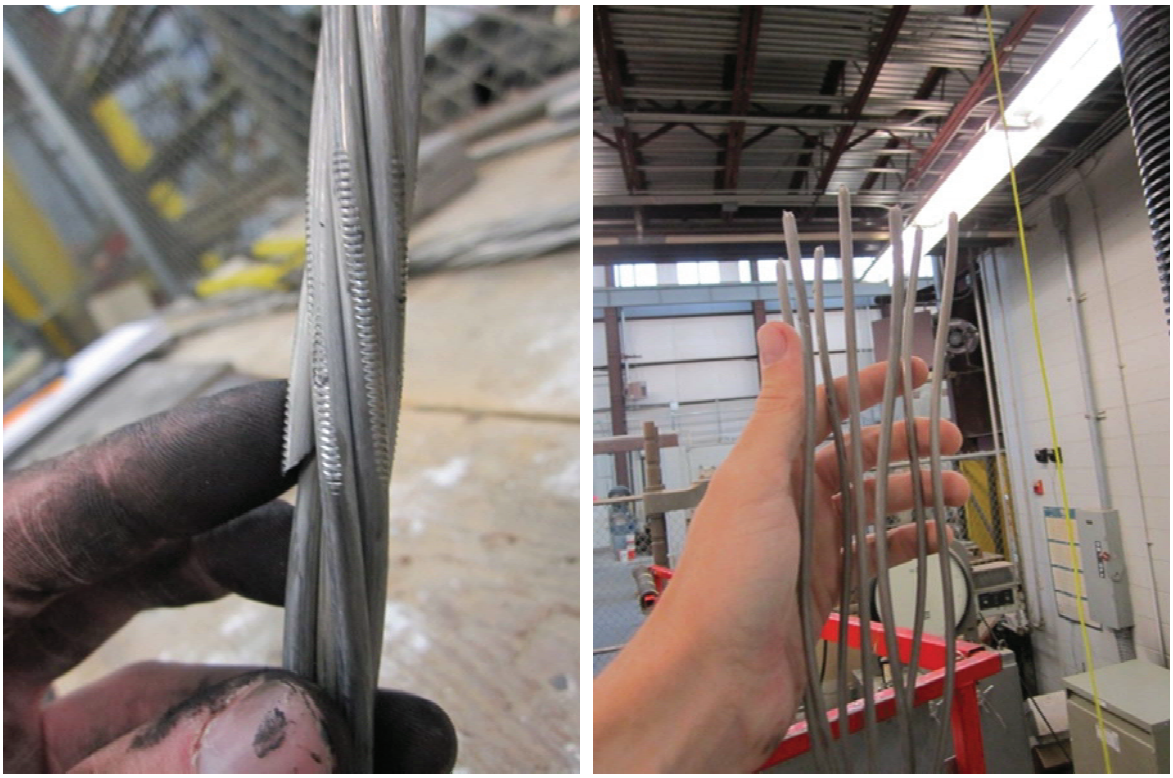

(a) (b)

Figure 4.3: Typical failure modes from (a) notching of 2304 strand, (b) uniform failure of 2205 and 2304 strand

4.2 Stress-Strain Behavior of Wire Samples

4.2.1 Experimental Methods

Wire samples were tested in direct tension using an INSTRON universal testing machine, as shown in Figure 4.4. Wire rod, and wires taken after reduction from dies #3, #5, #7 UW (untreated), and #7 HW (thermomechanically treated) were tested in triplicate from both 2205 and 2304 strand production samples. A gage length of approximately 8-in. (20 cm) and a displacement rate of 0.1 in/min (0.25 cm/min, strain rate of 0.0125 in/in/min) were used for all direct tension tests on single wires. A 2-in. (5 cm) extensometer was used and removed at 90% UTS, and position data generated from the testing machine were used to calculate the remainder of the strain data.

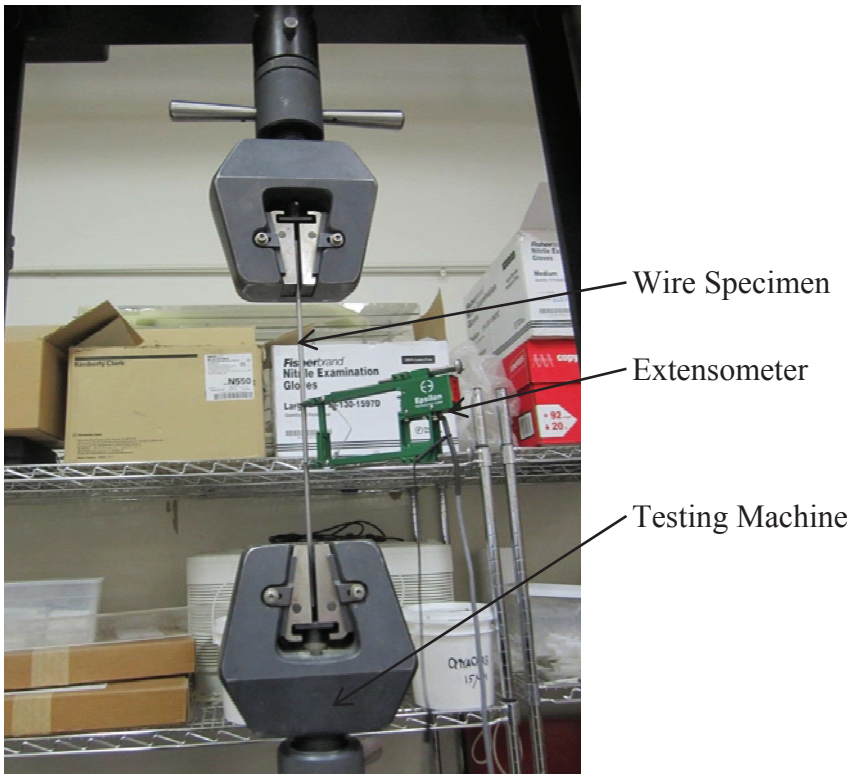

Figure 4.4: Wire tension testing apparatus

Stress-strain plots were constructed from these data. From these plots, 0.2% offset yield strength, UTS, E, and ultimate strain were determined, and average stress-strain curves were created. Tests were performed in triplicate when possible, but some wire types only received one or two tests due to limited quantities.

4.2.2 Results and Discussion

Figures 4.5 and 4.6 show the stress vs. strain behavior of drawn wire samples taken from varying points in the manufacture of the HSSS strand. Tables 4.3 and 4.4 detail the mechanical properties calculated from these curves along with the reduction of area (RA) from drawing. Individual test results are provided in Appendix C.

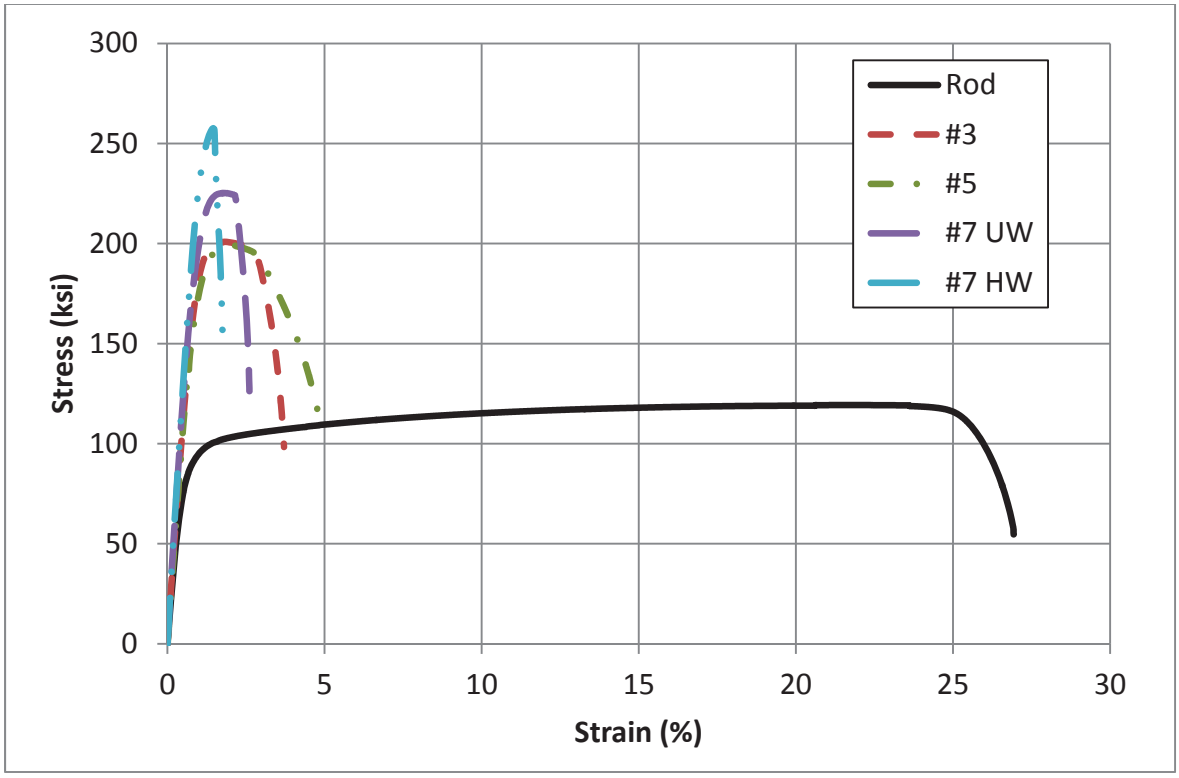

Figure 4.5: Stress-strain curves of 2205 wire samples

Table 4.3: Mechanical properties of 2205 wire samples*

Material	RA (%)	f_y ksi / MPa	UTS ksi / MPa	Ultimate Strain (%)	E ksi / GPa
Wire Rod	0	85.5 [1.0] / 589 [7.2]	119.1 [0.30] / 821 [2.1]	26.9 [2.1]	18400 [1440] / 126 [9.9]
#3	55.6	185.0 [3.2] / 1275 [22]	201.0 [0.35] / 1386 [2.3]	3.71 [0.30]	22200 [300] / 153 [2.1]
#5^	69.5	175.6 / 1211	199.3 / 1374	4.91	21700 / 150
#7 UW	78.7	207.3 [7.6] / 1429 [52]	225.2 [0.65] / 1553 [4.5]	2.62 [0.35]	24100 [1650] / 166 [11]
#7 HW	-	244.2 [2.8] / 1684 [19]	258.0 [0.57] / 1779 [3.9]	1.76 [0.053]	25500 [927] / 176 [6.4]

*Standard deviation shown in brackets.
^Due to limited materials, a shorter segment was tested in a different testing machine. Increased ultimate strain is likely caused by the magnification of strain localization caused by the smaller gage length. Other variability is likely due to the machine used.

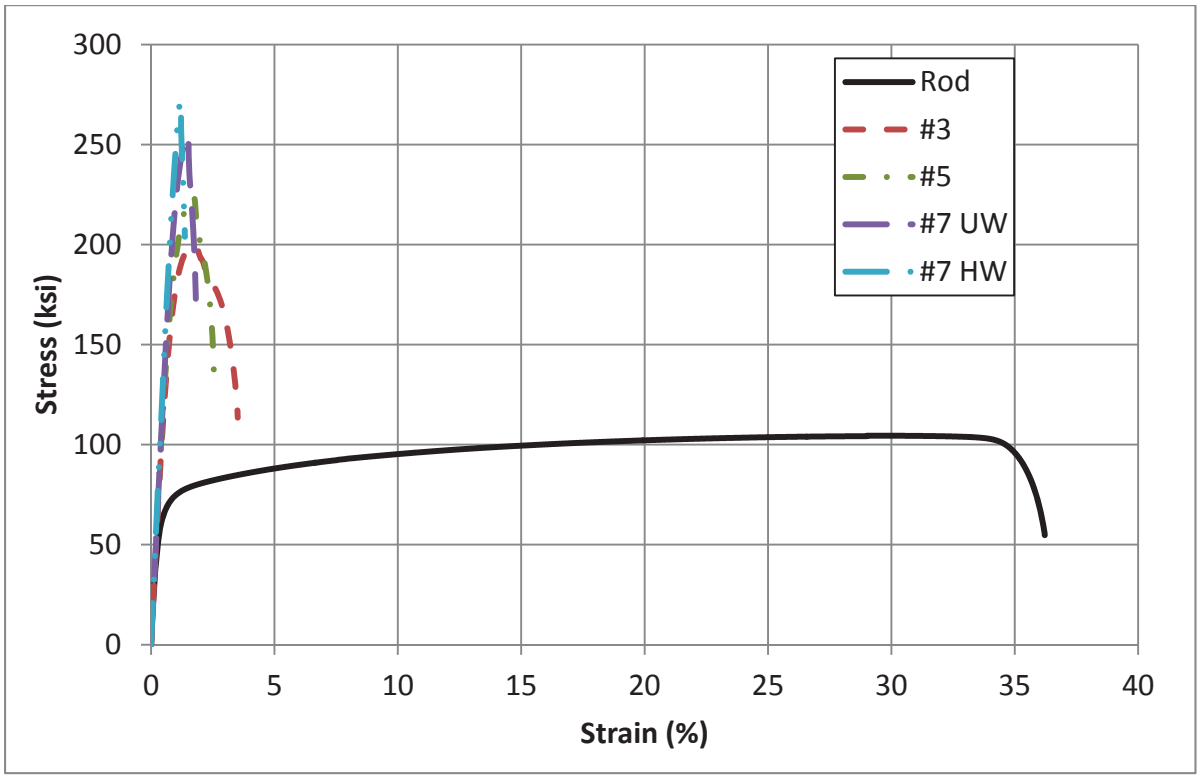

Figure 4.6: Stress-strain curves of 2304 wire samples

Table 4.4: Mechanical properties of 2304 wire samples*

Material	RA (%)	f_y (ksi)	UTS (ksi)	Ultimate Strain (%)	E (ksi)
Wire Rod	0	67.3 [2.3] / 464 [16]	104.3 [0.55] / 719 [3.8]	36.22 [1.22]	18100 [1850] / 125 [12]
#3	54.6	176.7 [3.0]/ 1218 [21]	199.7 [0.63] / 1377 [4.4]	3.51 [0.24]	22600 [50]/ 157 [0.3]
#5^	68.9	198.9 / 1371	224.0 / 1545	2.54	23000 / 159
#7 UW	78.3	238.3 [3.7] / 1642 [25]	254.7 [0.28] / 1756 [1.9]	1.81 [0.10]	25200 [1500] / 174 [10]
#7 HW	-	263.4 [7.4] / 1816 [51]	271.8 / [0.26] 1874 [1.8]	1.38 [0.031]	25600 [1100] / 177 [7.6]

*Standard deviation shown in brackets.
^Single test due to limited materials.

Reduction of area by cold drawing led to clear increases in yield stress, UTS, and Young's modulus, but significant decreases in ultimate strain in both stainless steels. While wire rods showed high ultimate strain (above 25%), none of the drawn samples exhibited significant post-yield plasticity or strain hardening, and necking occurred short after yield. Of the two materials, 2304 gained strength more effectively with reduction of area. This is potentially due to the formation of strain-induced martensite in the austenite fraction.

Thermomechanical treatment led to significant increases in UTS and further decreases in ductility. These effects can be accounted for by a decrease in residual stresses caused by the treatment. During drawing, high compressive residual stresses are believed to be unevenly induced along the length of the wire. These areas of high residual stress yield before areas of low residual stress. Therefore, after treatment which reduces residual stresses and provides a more uniform distribution, an increase in UTS is observed. In the untreated wire, more strain is required to overcome residual compressive

strains. Therefore, a higher ultimate strain is observed prior to treatment. However, these ultimate strains are based on the magnification of strain localization due to the gage length. At larger scales, ultimate strains would be reduced to approximately the yield strain since there is little ductility in any of the drawn wires after this point.

CHAPTER 5

STRESS RELAXATION BEHAVIOR

5.1 Stress Relaxation Behavior of Strand Samples

5.1.1 Experimental Methods

Stress relaxation testing on strand specimens was performed in a temperature controlled room (68° F or 20° C and 50% RH) in accordance with ASTM E328. 10-ft. (3 m) long HSS steel sections were used as a testing frame for strand relaxation tests, as illustrated in Figure 5.1. The ½-in. strand was places through holes in plates at each end of the HSS section. At the anchorage, dead end of the frame, a hollow core steel vibrating wire load cell was placed around the strand and anchored at the end with a standard strand chuck. At the jacked end, the strand was run through a hollowed bolt and nut, and a chuck was placed at the face of the bolt prior to loading. A steel housing was then set at the face of the frame; and a U-washer, jack, load cell and chuck were placed on the strand. The U-washer allowed for easier removal while the load cell was used to monitor load during jacking. After the strand was jacked to its desired load, the bolt was turned until tight with the chuck inside the housing. Load was then taken off the jack and initial load was confirmed by the vibrating wire load cell at the opposite end. The jacking apparatus was removed and load data were collected using a data acquisition box at 30 second increments for the first 20 minutes, 5 minute intervals for the next 24 hours, and 1 hour intervals for the remainder of the test. Data points were removed to provide a more uniform logarithmic distribution of data. The time required for jacking was about 5

minutes, and the time required for securing the bolts was approximately 30 seconds. Relaxation time was measured from the time the bolts were secured.

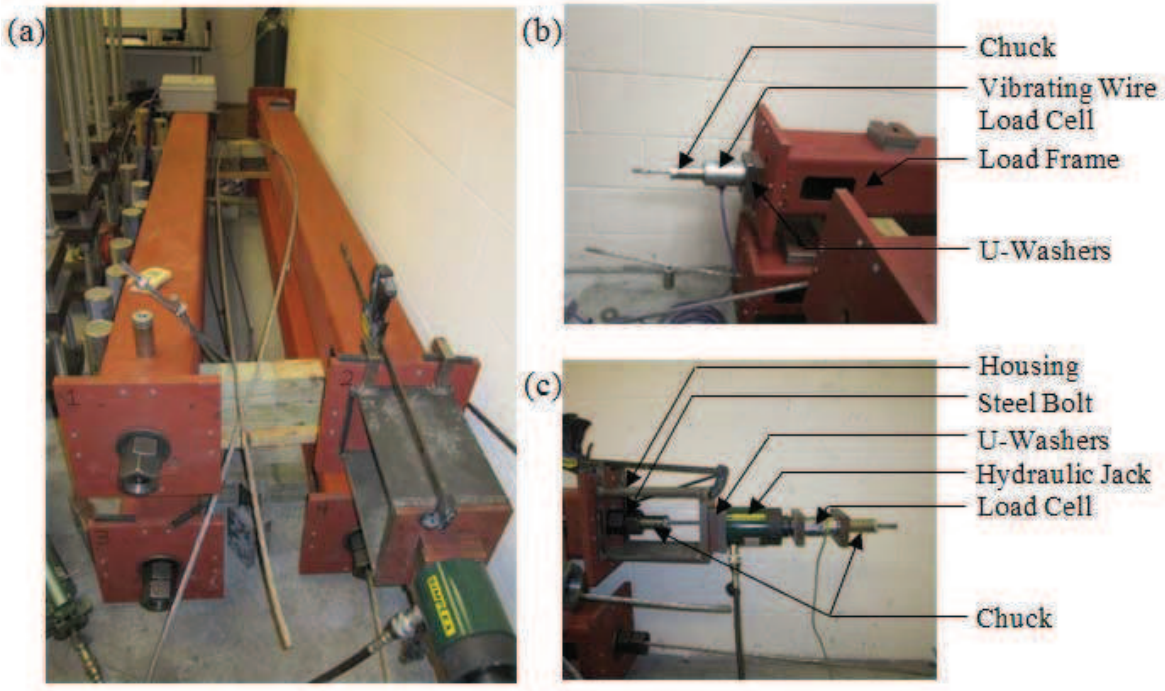

Figure 5.1 (a) Relaxation frame, (b) dead end of frame, (c) jacked end of frame during loading

Stress relaxation plots were generated by calculating the percent of initial stress at each data point and plotting the results versus logarithmic time. Average stress relaxation curves were generated where multiple tests were performed. Logarithmic best fit curves were fit to the data and were used to extrapolate the 1000 hour stress relaxation in the 200 hour tests. Despite having experimental values for stress relaxation at 1000 hours, best fit curves were also used to calculate the 1000 hour stress in 1000 hour tests to account for the potential random error of the final point.

For 2205 strand, triplicate tests were conducted at 70% UTS for a 1000 hr term as well as single tests loaded to 50% and 80% UTS for 200 hr each. The shorter term tests were extrapolated to provide 1000 hr relaxation values. Due to notch sensitivity of the 2304 material, the 2304 strand could not be stressed to the same load levels. Instead, three 1000 hr tests at 40% UTS were performed.

5.1.2 Results and Discussion

Figure 5.2 shows the stress relaxation of both HSSS alloys at differing initial stresses, and their 1000 hr losses are summarized in Table 5.1. Individual stress relaxation curves for the different HSSS strands at each stress level along with their line of best fit are shown in Figures 5.3 to 5.6. 1000 hr losses were extrapolated from the 200 hour tests using logarithmic regression. Though there is variation due to cyclic temperature fluctuation in the room, the data adheres well to logarithmic trend.

Three 1000 hr tests at 70% UTS initial stresses revealed an average loss of 2.49% for 2205 strand, slightly less than the limit of 2.5% set by ASTM A416 for low relaxation prestressing strand. At an initial stress of 80% UTS, 1000 hr relaxation was measured to be 1.91%, satisfying the limit of 3.5% from ASTM A416, which is also less relaxation loss than measured in the tests conducted at 70% UTS (2.49%). More tests are necessary to verify these data, as it is unexpected that less relaxation would occur when higher initial stress is applied.

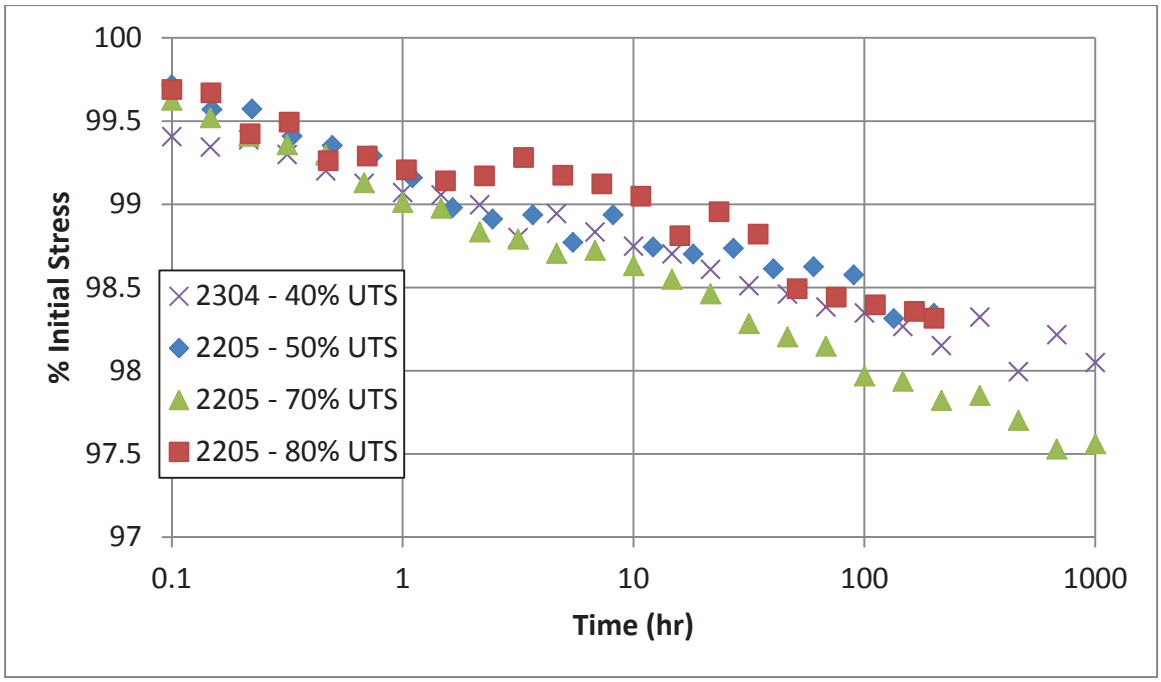

Figure 5.2 Stress relaxation of strand specimens

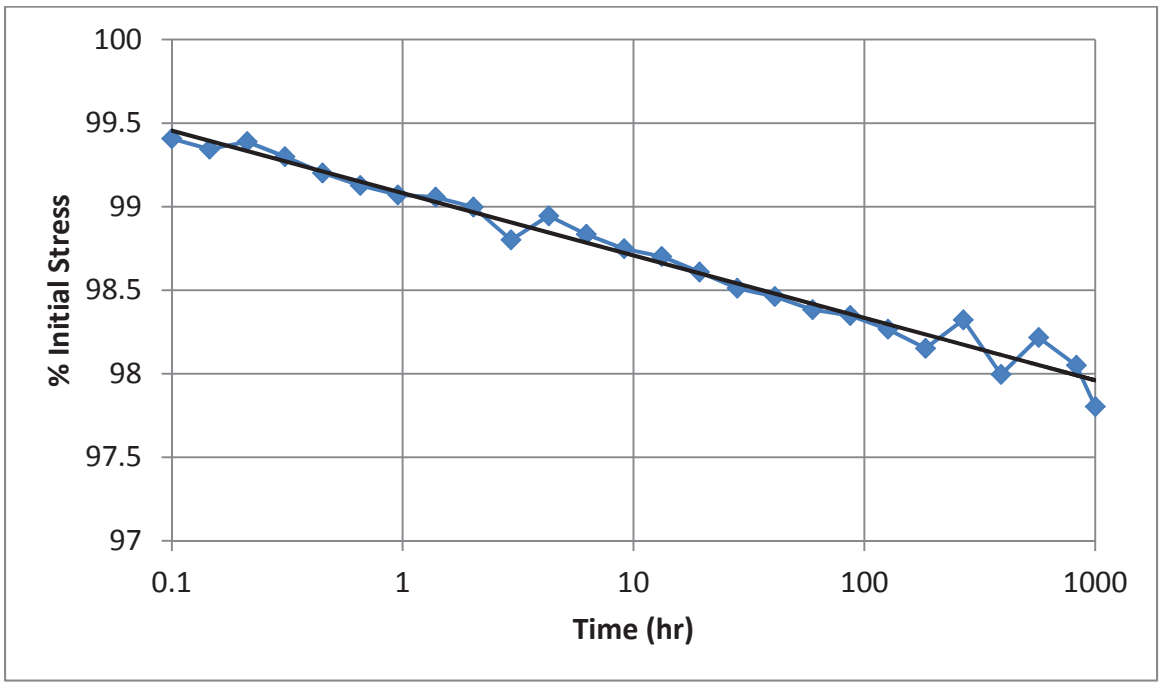

Figure 5.3 Average stress relaxation of 2304 strand at an initial stress of 40% UTS

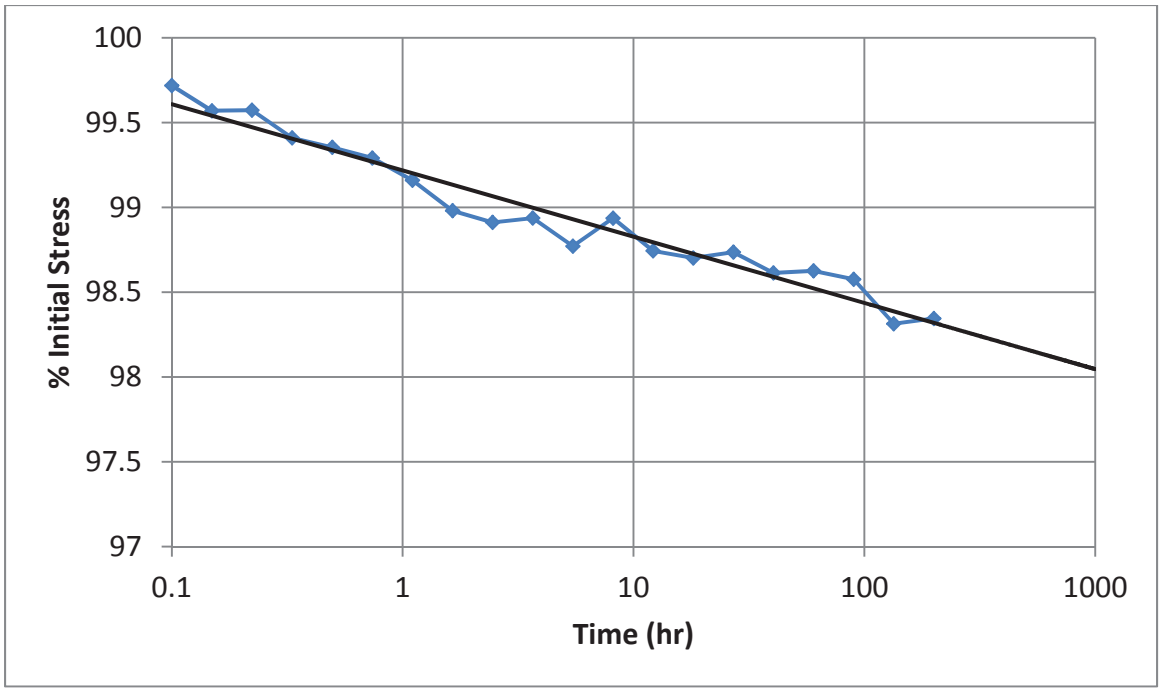

Figure 5.4 Stress relaxation of 2205 strand at an initial stress of 50% UTS

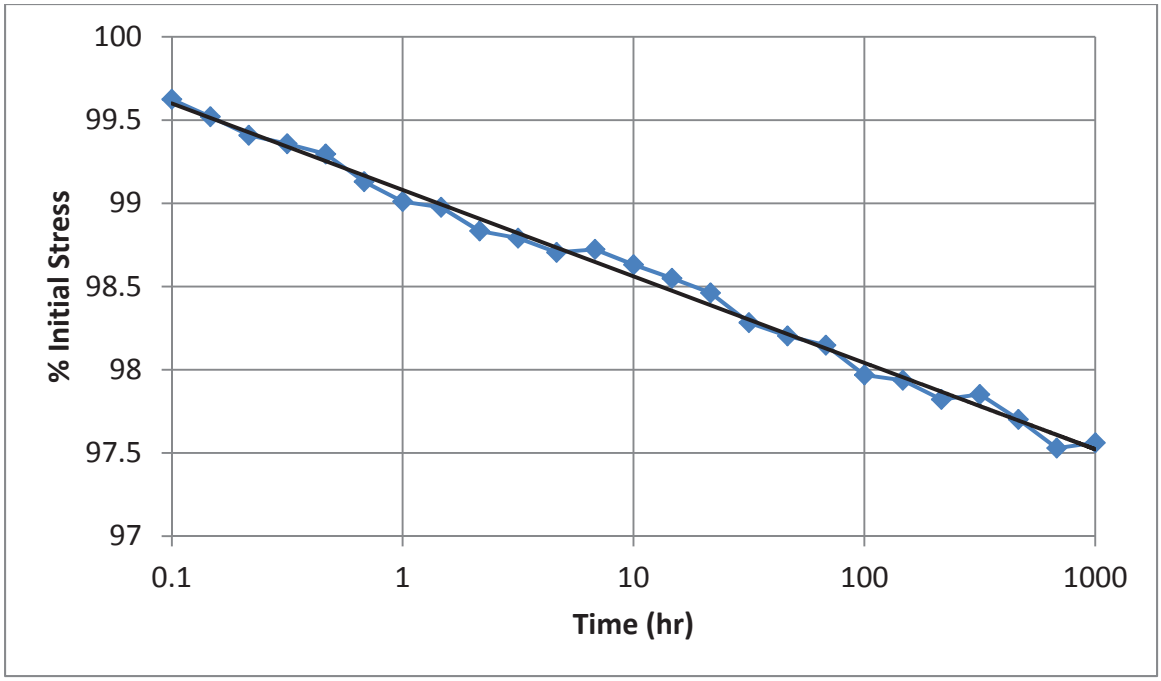

Figure 5.5 Average stress relaxation of 2205 strand at an initial stress of 70% UTS

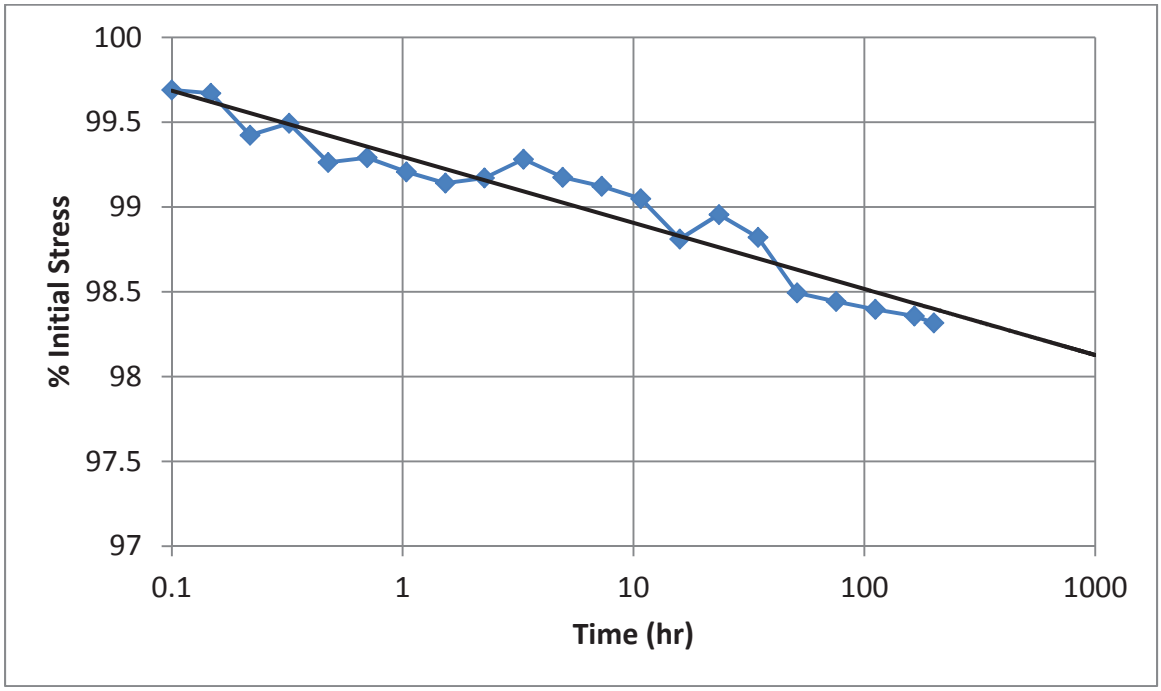

Figure 5.6 Stress relaxation of 2205 strand at an initial stress of 80% UTS

Table 5.1: Mean stress relaxation losses of strand specimens at 1000 hours*

Test	1000 hr Stress (% Initial)	% Loss	Lo-Lax Limit
2304 - 40% UTS 1000 HR	97.93 [0.0]	2.07 [0.0]	-
2205 - 50% UTS 200 HR^	97.99	2.01	-
2205 - 70% UTS 1000 HR	97.51 [0.24]	2.49 [0.24]	<2.5 %
2205 - 80% UTS 200 HR^	98.09	1.91	<3.5 %

*Standard deviation shown in brackets.
^Single test conducted.

All 1000 hour tests were truncated to 100 and 200 hr terms in order to assess the validity of the predicted 1000 hour stress relaxation value from the shorter term tests. 50 logarithmically spaced data points were selected for each test and a logarithmic trend-line was fit to the data and used to extrapolate the 1000 hour stress. The summary of these results for three tests of 2205 strand initially stressed to 70% UTS and two 2304 tests

initially stressed to 40% UTS are presented in Tables 5.2 and 5.3. The third test of 2304 at 40% UTS was excluded due to excessive random error in the data. The results of each test are presented in Appendix D.

Table 5.2: Comparison of 1000 hr stress relaxation losses—2205 strand at 70% UTS

Term (hr)	Test							
	1		2		3		Average	
	Loss (%)	% diff	Loss (%)	% diff	Loss (%)	% diff	Loss (%)	% diff*
1000	2.43	-	2.86	-	2.06	-	2.45	-
100	2.61	7.43	2.81	-1.59	1.97	-4.07	2.46	4.36
200	2.59	6.91	2.82	-1.34	2.06	0.01	2.49	2.75

*Based on absolute values of % difference.

Table 5.3: Comparison of 1000 hr stress relaxation values—2304 strand at 40% UTS

Term (hr)	Test					
	1		2		Average	
	Loss (%)	% diff	Loss (%)	% diff	Loss (%)	% diff*
1000	2.06	-	2.04	-	2.05	-
100	2.12	2.93	1.96	-3.73	2.04	3.33
200	2.11	2.45	1.98	-3.00	2.04	2.72

*Based on absolute values of % difference.

From the five 1000 hr tests, 200 hour term tests were shown to give stress relaxation values at an average 2.7% difference from the values taken from 1000 hour tests; 100 hour tests showed approximately 4% difference on average. The shorter term tests did not consistently overestimate or underestimate the 1000 hour relaxation value; therefore, the average of multiple short term tests is likely to be a much better approximation than each individual test. In the tests on 2205 strand, there was a significantly high standard deviation of 0.24% (or 9.6% of the average loss) in the 1000

hour stress from test to test, which reduces the significance of the random error caused by shortening the test duration. Extrapolated relaxation loss values from 100 and 200 hour tests each fell within 9.6% of the 1000 hour loss calculated from the full length test—i.e. the error incurred by reducing the testing term is insignificant compared to the error inherent to the test setup and material. Overall, the relaxation data exhibited strong logarithmic behavior, with R^2 values typically between 0.90 and 0.95 for short and long term tests. The difference in relaxation from the shorter term tests can most likely be attributed to the inherent random scatter in the data. Overall, the strand relaxation data show that the HSSS strand satisfied the ASTM A416 criteria for low relaxation strand.

5.2 Stress Relaxation Behavior of Wire Samples

5.2.1 Experimental Methods

Tests were conducted in a temperature controlled room (68° F or 20° C and 50% RH) using a vertical steel HSS load frame with a lever arm loading mechanism. A 10-ft. (3 m) length of wire was fit into the load frame and secured at the bottom end using a chuck and a bearing plate. The bottom end of the frame was the live end; it was hinged such that rotation of the HSS lever arm caused loading or unloading in the wire as shown in Figure 5.7. The mechanism provided enough mechanical advantage that wires could be loaded up to 5 kips (22 kN) by hand. The top end of the frame was fully fixed and was referred to as the dead end. A 10-kip (45 kN) capacity load cell was fit around the wire specimen with bearing plates at both ends, and a centering ring was placed to maintain the wire at the center of the load cell. The wire was secured above the top plate with

another chuck. Load readings were taken using a strain indicator box and switch and balance unit.

Tests were conducted in accordance with ASTM E 328. The wires were loaded gradually and the frame was locked in place between 3 to 5 minutes from the time loading began. Prior to loading, the lever arm at the live end of the frame was lifted and the bottom chuck was cinched as high as possible to minimize the travel of the arm required to straighten the strand. The wire was then centered in the frame and the weight of the lever arm was released onto the wire. A steel bar was inserted into the HSS lever arm for further mechanical advantage in loading. The rod was depressed slowly until the target load was reached (maximum loads were between 2.6 and 4.9 kips, 11.6 and 21.8 kN). The arm was then locked in place on a threaded rod that was anchored in the base of the frame. The steel bar was removed and the initial load reading was recorded. Initial loads on treated wires were based on the UTS of the strand in order to compare the relaxation loss of wire and strand at the same stress level.

Due to the logarithmic nature of stress relaxation, a higher volume of measurements were taken at early ages than later ages. These intervals are summarized in Table 5.4. These increments provided a near even logarithmic spacing of approximately 100 points over the course of 1000 hours.

Table 5.4: Wire relaxation measurement increments

Elapsed Time in Test	Maximum Interval Between Readings
0 - 1 min	10 s
1 - 10 min	30 s
10 - 25 min	3 min
25 min - 1 hr	5 min
1 - 3 hr	15 min
3 - 5 hr	30 min
5 - 10 hr	1 hr
10 hr - 1 week	8 hr
1 - 2 weeks	14 hr
2 - 3 weeks	28 hr
Remainder of Test	72 hr

Stress relaxation plots were generated by calculating the percent of initial stress at each data point and plotting the results versus logarithmic time. Average stress relaxation curves were generated where multiple tests were performed. Logarithmic best fit curves were fit to the data and used to extrapolate the 1000 hour stress relaxation in 200 hour tests. Despite having experimental values for stress relaxation at 1000 hours, best fit curves were also used to calculate the 1000 hour stress in 1000 hour tests to account for the potential random error of the final point.

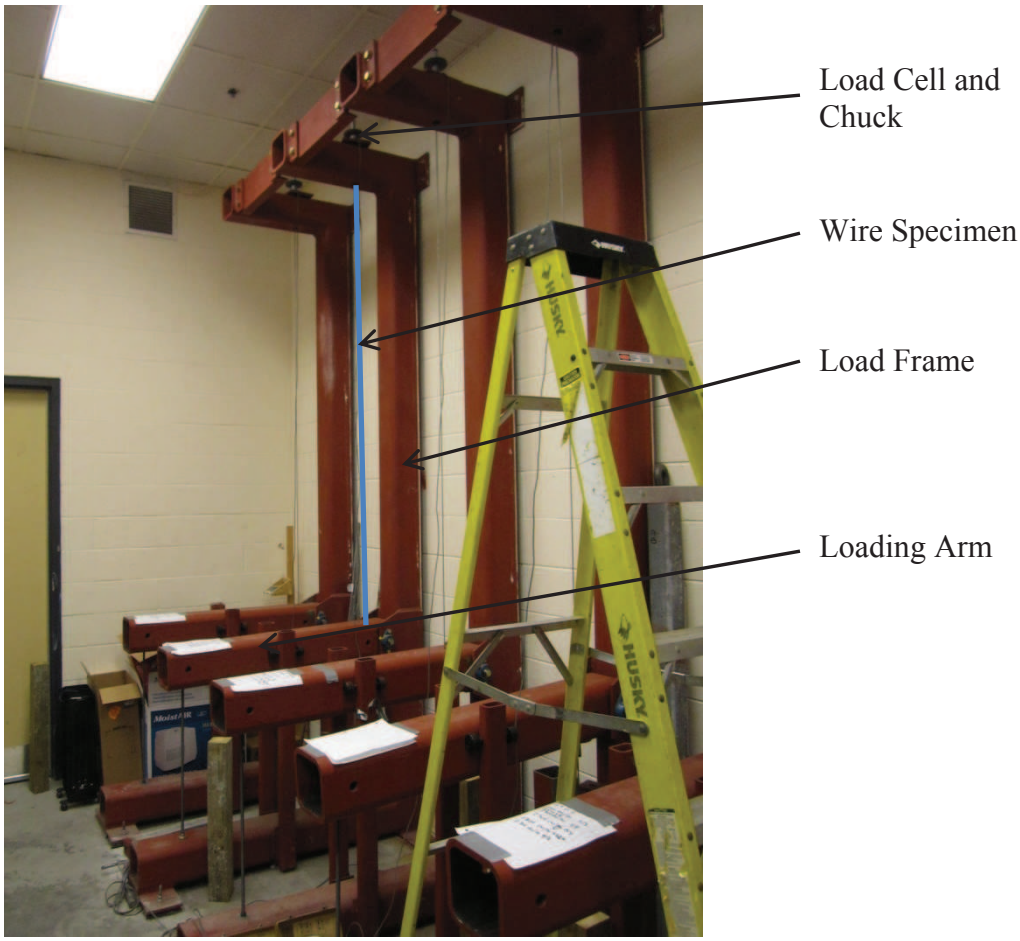

Figure 5.7 Wire relaxation test setup

Stress relaxation testing performed on wire samples included three 1000 hour tests initially stressed to 70% UTS and single 200 hour tests initially stressed to 50% and 80% UTS for each 2205 #7 UW, 2205 #7 HW, 2304 #7 UW, and 2304 #7 HW wires.

5.2.2 Results and Discussion

Figure 5.8 shows the stress relaxation of the HSSS wires stressed to 70% UTS, and their 1000 hr losses are summarized in Table 5.5. Average stress relaxation curves for the different HSSS wires along with their lines of best fit are shown in Figures 5.9 to 5.12. Logarithmic best fit lines were used for all the wire specimens, although

non-logarithmic behavior was observed in some wire samples. 1000 hr relaxation loss was calculated based on the best fit curves. While these curves show 20 evenly spaced data points, best fit curves were determined using the full data set of approximately 100 data points. Individual curves for each test are given in Appendix D.

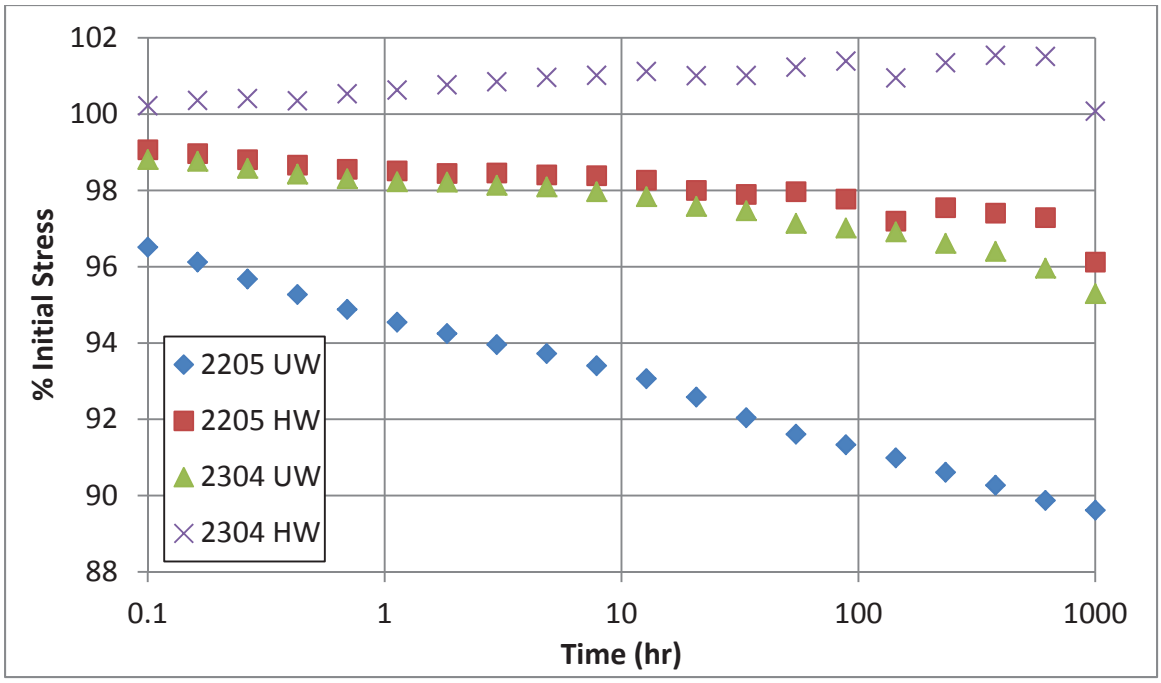

Figure 5.8 Stress relaxation of wire specimens

Table 5.5: Mean stress relaxation losses of wire specimens stressed to 70% UTS at 1000 hours*

Test	1000 hr Stress (% Initial)	% Loss
2205 UW	89.56 [1.34]	10.44 [1.34]
2205 HW	97.33 [0.71]	2.67 [0.71]
2304 UW	96.12 [0.87]	3.88 [0.87]
2304 HW^	101.79 [0.075]	-1.79 [0.075]

*Standard deviation shown in brackets.
^Average of two tests that exhibited negative relaxation.

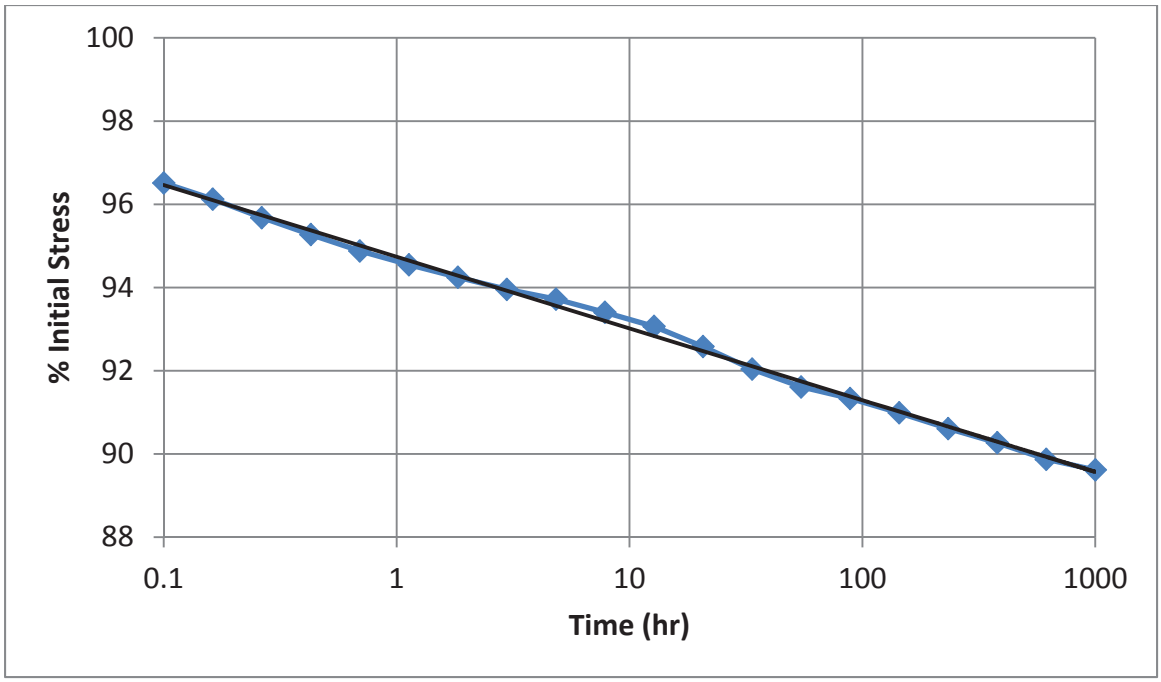

Figure 5.9 Stress relaxation of 2205 untreated wire at an initial stress of 70% UTS

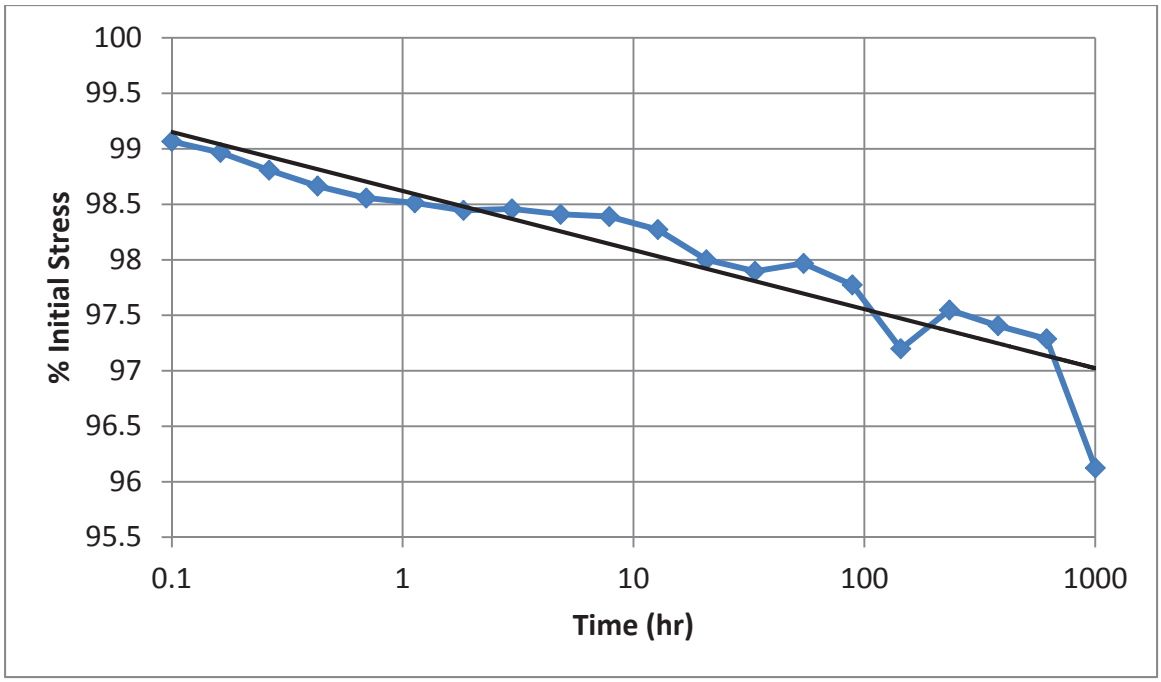

Figure 5.10 Stress relaxation of 2205 thermomechanically treated wire at an initial stress of 70% UTS

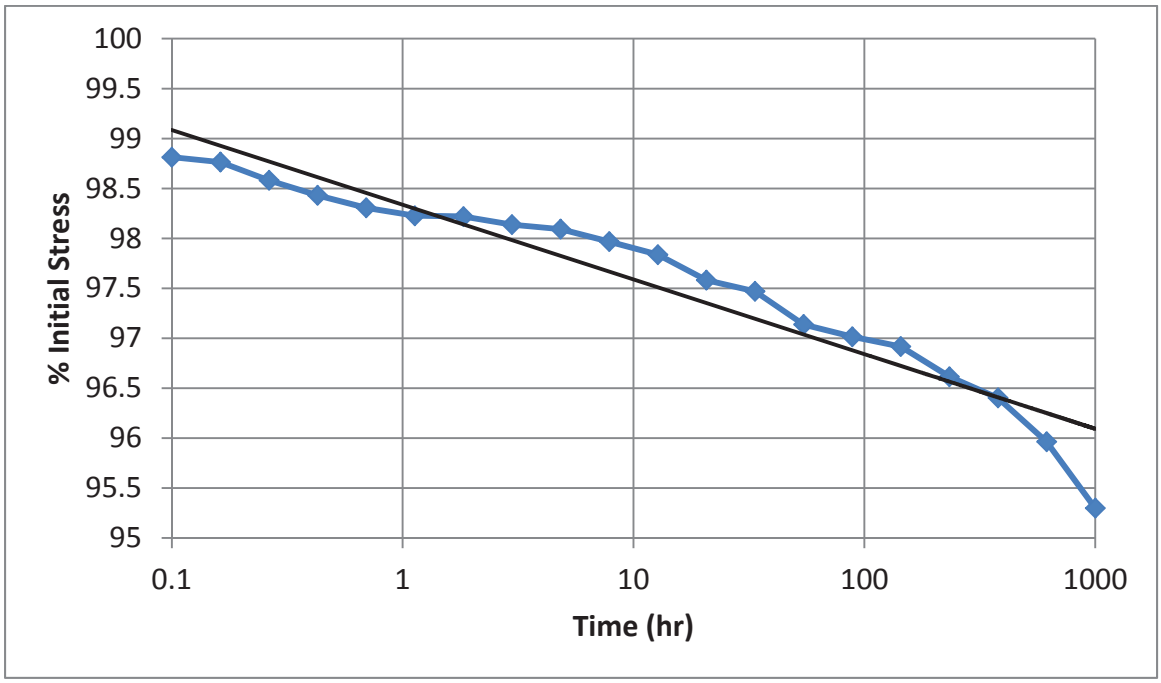

Figure 5.11 Stress relaxation of 2304 untreated wire at an initial stress of 70% UTS

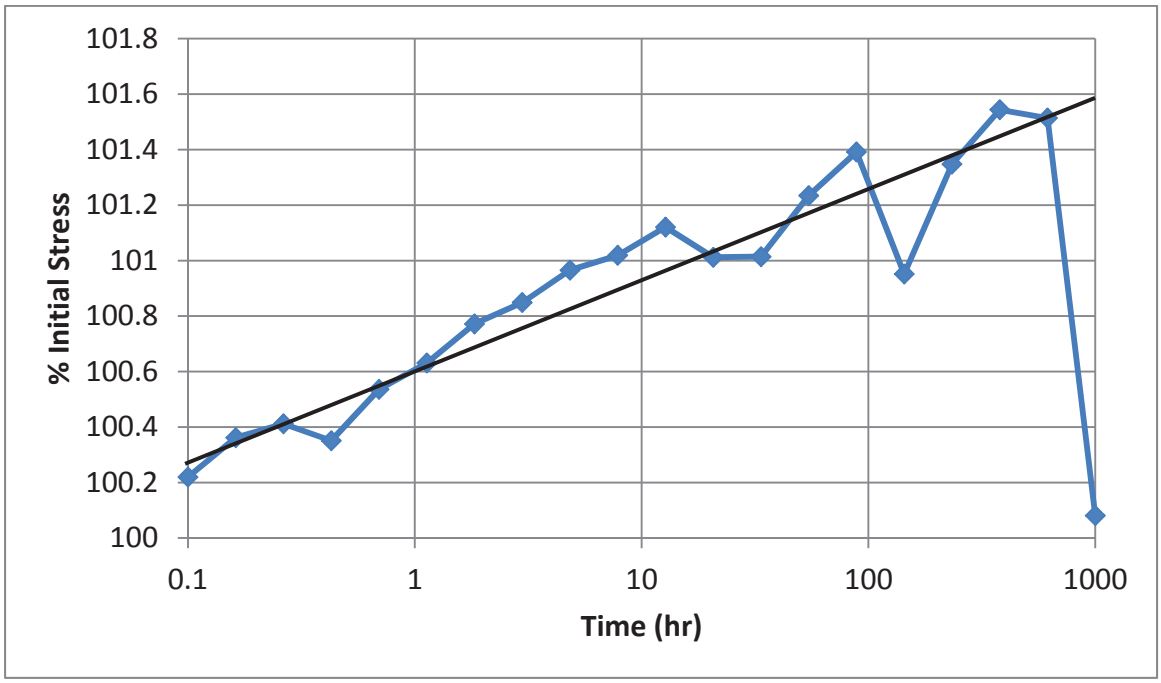

Figure 5.12 Stress relaxation of 2304 thermomechanically treated wire at an initial stress of 70% UTS

The 2205 untreated (UW) wire exhibited an average relaxation loss of 10.44%, while the 2205 wire subjected to thermomechanical treatment (HW) exhibited an average relaxation loss of 2.67%, resulting in a reduction of relaxation loss of 7.77% that can be attributed to the thermomechanical treatment. These results adhered well to the logarithmic best fit model; each test on 2205 UW wire yielded an R^2 over 0.98. R^2 values for 2205 HW testing ranged from 0.88 to 0.98.

The relaxation loss of 2205 HW strand, as given in Section 5.1.2, was 2.49%, with a standard deviation of 0.24%. The average relaxation of 2205 HW wire was measured to be 2.67%, which is within one standard deviation of the strand result. However, wire tests exhibited a much higher standard deviation of 0.71%, which reduces the confidence in the hypothesis that wire and strand relaxation tests yield the same results. The higher deviation in wire results may be attributed to temperature changes in the room, or issues with the data acquisition equipment. Further testing is required to adequately compare the two methods.

The 2304 wire samples exhibited unexpected behavior. Each test on 2304 UW wire exhibited a well-defined negative curvature on a single logarithmic plot, similar to the shape of the average curve shown in Figure 5.11. Of the three tests conducted on 2304 HW, two exhibited negative stress relaxation. The average of these two tests is presented in Figure 5.12. It is possible that these results are due to unknown error in the data acquisition system, but other mechanisms may account for this behavior.

While further investigation is still required, it is possible that this behavior can be accounted for by phase transformation in the microstructure of the steel. 2304, a lean

duplex stainless steel, is susceptible to a transformation from austenite to martensite under plastic strain (Lee et. al. 2003; Padilha et. al. 2012). The slippage of grains causing forest dislocations which characterizes the stress relaxation mechanism may serve the same purpose as plastic strain in inducing phase transformations. Martensite, a lower volume phase, would serve to increase stress in the wire to maintain a constant global strain in the material. The mechanisms of phase transformation and stress relaxation were theoretically both present in each test, acting to respectively increase and decrease the stress in the wire.

The results from 2304 UW show a negative curvature in each test, and a lower than expected 1000 hour stress relaxation loss of 3.88%. The relaxation in 2304 UW was expected to be close to the 2205 UW value of 10.44% over 1000 hours since the two samples are similar in microstructure and treatment, agreeing with similar tests conducted by Moser (2011). It is theorized that the negative curvature in the 2304 UW test was due to the exhaustion of austenite in the microstructure. As the rate of phase transformation slowed due to the exhaustion of austenite, the contribution of the stressing mechanism diminished, and eventually, the only significant mechanism present to change the stress in the strand would be stress relaxation. The diminishing of the stressing mechanism may explain the negative curvature in the stress relaxation curves of 2304 UW wire.

The tests on 2304 HW wire exhibited considerably more scatter and an actual increase in apparent stress in the wire during the test. It is possible that the phase transformation stressing mechanism was stronger than the relaxation mechanism in this case. Since these wires had undergone a low-relaxation treatment, the relaxation in the wires was expected to be smaller than the tests on 2304 UW. It is expected that the stress

in wire would begin to decrease due to the exhaustion of austenite, but this point was not clearly observed in the 1000 hour term of the test, either because the austenite was not completely exhausted before 1000 hours or because the data exhibited too much noise to notice this point.

Further studies are required into these results to verify this theory. The test on 2304 HW which exhibited a positive relaxation of 1.79% cannot be explained, except for the possibility that this test was loaded to a lower level than the others, and the phase transformation was not triggered. Magnetic analysis, metallography, and X-ray diffraction performed on samples prior to and after relaxation may provide further information on any microstructural changes that may occur during stress relaxation testing.

CHAPTER 6

PILE SPECIMEN EXPERIMENT DESIGN

In order to assess the performance of HSSS strand in real bridge structures, full scale prestressed piles are to be produced with 2205, 2304, and standard low relaxation 1080 strand. A series of tests are planned (1) to evaluate the performance of the HSSS strand during pile construction and pile driving, (2) to determine transfer and development length of the HSSS strand in comparison to 1080 strand, (3) to experimentally study the behavior of the HSSS reinforced piles in flexure and shear and compare that behavior with standard piles and with AASHTO design equations, (4) to measure prestress losses, and (5) to investigate the durability of the concrete and of the HSSS in actual Georgia coastal environment and to compare that durability with previous laboratory investigations.

6.1 Fabrication of Pile Specimens

6.1.1 Design of Steel Reinforcement

Piles constructed with 1080 strand were designed according to GDOT standards while analogous HSSS reinforced piles were detailed for equivalent initial prestressing force. While $^{7}/_{16}$-in. (11 mm) strand is used in GDOT standard piles, ½-in. (13 mm) stainless steel strand was used to compensate for the decrease in material strength with an increase in cross-sectional area. GDOT officials recommended testing on 18-in. (46 cm) square piles, as these piles are both commonly used and have one of the lowest precompressive stresses of the standard pile designs. 18-in. (46 cm) sq. piles were selected for testing with 2205 and 1080 strand. Due to the low prestressing capacity of 2304 strand due to notch sensitivity, 12-in. (30 cm) square piles were selected with a 12 strand cross-section, 4 more strands than typically used for this size pile. Standard 12-in. (30 cm) sq. piles will also be constructed with 1080 strand using the 8 strand

layout. Clear cover is 3-in. (76 mm) for all piles, shown in Figure 6.1. Piles are referred to based on their dimensions and strand metallurgy.

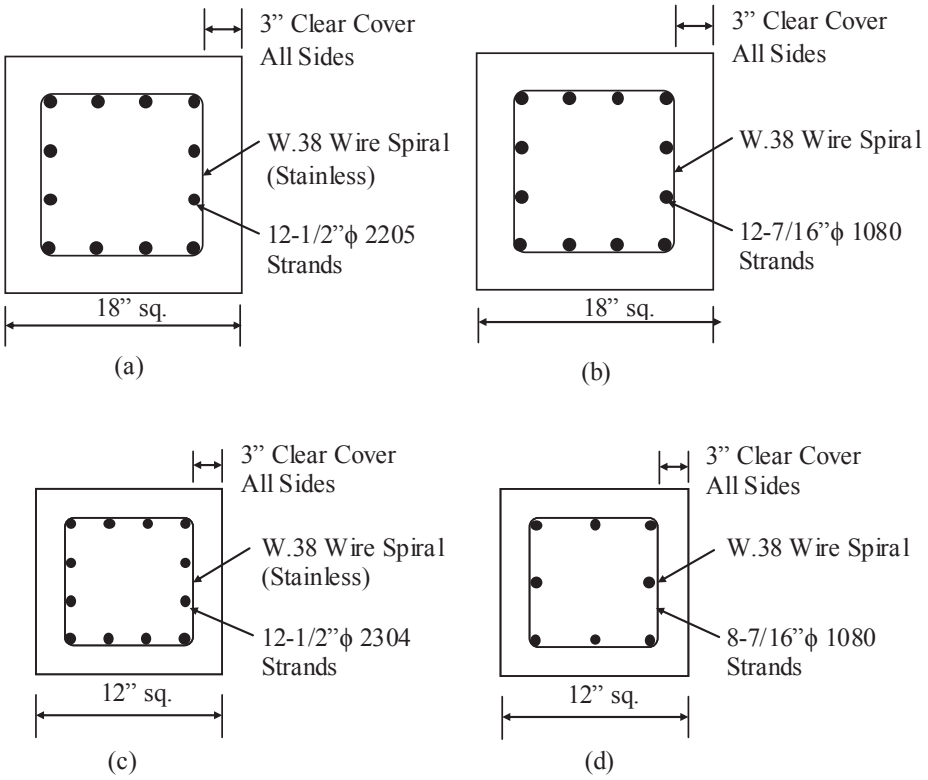

Figure 6.1 Cross sections of (a) 18-in. (46 cm) 2205, (b) 18-in. (46 cm) 1080, (c) 12-in. (30 cm) 2304, and (d) 12-in. (30 cm) 1080 piles

Shear reinforcement in GDOT standard piles is W-3.8, or No. 5 Birmingham wire spiral, corresponding to ASTM A82 "Standard Specification for Steel Wire, Plain, for Concrete Reinforcement". This wire has a diameter of 0.220-in. (5.5 mm) and yield strength of 70 ksi (483 MPa). The wire spiral is at a 1-in (25 mm) pitch at each end for the first 8-in. (20 cm), then 16 turns at 3-in. (76 mm), and the remainder of the wire spiral is at a 6-in. (152 mm) pitch. The

transverse reinforcement layout for the piles is given in Figure 6.2. These dimensions are typical for all piles except the 20-in. (51 cm) long samples, which will be reinforced at a 3-in. (76 mm) pitch along the entire length.

Stainless steel transverse reinforcement is required for piles reinforced with stainless steel strand, not only because the shear reinforcement needs to be resistant to corrosion caused by its environment as well, but also because the contact between plain steel wire and stainless steel strand would lead to accelerated galvanic corrosion of the wire. Stainless steel wire will be selected to match the mechanical properties of the current plain steel reinforcement. While this wire has not yet been selected, it is likely that Type 304 or 316 stainless steel will be used due to their availability and low cost.

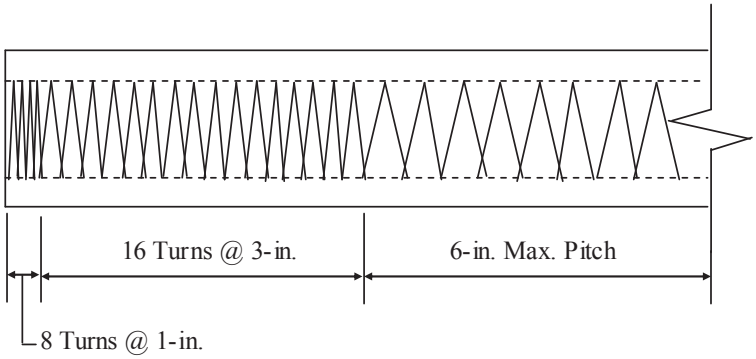

Figure 6.2 Typical wire spiral layout

6.1.2 Lengths of Pile Specimens

Pile testing is limited by the amount of HSSS strand available. After mechanical testing, approximately 2,300-ft. (700 m) of 2205 and 2,000-ft. (610 m) of 2304 remained—another 300 feet of 2304 was available, but it was from a different heat treatment. As a result, the maximum practical bed length allowed was 180-ft. (55 m) for 2205 piles and 165-ft. (50 m) for 2304 piles. Testing is confined to piles that may fit in these spans.

Pile sizes were chosen based on the tests to be performed and the available length in the casting bed. The lengths chosen for 18-in. (46 cm) sq. piles were two 70-ft. (21 m) long piles and four 20-in. (51 cm) long material

samples. Identical sets of these piles are to be constructed using 2205 and 1080 strands. The lengths chosen for 12-in. (30 cm) sq. piles were one 70-ft. long (21 m), two 27-ft. (8 m) long, one 10-ft. (3 m) long, and three 20-in. (51 cm) long samples, to be cast with each 2304 and 1080 strand. The purpose of these lengths is discussed in the following sections. The bed layout is shown in Figure 6.3.

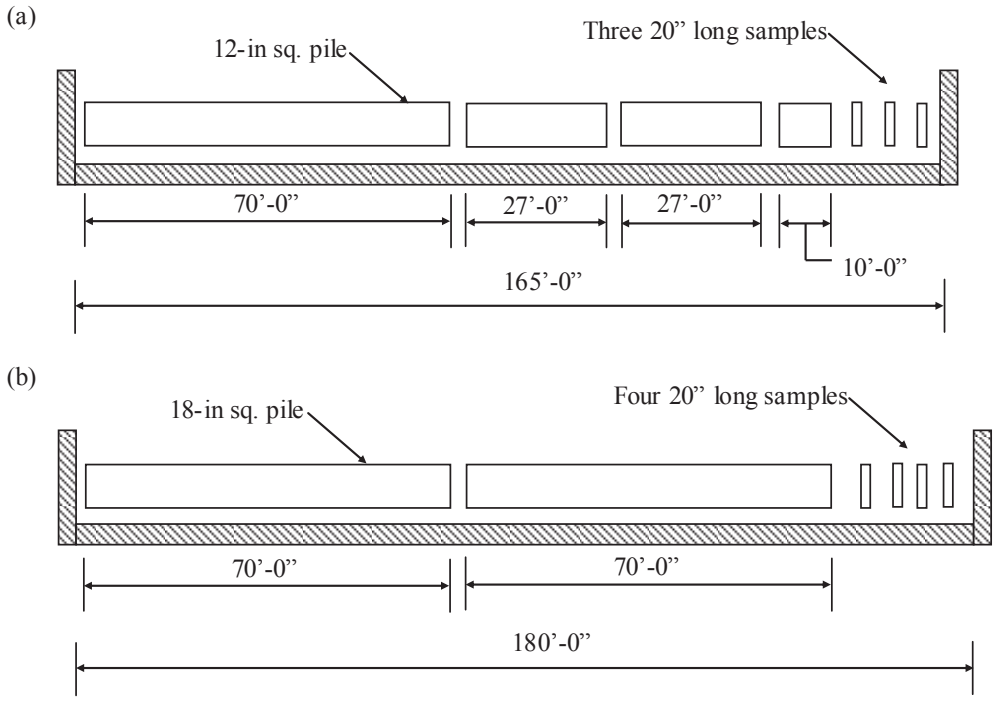

Figure 6.3 Construction layouts for (a) 12-in. (30 cm) sq. and (b) 18-in. (46 cm) sq.

6.1.3 Mix Designs

A High Performance Marine Concrete (HPMC) mix design developed by Holland (2012) is to be used in the HSSS piles. This is a ternary mix utilizing both Class F fly ash and silica fume as SCMs, shown in Table 6.1. The mix was designed specifically for durability—i.e. low permeability, high sulfate resistance, high carbonation resistance, and

self-healing. 1080 piles will be cast using a GDOT standard HPC mix. 4-in x 8-in cylinders will be cast alongside the piles for compression testing at 7, 28, and 56 days as well as rapid chloride permeability testing at 56 days.

Table 6.1 Mix designs for both girder types

	Weight, lb/yd^3 [kg/m^3]	
Material	HPC Mix	HPMC Mix
Water	237 [140]	285 [168]
Type I/II Cement	-	665 [393]
Type III Cement	796 [472]	-
Class F Fly Ash	98 [58]	238 [141]
Silica Fume	70 [41]	48 [28]
Natural Sand	965 [573]	866 [512]
#67 Stone	1837 [1090]	1905 [1125]
Admixture	oz./yd^3 [mL/m^3]	
AEA 14	7 [271]	9.5 [367]
V2100	-	54 [2089]
WRDA 35	35 [1354]	-
HRWR, Adva 100	169 [6537]	-

6.2 Pile Driving

Each 70-ft pile will be driven using a hydraulic hammer in the Savannah River, at Savannah, Georgia, where salinity and sulfate values match that of seawater. Pile driving force is to be determined by the pile driving contractor. Piles will be driven until refusal, defined as 10 blows per ½-in. (13 mm).

Pile driving will be closely observed with special attention to cracking. The form of cracking most prominent in pile driving is reflective cracking, where the compression wave reflects back up the pile in tension. This is typically caused by the transition of a layer of hard soil to a layer of soft soil, or soft soil to rock, or improper pile driving techniques. Due to the precompression on the piles, reflective cracks are typically hairline and difficult to detect. However, reflective cracking can be identified by a small cloud of powder that forms as the pile cracks. Cracks will be

mapped when possible to assess the pile performance during driving. Prior to driving, the piles will also be fit with a pile analyzer, which measures the stress wave and the strains in the pile due to impact, which will be used to detect cracks.

After driving, one 18-in. (46 cm) sq. 2205 pile and one 18-in. (46 cm) sq. 1080 pile will be pulled from the ground, sawn in half, and taken back to the Georgia Institute of Technology Structures Lab for flexural and shear testing. Prior to testing, these piles will be examined for cracking. The remainder of the piles will be left for long term monitoring of durability and prestress losses.

6.3 Flexural Behavior

6.3.1 Experimental Methods

Flexural testing will be performed on 35-ft. (10.7 m) long pile samples—previously driven 70-ft. (21.4 m) piles that will be cut in half. The choice to cut the piles in half was made to facilitate transportation, to provide two independent flexure tests, and to avoid high very large deflections. Two 18-in. (46 cm) sq. piles will be removed after driving and may be tested immediately, one with 2205 strand and one with 1080 strand. The remainder of the piles will be tested in flexure after 2 years. It is not expected that these piles will exhibit any significant deterioration over this term.

As shown in Figure 6.4, testing consists of 4-point bending; the pile will be simply supported at the ends, and load will be applied at midspan until failure. Midspan deflection will be measured continuously, and midspan curvature will be calculated from 2 opposing LVDT displacement gages placed longitudinally at the top and bottom of the vertical face of the pile at midspan. The piles will be loaded at a rate slow enough to avoid dynamic loading effects and to gather sufficient data.

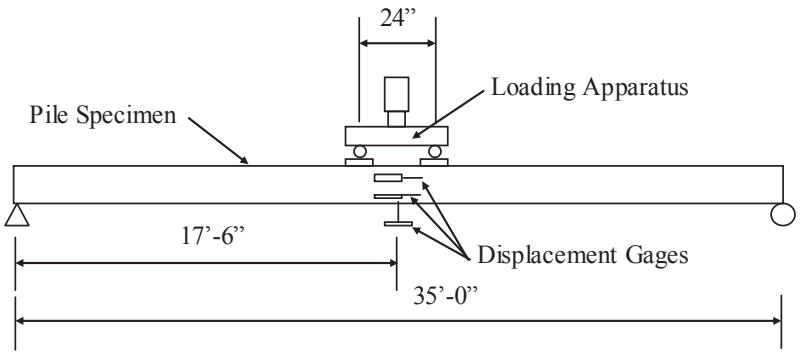

Figure 6.4 Flexural test apparatus

6.3.2 Moment-Curvature and Force-Displacement Curves

Moment-curvature behavior plots were created for each pile type. Moment and curvature calculations were made for cracking, yield, and ultimate conditions. The yield moment was defined as the moment corresponding to a strain in the bottom layer of strand of 1.0% for 1080 strand and 1.2% for 2205 and 2304 strands. This analysis was conducted for concrete compressive strengths of 5 ksi (34 MPa) and 10 ksi (69 MPa). This value may be changed based on the results of cylinder compression tests. Moment curvature diagrams are shown in Figures 6.5 and 6.6.

From the moment-curvature diagrams, force-displacement relationships were determined based on the flexure test configuration in Figure 6.4. These diagrams are shown in Figures 6.7 and 6.8, and the moment-curvature and load-displacement calculations are given in Appendix E. The load in the force-displacement diagrams refers to the overall load on the pile—i.e. the sum of both midspan point loads in the four-point bending setup.

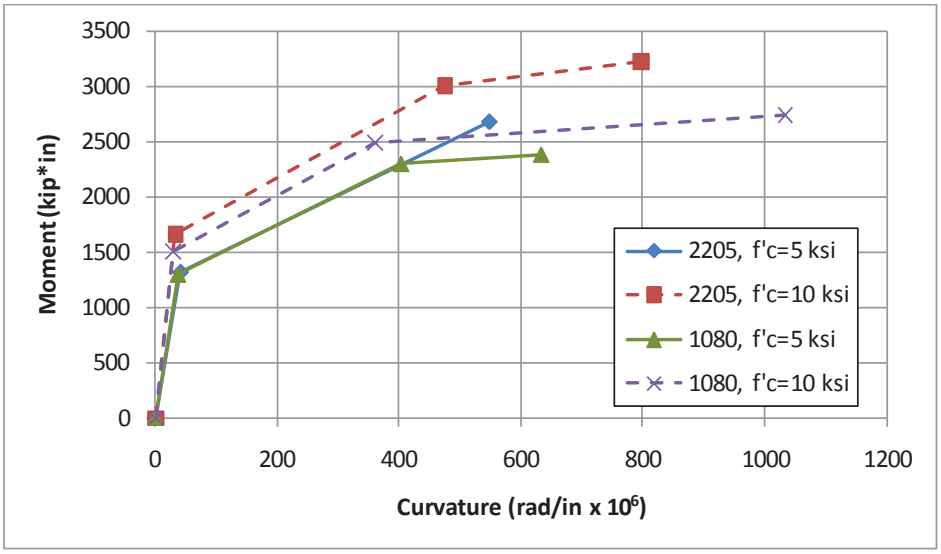

Figure 6.5 Moment-curvature relationships for 18-in. (46 cm) sq. piles

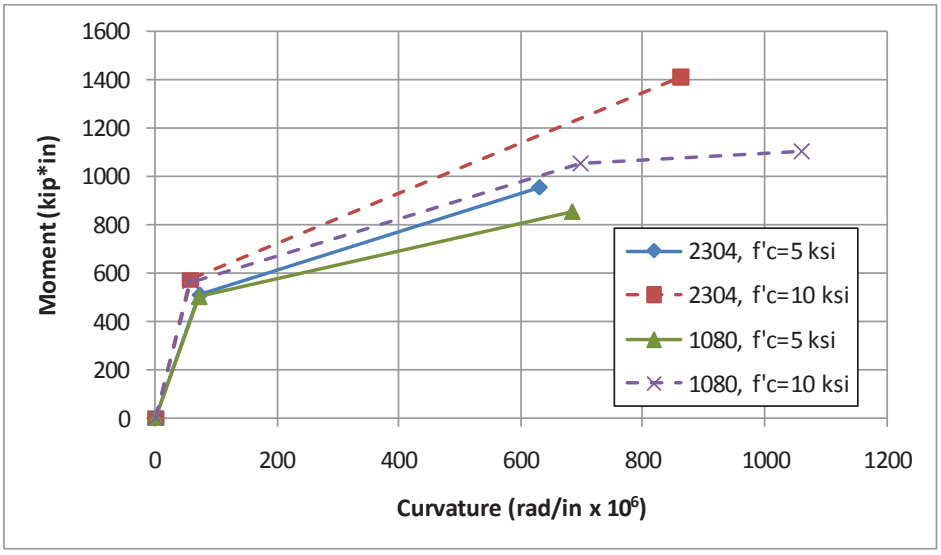

Figure 6.6 Moment-curvature relationships for 12-in. (30 cm) sq. piles

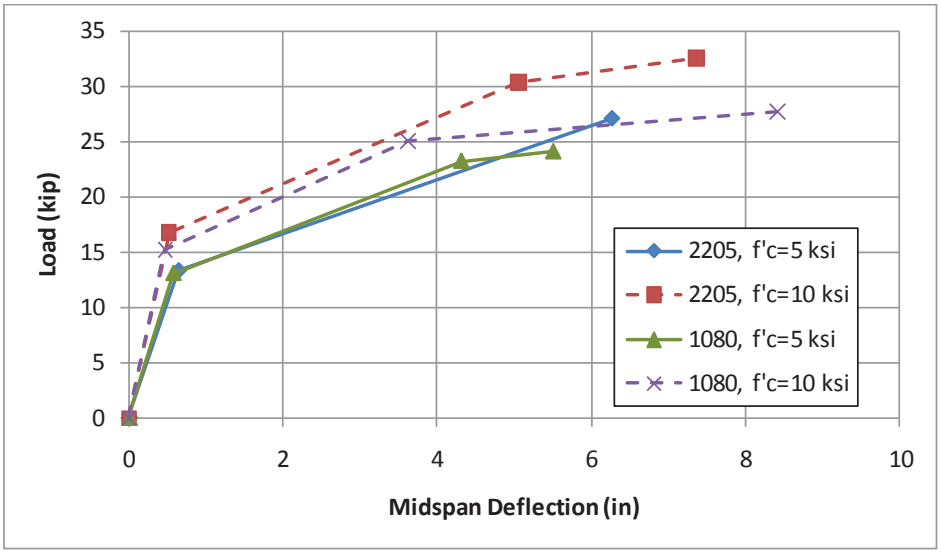

Figure 6.7 Load-displacement relationships for 18-in. (46 cm) sq. piles

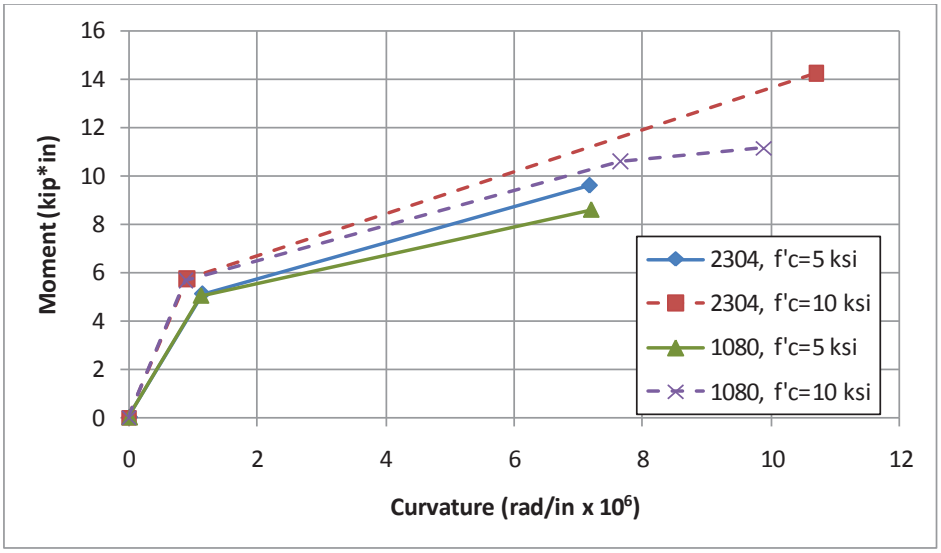

Figure 6.8 Load-displacement relationships for 12-in. (30 cm) sq. piles

With zero externally applied moment, curvature is also zero for all piles since the cross-sections are perfectly symmetric. The cracking moment was typically higher for HSSS piles since the initial prestressing force on these piles was higher than their 1080 counterparts. The stainless steel typically exceeded the strength of their 1080 counterparts because the increased cross-sectional area of strand allowed for higher force in the strand despite its decreased strength. Curvature in the ultimate condition was typically lower for piles reinforced with HSSS strand due to the increased force capacity in the strand. Ultimate displacements were typically comparable for analogous HSSS and 1080 strand piles, as the lower ultimate curvatures in the HSSS piles were offset by extra displacement due to their higher moment capacity.

Failure mode was characterized by crushing of the concrete in the compression zone for all piles with the exception of the 18-in. (46 cm) sq. pile with 2205 strand and 10 ksi (69 MPa) concrete compressive strength. Due to the smaller depth and lower initial strain due to prestressing, neither of the 12-in. (30 cm) sq. piles reached their yield point. The largest ultimate strains in piles reinforced with 2304 were 0.62% and 0.83% for 5 ksi (34 MPa) and 10 ksi (69 MPa) concrete, respectively. The only other pile that did not reach yield was the 12-in. (30 cm) sq. pile with 1080 strand and 5 ksi (34 MPa) concrete, which reached an ultimate strain of 0.91%. The 18-in. (46 cm) pile with 2205 strand and 5 ksi (34 MPa) concrete failed due to crushing of the compression zone of the concrete as the strand reaches its yield point of 1.2%. Since the ultimate strain of the stainless steel prestressing strand is a concern, the compressive strength of the concrete was manipulated in the calculations to find the minimum strength where failure is caused by strand rupture. It was found that failure would only be caused by strand rupture for strengths over 9 ksi (62 MPa) in the 2205 piles, and strand rupture would not occur for concrete strengths well over 20 ksi (138 MPa) in 2304 piles.

6.4 Shear Behavior

6.4.1 Experimental Methods

Shear testing will be performed on the end sections of the piles used for flexural testing and on the 10-ft (3 m) long 12-in. (30 cm) sq. pile samples. It is estimated that 6 to 8 ft. (1.8 to 2.4 m) of pile will remain uncracked at each end after the pile fails in flexure at midspan. These sections will be salvaged and a shorter span 3-point bending tests will be performed to induce shear failure of the piles, as shown in Figure 6.9. 3-point bending was chosen to provide a constant shear force in the piles as they are loaded. The span of the 3-point bending tests will be 3.0 times the depth of the pile, or 54-in. (138 cm) for 18-in. (46 cm) sq. piles, and 36-in. (90 cm) for 12-in. (30 cm) sq. piles), resulting in a shear span to depth ratio of 3 The ends of the pile will be simply supported and load will be applied monotonically until failure. Shear tests will be conducted in the region of the pile with either a 3-in. (76 mm) or 6-in. (152 mm) wire pitch, depending on the section to be tested.

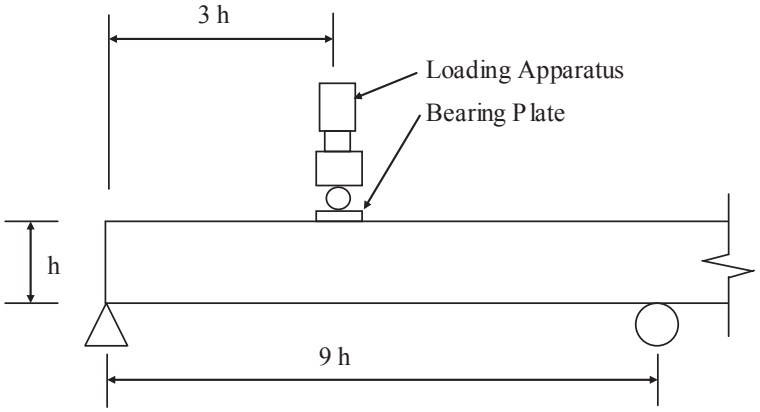

Figure 6.9 Shear test apparatus

6.4.2 Shear Capacity

Shear calculations were performed in accordance with ACI 318 Section 11.3.2. Flexure-shear (V_{ci}) and web-shear (V_{cw}) capacity of the pile were calculated according to equations 6.1 and 6.2.

$$V_{ci} = 0.6\lambda\sqrt{f'_c}\,b_w d_p + V_d + \frac{V_i M_{cre}}{M_{\max}} \tag{6.1}$$

Where:
λ = Lightweight concrete adjustment factor
f'_c = Compressive strength of concrete
b_w = Width of section
d_p = Depth of strand
V_d = Shear due to dead load
V_i = Shear force in pile
M_{cre} = Cracking moment
M_{max} = Moment in pile

$$V_{cw} = \left(3.5\lambda\sqrt{f'_c} + 0.3 f_{pc}\right) b_w d_p + V_p \tag{6.2}$$

Where:
f_{pc} = Precompression stress on the pile
V_p = Shear Resistance from prestressing strand

The contribution of steel reinforcement to the overall shear capacity (V_s) is given as:

$$V_s = \frac{A_v f_{yt} d_p}{s} \tag{6.3}$$

Where:
A_v = Area of shear reinforcement
f_{yt} = Yield strength of shear reinforcement
s = Spacing of shear reinforcement

Since all strands are perpendicular to the direction of the shear force, $V_p = 0$, and V_{cw} was a constant value along the entire length of the pile. V_{ci} was at a minimum at the midspan of the pile. The minimum value was taken since the shear force was constant along the length of the pile. V_d was assumed to be negligible due to the short span.

To calculate total shear capacity of the pile, the minimum value between these values was added to the shear capacity of the steel wire spiral. Since shear reinforcement and precompression stress were the same in stainless and carbon steel reinforced piles, the shear strength calculations were identical. The results of shear calculations are summarized in Table 6.2.

Table 6.2 Shear strength of pile specimens

Shear Strength		18-in. (46 cm) sq.	12-in. (30 cm) sq.
Min. V_{ci}, kip [kN]		74.5 [331]	39.1 [174]
V_{cw}, kip [kN]		94.0 [418]	41.8 [186]
V_s, kip [kN]	3-in. (76 mm) pitch	25.5 [113]	17.0 [76]
	6-in. (152 mm) pitch	12.8 [57]	8.5 [38]
V_n, kip [kN]	3-in. (76 mm) pitch	100.0 [445]	56.1 [250]
	6-in. (152 mm) pitch	87.3 [388]	47.6 [212]

6.5 Transfer and Development Length

6.5.1 Introduction

Transfer length (l_t) is defined according to the American Concrete Institute (ACI 318-11) as the "length of embedded pretensioned strand required to transfer the effective prestress to the concrete" The effective prestress (f_{se}) is the stress in the reinforcement after allowance for all prestress losses. Development length (l_d) is defined according to ACI as the "length of embedded reinforcement, including pretensioned strand, required to develop the design strength of reinforcement at a critical section". Flexural bond length in prestressed concrete is the difference between development length and transfer length. Figure 6.10 presents an idealized strand stress profile in a pretensioned element under applied load.

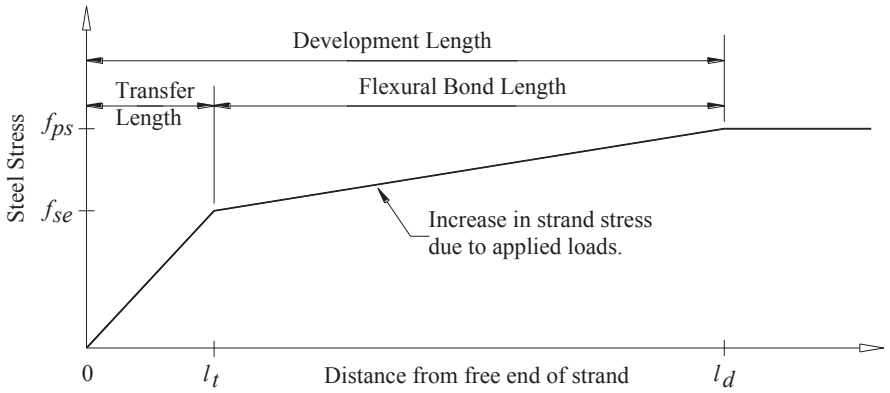

Figure 6.10 Idealized strand stress profile in a pretensioned element under applied load (from (Reutlinger, 1999))

The American Association of State Highway and Transportation Officials specifications (AASHTO LRFD) suggest the transfer length be taken as 60 times the strand diameter (60*d_b). Both the ACI and AASHTO codes suggest that the development length can be calculated from the following expression (units in kips, in):

$$l_d = \left(f_{ps} - \frac{2}{3} f_{se} \right) d_b \tag{6.4}$$

Where:
l_d = Development length (in.)
f_{ps} = Prestressing strand stress (ksi)
f_{se} = Prestressing strand stress after transfer (ksi)
d_b = Strand diameter (in)

As a corollary to Equation 6.4, transfer length may also be calculated as the length in which f_{ps} equals f_{se}, given in Equation 6.5.

$$l_d = \frac{f_{ps} d_b}{3} \tag{6.5}$$

6.5.2 Elements of Bond

In pretensioned concrete members, there are three primary mechanisms that allow for force transfer from the prestressing strand to the concrete, governing transfer and development length. These elements of bond are adhesion, Hoyer's effect, and mechanical interlocking (Russell 1992). Friction is not mentioned here as a separate mechanical process, but included as a component and contributor to both Hoyer's effect and mechanical interlocking. While these mechanisms are not easily quantified, a qualitative understanding of the mechanisms generating bond appears to sufficiently describe the anchorage and development of pretensioned strand.

6.5.2.1 Adhesion

Adhesion is the glue between the concrete and the steel. Adhesion effectively prevents displacement of the strand relative to the concrete until some critical stress is reached. At that critical stress, the glue fails and its resistance reduces to zero. This failure is always brittle. Because of this rigid-brittle behavior, adhesion contributes little or nothing to either prestress transfer bond or the bond developed to resist additional strand tension from applied loads. At transfer, the prestressing strands slip relative to the concrete. In fact, the transfer zone is characterized by strand slip. The transfer length is defined as the length from the free end of the strand to the point where the change in strand strain resulting from the prestress transfer equals the change in concrete strain—where there is no slip between the concrete and strand.

6.5.2.2 Hoyer's Effect

Hoyer's effect, also referred to as wedge action, results from lateral expansion of the strand at transfer. When steel is pretensioned, the diameter of the strand reduces by Poisson's ratio as the strand is elongated. Then, concrete is cast surrounding the strand. Upon release, the strands lose their initial prestress and expand laterally. When this lateral expansion is resisted by concrete surrounding the strand, a normal force is imposed at the boundary between concrete and steel. This normal force increases the frictional force between concrete and strand, restraining the strand and holding it in tension.

6.5.2.3 Mechanical Interlocking

When prestressing strand is cast in concrete, the concrete completely surrounds the strand, filling the narrow crevices, or interstices, between individual wires. If the strand attempts to pull through the concrete without twisting, movement is resisted by the concrete ridges acting on the outside wires of the strand. This resistance is called mechanical interlocking. If twisting is restrained, bond between strand and concrete behaves somewhat like pullout of mild reinforcement.

Mechanical interlocking is the largest contributor to flexural bond, especially in cracked regions. As a flexural crack forms, strand slip must occur for some small finite distance on either side of the crack to preserve compatibility of the strand. When slip occurs, mechanical interlocking is activated by the reaction of the outside wires interlocking with the concrete envelope.

6.5.3 Transfer Length: Experimental Methods

Transfer length testing will be performed on both ends of all 70-ft and 27-ft long specimens. This results in 4 tests on each 2205 and 1080 18-in. (46 cm) sq. piles, and 6 tests for each 2304 and 1080 12-in. (30 cm) sq. piles. Concrete surface strain (CSS) and end slip measurements will be used to calculate transfer length.

6.5.3.1 Concrete Surface Strain Measurements

In order to obtain the concrete surface strain, gage points will be embedded into the concrete section at the level of the prestressing strand. These gage points are located at each pile end. The concrete surface strain is measured using a detachable mechanical strain gage (DEMEC gage) which measures the change in distance of adjacent points. The DEMEC gage contains two conical points spaced a given distance apart; an 8-in gage length is used for these strain measurements. The points are inserted into cylindrical holes of embedded gage points.

Measurements will be taken prior to and after release in order to calculate the strain across each 8-in segment. These strains will then be plotted against the length from the end of the pile, and a bilinear curve will be fit to the data,

similar to Figure 6.11. Transfer length will be determined as the point where strains are no longer increasing along the length of the pile.

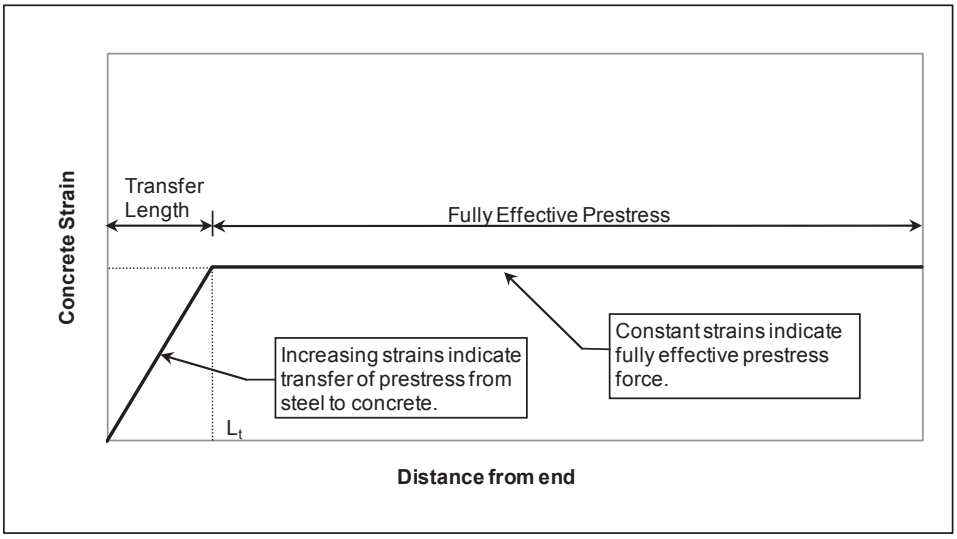

Figure 6.11 Sample idealized concrete surface strain profile for transfer length (from (Reutlinger, 1999))

Gage points will be placed across 8-ft. (2.4 m) on the ends. The first gage point will be 1-in. (25mm) from the end, and the remainder will be spaced at 2-in. (51 mm), a total of 48 points per end. Since there is no information on the transfer length of stainless steel prestressing strand, the 8-ft. (2.4 m) length was used because it is unlikely that the transfer length is out of this range. The two methods discussed above for estimating transfer length were used as a baseline for estimating the transfer length of stainless steel strand, summarized in Table 6.3. They will also be compared to the test results to determine if a special provision in ACI or AASHTO is required for transfer length of stainless steel strand.

Table 6.3 Estimated transfer lengths of each strand

Strand	Transfer Length, in [cm]	
	$l_t = 60\ d_b$	$l_t = f_{se} d_b / 3$
1080	26.3 [66.8]	27.6 [70.0]
2205	30.0 [76.2]	23.7 [60.2]
2304	30.0 [76.2]	17.3 [43.9]

The gage points consist of an 8-32 x 1-in. (25 mm) long machine screw and a corresponding ¼-in (6.4 mm) long threaded brass anchor, shown in Figure 7.12. Embedments are held in place on 2-in. (51 mm) wide x 3/16-in. (4.8 mm) thick steel flat bar embedment strips that are anchored in the formwork. Holes were drilled in the embedment strips at the location of each gage point, and then countersunk such that 8-32 x 3/16-in. (4.8 mm) slotted machine screws that hold the embedments flush on the opposite side. Embedment strips must be flush to keep concrete out of the gap between the strip and the form and to allow for easier removal of the strip. The embedment strips are held to the form by similar countersunk screws oriented in the opposite direction, spaced at 18-in. (46 cm) o.c. After the concrete sets and the forms are removed, each machine screw will be removed from the embedments, and the embedment strips will be removed. To facilitate easy removal of the steel bars, the corners on the concrete side of the strip are removed using an angle grinder. Details for the embedment setup are shown in Figure 6.13.

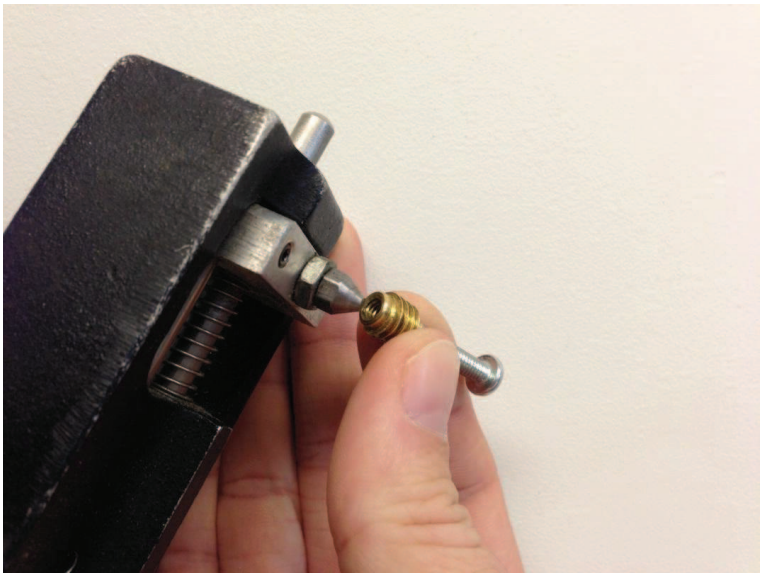

Figure 6.12 DEMEC gage and CSS gage point

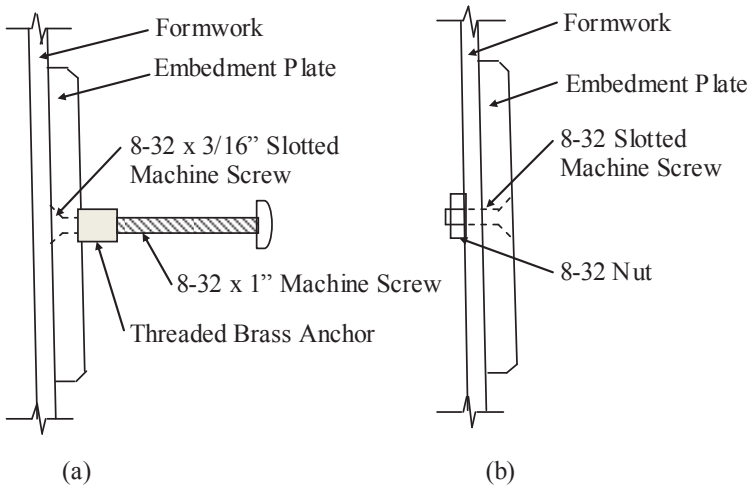

Figure 6.13 Embedment connection details for (a) embedment to embedment plate and (b) embedment plate to formwork

6.5.3.2 End-Slip Measurements

End slip measurements will also be used to estimate the development length of the strand. A pipe clamp will be placed on each strand 1-2-in. (25-51 mm) from the face of the pile prior to the strand release. An exact measurement from the face of the pile to the edge of the pipe clamp will be taken using calipers and recorded. After release, the measurement will be taken again. Assuming a linear variation in strand stress through the transfer length of the pile, development length can be estimated from the difference in these two readings using the equation:

$$\Delta = PL / AE = fL / E = f_{si,avg} l_t / E_{ps} \quad (6.6)$$

Where:
Δ = Measured end slip (in)
$f_{si,avg}$ = Average initial strand stress over the transfer length after release of prestress (ksi)
l_t = Transfer length (in)
E_{ps} = Elastic modulus of prestressing strand (ksi)

Assuming linear increase in stress over the transfer length and zero stress at the pile face, the equation may be rewritten as:

$$l_t = \frac{\Delta \cdot E_{ps}}{\frac{1}{2} \cdot f_{si}} \quad (6.7)$$

Where:
f_{si} = Initial strand stress after release of prestress

6.5.4 Development Length Experimental Methods

Development length testing will be performed on 27-ft long 12-in. (30 cm) sq. pile samples. Two piles of this size will be cast using each 2304 and 1080 steel strand. Due to their similar metallurgy, it is assumed that 2205 and 2304 will exhibit similar development length behavior.

Preliminary development length calculations were performed using Equation 6.4. This equation predicts a development length of 95.3-in for 2304 strand, and 63.0-in for 1080 strand. 2304 strand exhibits a higher development

length due to its increased diameter and decreased initial prestress. The equation also predicts a development length of 64.5-in for the 2205 strands, although this strand will not be tested.

In order to properly test development length, the strands in the tension face of the pile must be developed near their ultimate strength in a 3-point bending test. This means 2% strain is required for the developed strand, or rupture if the ultimate strain in the strand is less than 2%, which is the case for 2205 and 2304 strand. Based on moment-curvature calculations and discussed in Section 6.3.2, 12-in. (30 cm) sq. piles are not deep enough to induce these high strains in the strands. As a result, a concrete topping will be placed in the laboratory to increase the moment capacity of the concrete and to induce high strains or rupture in the strands. Shear reinforcement (2-leg #5 bars at 6-in. (152 mm). o.c.) will be placed in the 27-ft. (8.2 m) piles when the piles are cast and the top surface will be roughened to develop a good bond to the concrete topping. The topping will be 30-in. (76 cm) deep with a 24-in. (61 cm) wide flange to further increase the moment capacity of the section. The cross section of the composite section is shown in Figure 6.13. Related calculations are given in Appendix F.

Each 27-ft. (8.2 m) long pile will be tested twice for development length—once at each end. The pile will be supported by a pin at the end and a roller 18-ft. (5.5 m) along the section, shown in Figure 6.14. This maintains the outer third of the pile for the next test. A point load will be placed first at a distance equal to the predicted embedment length from the end of the pile and adjusted for later tests. Manipulating the point load changes the embedment length, the bonded length of strand from the beginning of the bond to the critical (maximum moment) section. When the embedment length is longer than the development length, a flexural failure (either crushing of concrete or strand rupture) is expected. When the embedment length is shorter than the development length, a shear/bond (S/bond) failure will occur. The location of the point load for the 2^{nd} to 4^{th} tests will be determined based on the results of the previous tests. The development length will be the shortest embedment length tested that exhibits flexural failure. Development length tests will be instrumented with two LVDT displacement gages to measure curvature under the point load. The strain in the strand will also be determined throughout the test using CSS measurements with DEMEC gage points.

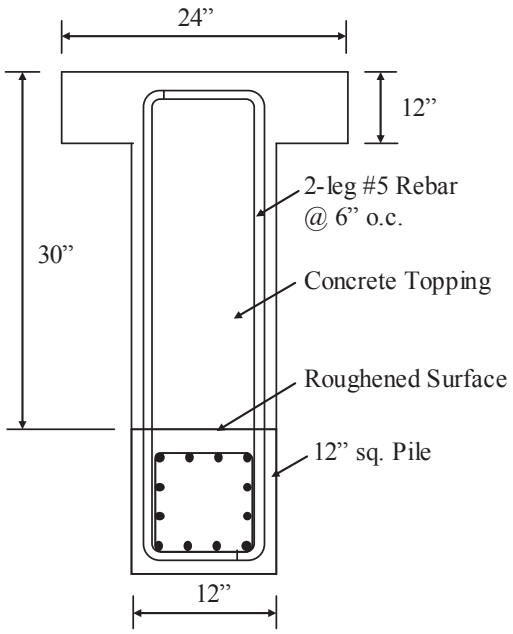

Figure 6.14 Concrete topping for development length testing

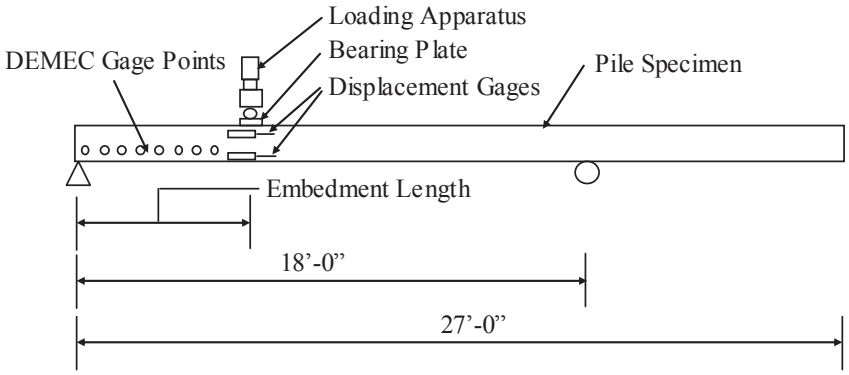

6.15 Development length test apparatus

6.6 Long-Term Prestressing Losses

One 70-ft. (21 m) pile of each of each type will be driven and left in place in the Savannah River for 2 years. Geokon Model 4200 vibrating wire strain gages were selected for their durability and will be placed at each quarter point of each pile to be left for long term testing, shown in Figure 6.15. Two strain gages will be zip-tied to the top and bottom strands at each quarter point for a total of 4 strain gages per pile. The strain gages will be applied to the strands after tensioning and monitored before and after release of the strand to capture elastic shortening. The gages will also be read before and after driving, and periodically over the next 2 years. Readings will be taken using a vibrating wire readout box. The strain gages measure internal strain in the concrete at the level of the strand; a decrease in compressive strain corresponds to loss. The modulus of the steel strand will be used to determine the stress lost from the strain data.

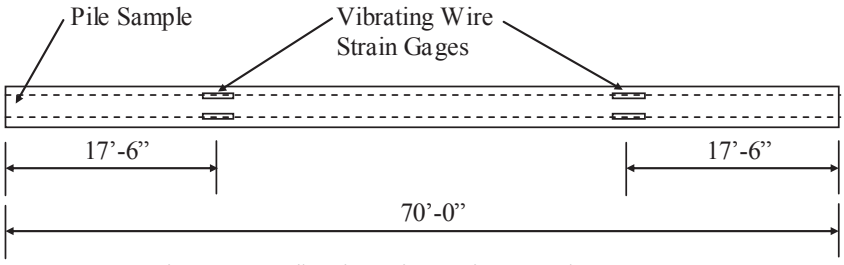

Figure 6.16 Vibrating wire strain gage placement

6.7 Durability

The 20-in. (51 cm) long samples of each pile type will be cast for the purpose of providing samples for long term study of concrete durability. These samples will be placed in the Savannah River to be brought to the surface periodically during the study period so that core samples may be taken for durability testing. Testing will be performed

on 3-in. (76 mm) diameter core samples to determine the degree of carbonation and depth of chloride and sulfate ingress.

To expose the strand in two faces of the concrete, foam blocks will be placed in the formwork on the sides of the strand in the area between the strand and the form, shown in Figure 6.16. This will create a zero cover situation, and the performance of the strand and shear reinforcement in a situation in which the concrete cover is compromised can be examined. This reduced cover mimics the carbonation of cover over a 35 year period.

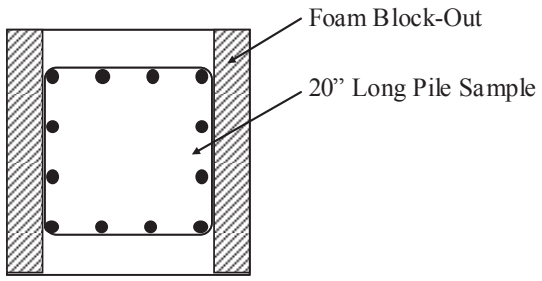

Figure 6.17 Material durability sample design

To place the samples into and lift the samples out of the river, a rebar lift loop will be placed at the center of each specimen. To avoid galvanic effects, stainless steel rebar will be used for stainless steel reinforced samples. A buoy will be tied to each rebar lift loop to locate the sample and raise it to the surface.

CHAPTER 7

CONCLUSIONS, RECOMMENDATIONS, AND FUTURE RESEARCH

7.1 Conclusions

The primary goal of this research was to advance the development of corrosion mitigation techniques for implementation in prestressed concrete (PSC) bridge substructures along the coastline. Specifically, corrosion resistant high strength stainless steel (HSSS) prestressing strands were produced based on the recommendations by Moser (2011). Two varieties of duplex stainless steel prestressing strand (grades 2205 and 2304) were produced using similar practices for the production of high carbon grade 1080 prestressing strand. The scope of this testing program involved characterization of the mechanical properties of the HSSS strands through tensile and stress relaxation testing. A future test program was also designed to determine the behavior of HSSS strand in bridge piles. The conclusions from this investigation are presented in the following sections.

7.1.1 Stress vs. Strain Behavior

HSSS strands were tested in tension using a universal testing machine in order to characterize stress vs. strain behavior. To determine the effects of cold drawing and thermomechanical treatment, additional tensile tests were performed on samples taken during strand production, including wire samples from the wire rod, #3, #5, and #7 dies, along with the center wire of the strand which received thermomechanical treatment.

1. 2205 and 2304 duplex stainless steels can both be used to create strands that achieve strengths comparable to strand currently in practice. The 2205 and 2304 strands exhibited ultimate strengths of 242 and 261 ksi (1670 and 1800 MPa), respectively.
2. Ultimate strain of the stainless steels is greatly diminished with reduction of area by cold drawing. Yielding of the strand was immediately followed by necking failure, and no general plastic deformation or strain hardening throughout the specimen was observed. Ultimate strains of the 2205 and 2304 stainless steel strands were 1.60% and 1.87% which equaled approximately 30% of the ultimate strain of 1080 strand.
3. The 2205 and 2304 strands exhibited elastic moduli of 23500 ksi (162 GPa) and 24100 ksi (166 GPa) which was approximately 18-20% lower than 1080 strand due to the presence of austenite in the microstructure.
4. The 2304 strand failed in the pretensioning chucks due to notch sensitivity at 62% UTS, and as a result may only be effectively stressed to around 40 % UTS in practice.

7.1.2 Stress Relaxation Behavior

Stress relaxation testing was performed on 2205 and 2304 strands, as well as on center wires before and after heat treatment.

1. The 2205 strand can be classified as low relaxation prestressing strand as defined in ASTM A416, i.e. less than 2.5% relaxation loss at 1000 hr when initially stressed to 70% UTS and less than 3.5% loss at 1000 hr when initially stressed to 80% UTS.

2. The 2304 strand could not be stressed to the levels specified by ASTM A416, but underwent approximately 2.1% loss over 1000 hr when initially stressed to 40% UTS.
3. While strand and wire relaxation tests yielded similar average results (within one standard deviation) on 2205 strand and the center wire of 2205 strand, a high standard deviation in the wire relaxation testing warrants further testing to develop a larger sample size.
4. When stressed to 70% of its UTS, 2205 wire that had not received heat treatment relaxed 10.44% over 1000 hours, while 2205 wire which had received a low-relaxation heat treatment relaxed 2.67% over the same time period, a difference of 7.77%.
5. When stressed to70% of its UTS, 2304 wire that had not received heat treatment relaxed 3.88%, while 2304 wire which had received low-relaxation treatment relaxed -1.79% over 1000 hours, a difference of 5.67%. The increase in stress over time in heat-treated 2304 wire and the downward curvature in untreated 2304 wire may be attributed to phase transformation in the steel, although further research is necessary.

7.1.3 General Conclusions

Corrosion resistant duplex stainless steels may be used to produce prestressing strand with adequate mechanical properties to be effectively used in PSC bridge substructures. While grade 2304 steel was originally produced as a low-cost alternative to 2205, the notch sensitivity of 2304 necessitates a lower initial prestressing force per

strand. Therefore, 2205 is both the more corrosion resistant and cost effective option per unit of initial prestressing force.

7.2 Recommendations

7.2.1 Implementation in Coastal Bridges

Based on the mechanical properties alone, it is clear that piles may be designed with 2205 strand to match the structural performance of the current standard precast, prestressed concrete piles. A slight increase in the area of prestressing strand may make up for the 10% reduction in ultimate strength associated with 2205 strand compared to conventional 270 ksi (1861 MPa) strand. While the ultimate strain of 2205 strand is only 40% of that of A416 strand, there is little demand for strand elongation in bridge piles. As presented in Section 6.3.2, rupture of the strand due to flexure may only become a concern for piles greater than 18-in. (46 cm) constructed with high strength concrete mixes.

It is recommended that a test bridge be constructed using piles reinforced with 2205 strand and detailed similar to the piles presented in Chapter 6. While the test program presented in Chapter 6 will provide valuable information about the behavior of HSSS prestressing strand in piles, the mechanical and stress relaxation properties presented herein are sufficient to warrant the construction of a test bridge. The piles should be monitored during construction and during the service life of the bridge to monitor their structural behavior and durability. Given the results of the first bridge, full

scale implementation is feasible for new bridges that are deemed to require special corrosion resistance.

7.2.2 Standards for HSSS Prestressing Strand

To facilitate the implementation of HSSS prestressing strand on a larger scale, it is recommended that certain standards be set to govern the mechanical properties of HSSS strand. ASTM A416 may be amended to include provisions for stainless steel strand to facilitate the mechanical properties of HSSS strand determined in this study. The only special considerations to be made for HSSS strand are the following:

1. Minimum ultimate tensile strength of 240 ksi (1650 MPa).
2. Minimum ultimate strain of 1.5% provided the strand is utilized in a member to be loaded primarily in compression.
3. The yield point may be determined as the stress corresponding to a strain of 1.2% or using the 0.2% offset method.

In this study, HSSS strand was shown to satisfy the provisions in ASTM A416 for low relaxation strand, and no special considerations would need to be made for the stress relaxation of HSSS strand.

7.3 Future Research

While this study has addressed many of the issues concerning the use of HSSS prestressing strand in PSC construction, more information is required prior to the full scale implementation of HSSS strand in bridge substructures. Further studies may also be

warranted to optimize the design of members with HSSS strand. Some of these key topics are listed below:

1. Prior to the implementation of HSSS prestressing strand in bridge substructures, it is necessary to determine its behavior in test piles. Using the test procedures outlined in Chapter 6, driving performance, transfer and development length, flexural and shear performance, prestress losses, and durability must be properly evaluated in order to properly design using HSSS prestressing reinforcement.
2. More investigation is necessary to streamline and optimize the production of HSSS strand if the strand is to be produced on a larger scale. This includes researching the most efficient means of limiting die blow-outs and thermally treating the strand. Production techniques that may improve the mechanical behavior of the HSSS strands (specifically, increasing ultimate strain and ultimate strength) should also be investigated. Furthermore, it is necessary to devise a means to set the geometry of HSSS strand during production, so that they will not tend to unwind during construction.
3. Further studies are required to explain the stress relaxation results of 2304 wire, particularly the non-logarithmic behavior of the untreated wires and the negative relaxation trend noticed in some of the heat treated samples. Metallography and X-ray diffraction testing is warranted to determine if a phase change occurred during relaxation, which may explain this behavior.
4. New stainless steels are constantly being developed for a wide variety of applications. Since 2304 is not a viable low cost alternative to 2205, it is desirable to develop another cost effective option for bridge substructures in less severe

environments that do not require the corrosion resistance of 2205. In particular, lean duplex grade 2003 stainless steel has shown promising corrosion resistance and mechanical behavior. While it does not provide the corrosion resistance of 2205, 2003 stainless steel has been shown to have similar mechanical properties and good corrosion resistance due to its relatively high Molybdenum proportion of 1.5 to 2.0 wt% (Allegheny, 2012).

5. GDOT standard pile sizes were designed using $^{7}/_{16}$–in. (11 mm) A416 Grade 270 prestressing strand. Further studies into the optimal strand diameter and arrangement may be desired to design efficient, analogous standard piles with HSSS strand. In addition to taking into account the HSSS mechanical properties in new design, other design considerations used to limit the corrosion of steel reinforcement (i.e. minimum cover distance, maximum crack size, and concrete quality) may be relaxed to allow for a more efficient and cost effective pile design.
6. The overall failure mode associated with flexural failure due to strand rupture at low strains must be assessed to determine the necessary resistance factors for design using HSSS strand. Although strands initially stressed to around 70% UTS will meet the minimum net strain of 0.5% prior to failure for flexural safety factors of 0.9 (ACI 318) and 1.0 (AASHTO LRFD), the strand's low ultimate strain will lead to rupture soon after this limit is reached.

APPENDIX A

STRAND GRIP METHODS

A.1 Wet Sand Grips

Due to the size and configuration of the 7-wire strand, standard wedge grips were not adequate for tensile testing. Other methods were required to provide a more uniform grip and avoid large stress concentrations, excessive slippage, and failure in the grip.

The first method used was a simple wet sand grip. First, 1" flange aluminum angles were cut to 8" lengths, placed in the wedge grips, and hammered to contour. Sand was then saturated with water, and a layer was spread over the inside surface of the aluminum angle. Two angles were then placed around the strand near each end and zip-tied in place. The corners of the angles were then fit into the wedge grips in the testing machine and the tensile test was performed. The grips are shown in Figures A.1 and A.2.

Figure A.1 Wet sand grip in universal testing machine

Figure A.2 Wet sand grip

A.2 Expansive Cement Grips

The wet sand grip method typically produced a fracture of every wire, just outside of the grip face when testing the 2205 strand. This signified a pure tension failure that was unaffected by the grips. When the 2304 strand was tested using the same method, failure was usually due to the fracture of a single wire located in the grip and occurred before the stress level in the strand was able to reach its ultimate strength. The wet sand grips were not able to transfer force very evenly around the circumference of the strand, and the 2304 strand failed in this manner because of its notch sensitivity. New grip

methods were required to reduce the stress concentrations in the grips and induce tension failure in the 2304 strand.

To provide a more uniform grip around the strand, expansive cement, commonly used for demolition of rock formations, was confined in an extra heavy steel pipe (1 $^{3}/_{4}$-in. inner diameter, ½-in. wall) to provide a high normal pressure on the strand. 1-ft. long pipe sections were set at the top and bottom of each strand specimen and held there by a wooden stand, as shown in Figure A.3. The bottoms of each pipe were plugged using rubber stoppers and each pipe was filled with expansive grout and allowed to set for 3 days prior to testing. The expansive cement was mixed with water to provide a water to cement ratio of 0.30, per manufacturer recommendations. Figure A.4 shows the final expansive cement grips as placed in the testing machine.

Figure A.3 Placement of expansive cement grips

Figure A.4 Expansive cement grip in universal testing machine

Expansive cement is commonly used to demolish rock formations; holes are pre-bored into the rock formations and filled with expansive grout. The grout sets and expands, exerting an outward pressure on the bore holes and fracturing the rock along the bore holes. Because of this, the expansion capacity of the cement was given by the manufacturer as a radial pressure, based on the set time, water to cement ratio, temperature, and hole diameter. These factors were used to determine the pressures exerted on the strand and inner face of the pipe (9.78 ksi and 5.96 ksi). The capacity of the grip was based on the static friction between the cement and strand, as shown in the appended calculations; mechanical interlocking was not considered. It was determined that the expansive cement grips have a capacity of 10.2 kips per inch for ½-in. strand. While only 42 kips of capacity were required of the grips, 12-in. grips were used to

assure tensile failure. It was also noticed that the ends of each grip are weaker due to drying while the grout sets, and the extra length helped to account for this effect.

Expansive Cement Grip Calculations

$v_s := .3$ $v_c := .15$

$E_s := 29000\text{ksi}$ $E_c := 2000\text{ksi}$

a: inner radius of steel tube
b: outer radius of steel tube
c: radius of strand

$a := .875\text{in}$ $b := 1.375\text{in}$ $c := .25\text{in}$

radial flexibility of steel tube to outward pressure:

$F_s := \frac{a}{E_s} \cdot \left(\frac{a^2 + b^2}{b^2 - a^2} + v_s \right) = 8.029 \times 10^{-5} \cdot \frac{\text{in}}{\text{ksi}}$ increase in radius at inside face per unit pressure at inside face

radial flexibility of concrete cylinder

$F_c := \frac{a}{E_c} \cdot (1 - v_c) = 3.719 \times 10^{-4} \cdot \frac{\text{in}}{\text{ksi}}$

$p := 50\text{MPa} = 7.252 \cdot \text{ksi}$ pressure exerted due to expansion, from manufacturer

$p_1 := \frac{2a^2}{(1 - v_c) \cdot c^2 + (1 + v_c) \cdot a^2} \cdot p = 11.894 \cdot \text{ksi}$ pressure at face of strand for fully confined cement

$d_2 := p \cdot \left(\frac{1}{\frac{1}{F_c} + \frac{1}{F_s}} \right) = 4.789 \times 10^{-4} \cdot \text{in}$ displacement when 50 MPa acts outward on the steel+cement

$p'_2 := \frac{d_2}{F_c} = 1.288 \cdot \text{ksi}$ pressure at the face of the concrete corresponding to d2

$p_2 := \frac{2a^2}{(1 - v_c) \cdot c^2 + (1 + v_c) \cdot a^2} \cdot p'_2 = 2.112 \cdot \text{ksi}$ pressure at face of strand corresponding to d2

$p_{tot} := p_1 - p_2 = 9.782 \cdot \text{ksi}$ final pressure at face of strand

$L := 10in$ assumed cement is effective from 1" on either end

$\mu := .5$ steel on concrete

Assume contact area of outer 2/3 of 6 outside wires (strand perimeter)

$C := 6 \cdot \frac{2}{3} \cdot \pi \cdot .167in = 2.099 \cdot in$ $A := C \cdot L = 20.986 \cdot in^2$

$P := p_{tot} \cdot A \cdot \mu = 102.644 \cdot kip$ 42 kip required

Friction calculation at face of steel pipe

$C_{pipe} := \pi \cdot a \cdot 2 = 5.498 \cdot in$ $A_{pipe} := C_{pipe} \cdot L = 54.978 \cdot in^2$

$p_{pipeface} := p - p'_2 = 5.964 \cdot ksi$

$F_{pipe} := A_{pipe} \cdot p_{pipeface} \cdot \mu = 163.948 \cdot kip$ >42 kip

Force per inch of grip:

$\frac{P}{L} = 10.264 \cdot \frac{kip}{in}$

APPENDIX B

STRESS-STRAIN CURVE FORMULATION

With the extensometer in place, the load on the strand was taken to approximately 10% UTS and the string potentiometer was attached to measure crosshead displacement. This small load was first applied to seat the grips and straighten the strand in order to limit the required travel of the string potentiometer, which could only extend 2.5-in. Load was then increased to 80% UTS and decreased to 50% UTS at which point the extensometer was removed. This was done not only for safety reasons, but also to calculate the gage length of the strand corresponding to crosshead displacement. After the extensometer was removed, the specimen was loaded until failure.

Load, extensometer displacements, and string potentiometer displacements were recorded at 2 second increments. The Baldwin universal testing machine in which these tests were performed does not support electronic readouts, but a linear variable displacement transformer (LVDT) was attached to the mechanism that controls the dial load readout. Since the displacements in the mechanism vary linearly with applied load, the LVDT readout was calibrated against an Interface load cell and used to read load for these tensile tests.

Load measurements were zeroed at the start of the test and divided by the individual strand area to generate the stress in the strand at each time increment. No adjustments were made to any of the stress readings.

The measured displacement from the extensometer was also zeroed and divided by its gage length of 24-in. In some tests, the strain measured by the extensometer was

shown to drift when the stress was held at 10% UTS as the string potentiometer was being attached. This is possibly due to slipping of the extensometer caused by working in close proximity to it. In order to account for this, the portion of the stress-strain curve above 10% UTS was shifted by the amount that strain had drifted as shown in Figure B.1.

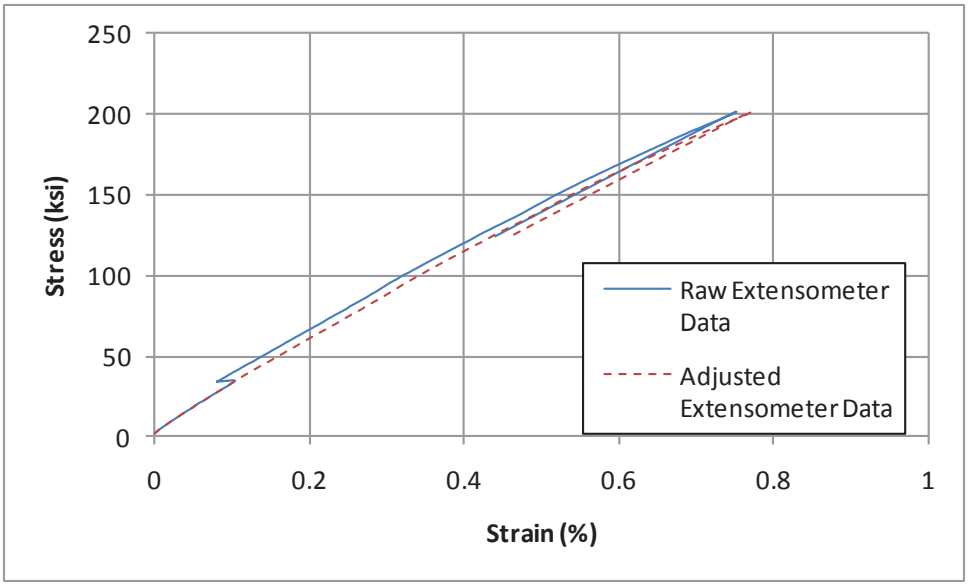

Figure B.1 Adjusted extensometer data

In order to calculate strain measurements from crosshead displacement data, the overall gage length of the strand needed to be determined first. This was accomplished by dividing the crosshead data by a gage factor and adjusting the gage factor until the slope of both curves along a given segment read the same value. However, it was seen that the crosshead data yielded different modulus results in the elastic range and when the strand was unloaded. It was assumed that this was due to slipping in the grips, and that slipping only occurred in "virgin tension" regions—i.e. unloading and reloading paths had zero

slipping, and the displacement recorded in this region was due solely to the strain in the strand. This assumption is supported by the fact that these segments were steeper that the rest of the curve and roughly coincidental with each other on the stress-strain curve. For this reason, the unloading segment was used to calculate the gage length for strain calculations. Crosshead displacements for virgin tension regions can be described by the relationship:

$$\Delta_{CH} = \Delta_{strand} + \Delta_{slip} \qquad \text{B.1}$$

Where:
Δ_{CH} = Total measured crosshead displacement
Δ_{strand} = Crosshead displacement due to elongation of the strand
Δ_{slip} = Crosshead displacement due to slippage

Similarly, the change in apparent strain due to each component between data points can be calculated by dividing by the gage length and taking the difference between data points:

$$\Delta\varepsilon_{CH} = \Delta\varepsilon_{strand} + \Delta\varepsilon_{slip} \qquad \text{B.2}$$

Where:
$\Delta\varepsilon_{CH}$ = Change in apparent strain from measured crosshead displacement
$\Delta\varepsilon_{strand}$ = Change in strain in the strand
$\Delta\varepsilon_{slip}$ = Change in apparent strain caused by slippage

Since ε_{strand} was known from extensometer data for the first portion of the curve, and ε_{CH} was also calculated from crosshead displacement data, Equation B.3 can be reordered to solve for ε_{slip} for this section as:

$$\Delta\varepsilon_{slip} = \Delta\varepsilon_{CH} - \Delta\varepsilon_{strand} \quad \text{B.3}$$

In order to correct the rest of the crosshead strain data for slipping, an assumption was made that displacement due to slip is directly correlated with the increase in force applied to the strand. This assumption was made by comparing the stress-strain data within the elastic range as calculated by crosshead displacement and extensometer. Since both curves were approximately linear in this region, their difference, which corresponds to total apparent strain caused by slippage, was also linear. A linear correction factor was introduced to account for the change in ε_{slip} with respect to the change in stress in the strand between data points, or:

$$\Delta\varepsilon_{slip} = K\Delta\sigma \quad \text{B.4}$$

Where:
K = Linear correction factor for apparent strain due to slip
$\Delta\sigma$ = Change in stress in the strand

Substituting this into equation B.3, the equation becomes:

$$K\Delta\sigma = \Delta\varepsilon_{CH} - \Delta\varepsilon_{strand} \quad \text{B.5}$$

By dividing both sides by $\Delta\sigma$ the equation for the correction factor becomes:

$$K = \frac{\Delta\varepsilon_{CH}}{\Delta\sigma} - \frac{\Delta\varepsilon_{strand}}{\Delta\sigma} \quad \text{B.6}$$

Since the correction factor is not dependent on strain in the strand, the same value applies for the linear range as the nonlinear range. By restricting Equation B.6 to the linear range, the following equation for K was obtained:

$$K = \frac{1}{E_{CH}} - \frac{1}{E_{strand}} \qquad \text{B.7}$$

Where:
E_{CH} = Apparent elastic modulus due to crosshead displacement data in virgin tension zones
E_{strand} = Elastic modulus of the strand calculated from extensometer data

Where extensometer data was not available, the strain between data points was calculated using the following relationship:

$$\Delta\varepsilon_{strand} = \Delta\varepsilon_{CH} - K\Delta\sigma \qquad \text{B.8}$$

A smooth curve was generated by eliminating the unloading and reloading portions of the curves and matching the portion of the curve calculated from extensometer data with the segment generated from crosshead displacement data at the point where the strand was begun to be unloaded (stress level of 80% UTS). This correction provided a smooth curve and matched very well with extensometer data for strands tested using expansive cement grips, but provided a rougher estimate for tests conducted using sand grips. Slippage occurred at a higher rate and more randomly than tests performed with expansive cement grips. Figures B.2 and B.3 provide examples of this corrected data for both types of grip.

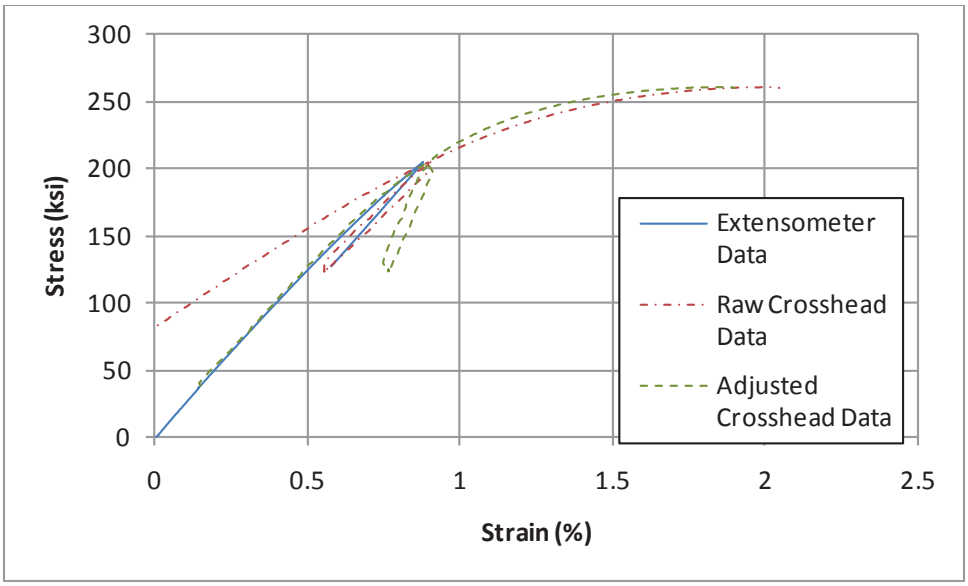

Figure B.2 Corrected crosshead position data for tests conducted using expansive cement grips

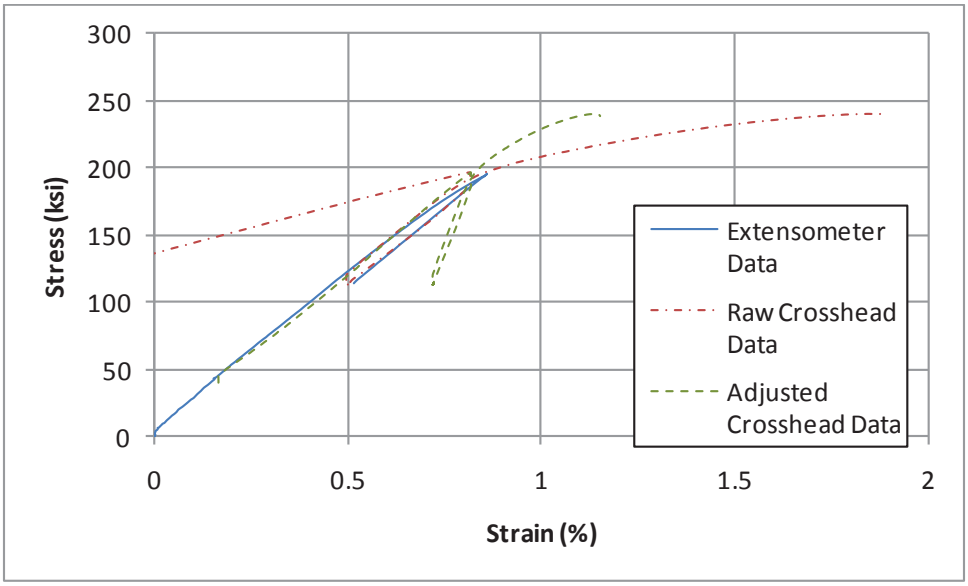

Figure B.3 Corrected crosshead position data for tests conducted using wet sand grips

APPENDIX C

STRESS-STRAIN RESULTS

C.1 Strand Testing

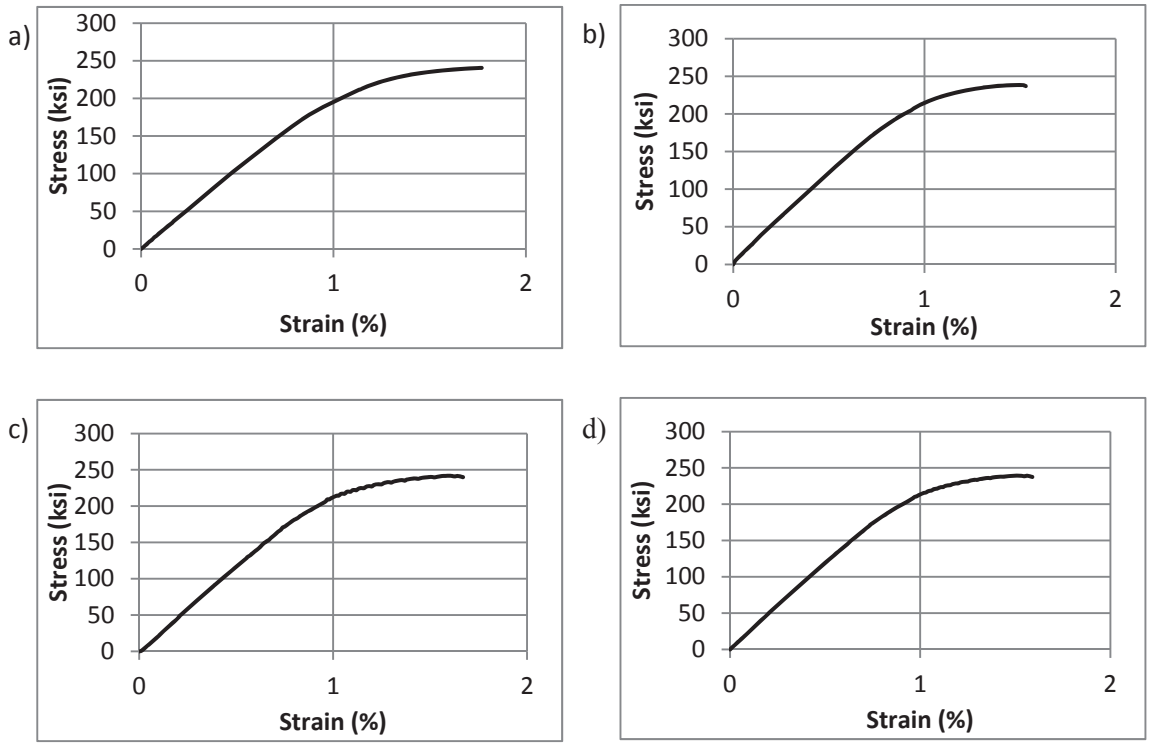

Figure C.1 2205 strand stress-strain curves for a) test 1, b) test 2, c) test 3, and d) average

Table C.1 Mechanical properties of 2205 strand

Test	fy – 0.2% Offset (ksi)	fy – 1% (ksi)	UTS (ksi)	Ultimate Strain (%)	E (ksi)
1*	223.5	197.1	242.8	1.77	21400
2	231.0	216.2	239.9	1.53	23300
3	226.3	213.3	243.1	1.67	23700
Average	228.7	214.8	241.5	1.60	23500

*Test not included in average calculations.

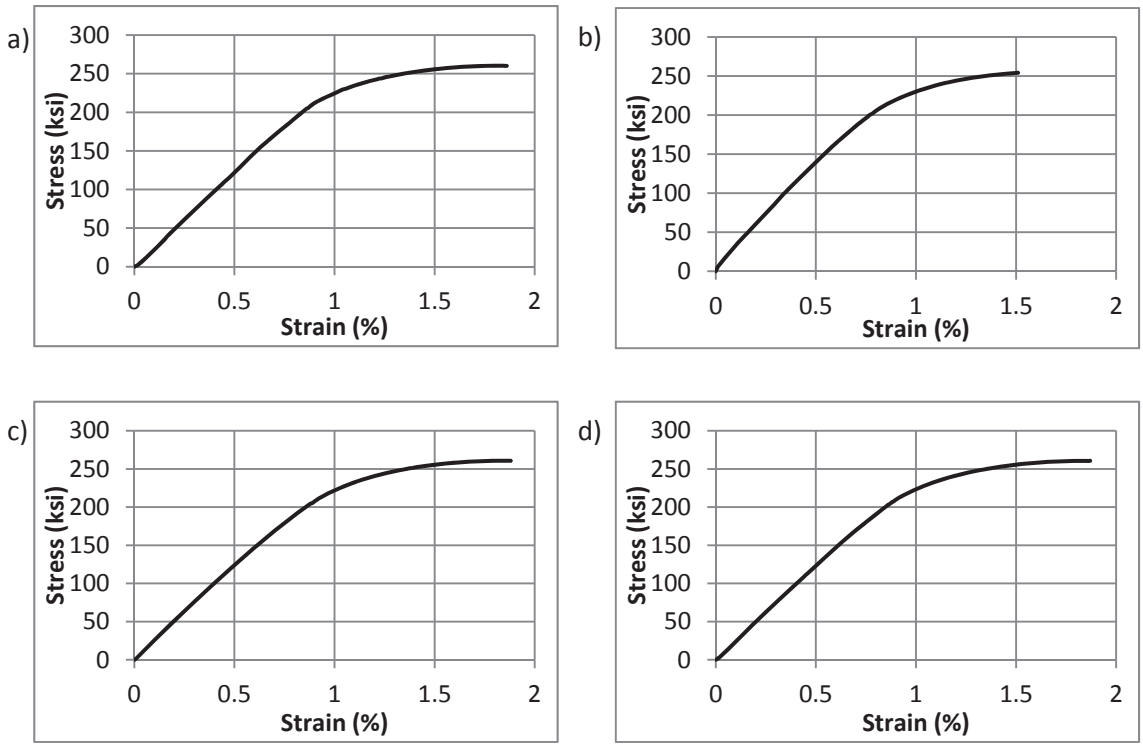

Figure C.2 2304 strand stress-strain curves for a) test 1, b) test 2, c) test 3, and d) average

Table C.2 Mechanical properties of 2304 strand

Test	f_y – 0.2% Offset (ksi)	f_y – 1% (ksi)	UTS (ksi)	Ultimate Strain (%)	E (ksi)
1	241.7	224.7	260.3	1.87	24400
2*	235.2	230.4	254.5	1.54	27700
3	242.2	222.3	260.8	1.88	23800
Average	242.0	223.5	260.6	1.87	24100

*Test not included in average calculations.

C.2 Wire Testing

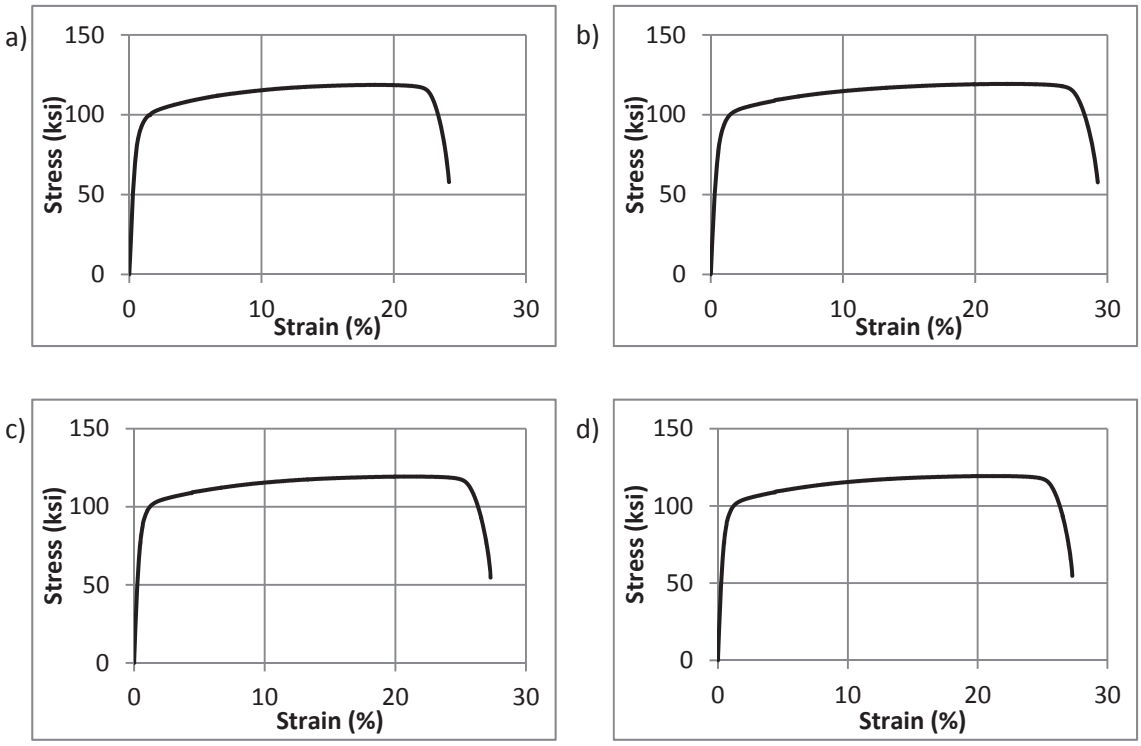

Figure C.3 2205 rod stress-strain curves for a) test 1, b) test 2, c) test 3, and d) average

Table C.3 Mechanical properties of 2205 rod

Test	f_y - 0.2% Offset (ksi)	UTS (ksi)	Ultimate Strain (%)	E (ksi)
1	84.5	118.7	24.21	18700
2	85.0	119.3	29.30	16500
3	86.9	119.3	27.32	20000
Average	85.5	119.1	26.94	18400

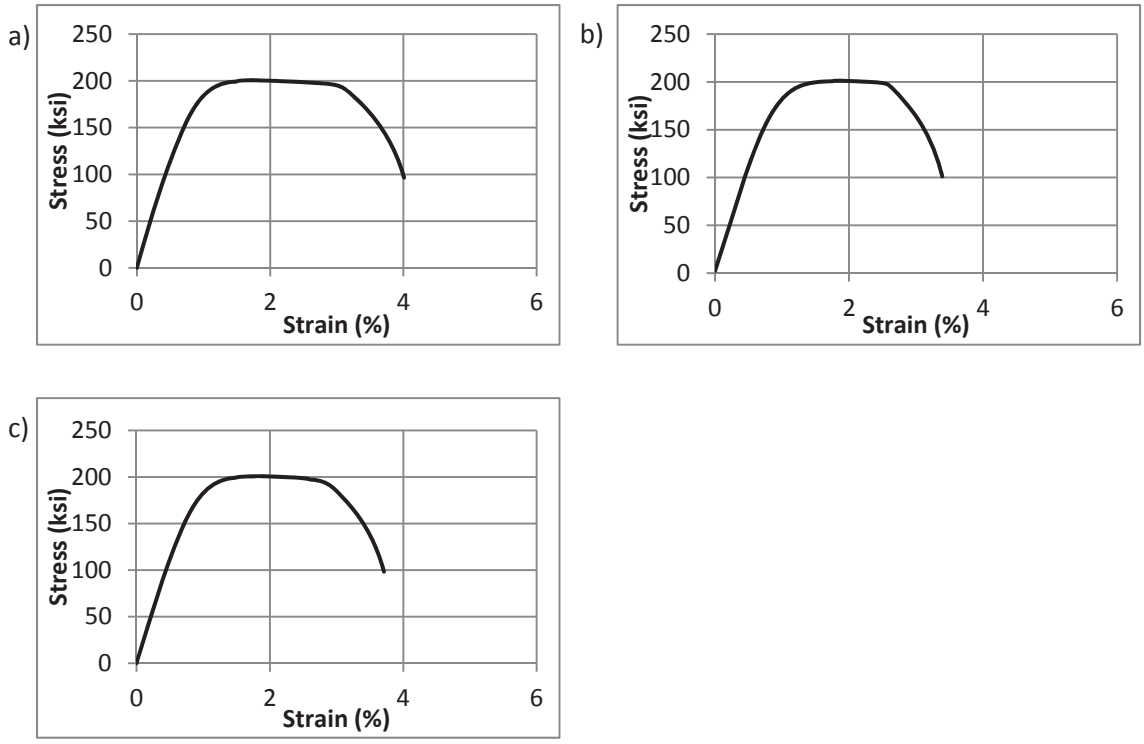

Figure C.4 2205 #3 wire stress-strain curves for a) test 1, b) test 2, and c) average

Table C.4 Mechanical properties of 2205 #3 wire

Test	f_y - 0.2% Offset (ksi)	UTS (ksi)	Ultimate Strain (%)	E (ksi)
1	188.1	200.6	4.01	21900
2	181.8	201.3	3.41	22500
Average	185.0	201.0	3.71	22200

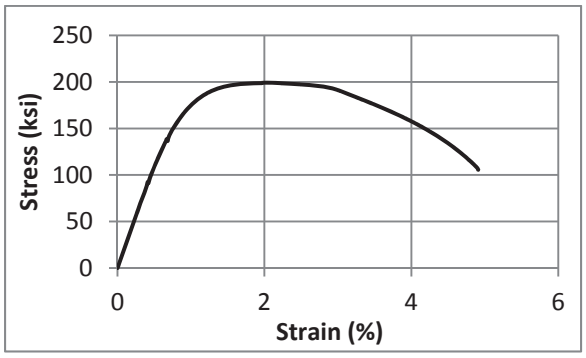

Figure C.5 2205 #5 wire stress-strain curve

Table C.5 Mechanical properties of 2205 #5 wire

Test	f_y - 0.2% Offset (ksi)	UTS (ksi)	Ultimate Strain (%)	E (ksi)
1	199.3	175.6	4.91	21700

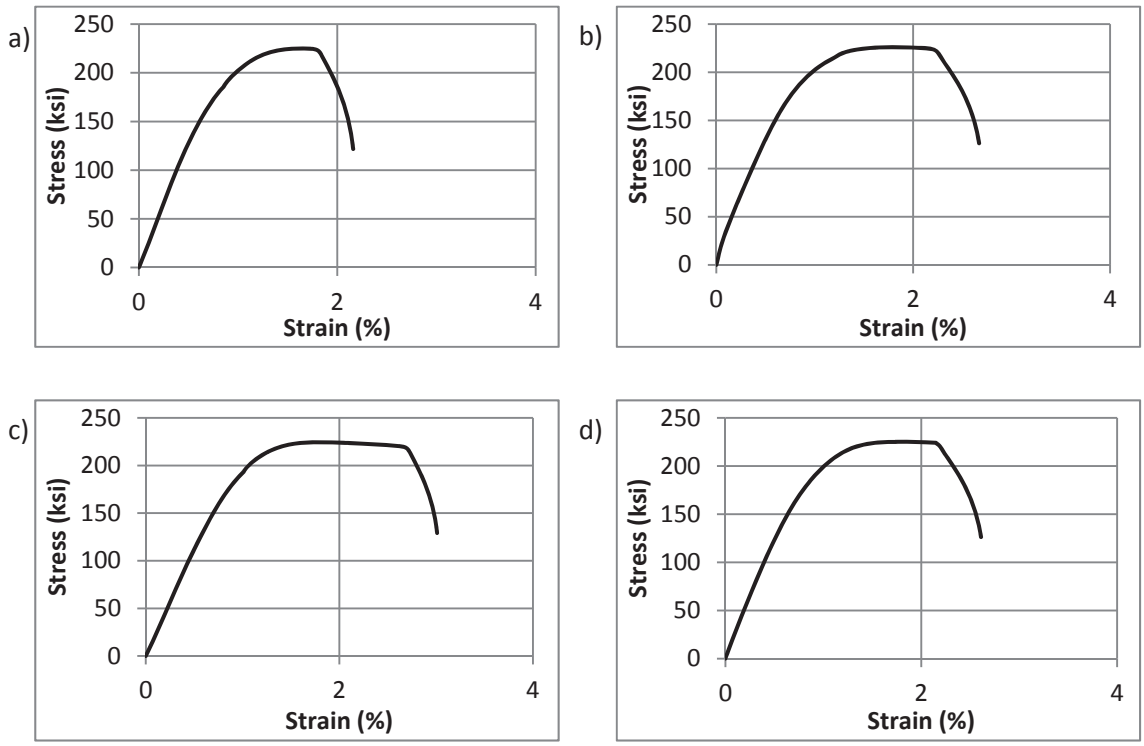

Figure C.6 2205 #7 UW wire stress-strain curves for a) test 1, b) test 2, c) test 3, and d) average

Table C.6 Mechanical properties of 2205 #7 UW wire

Test	f_y - 0.2% Offset (ksi)	UTS (ksi)	Ultimate Strain (%)	E (ksi)
1	197.7	225.0	2.17	26300
2	208	226.0	2.68	23800
3	216.2	224.5	3.01	22300
Average	207.3	225.2	2.62	24100

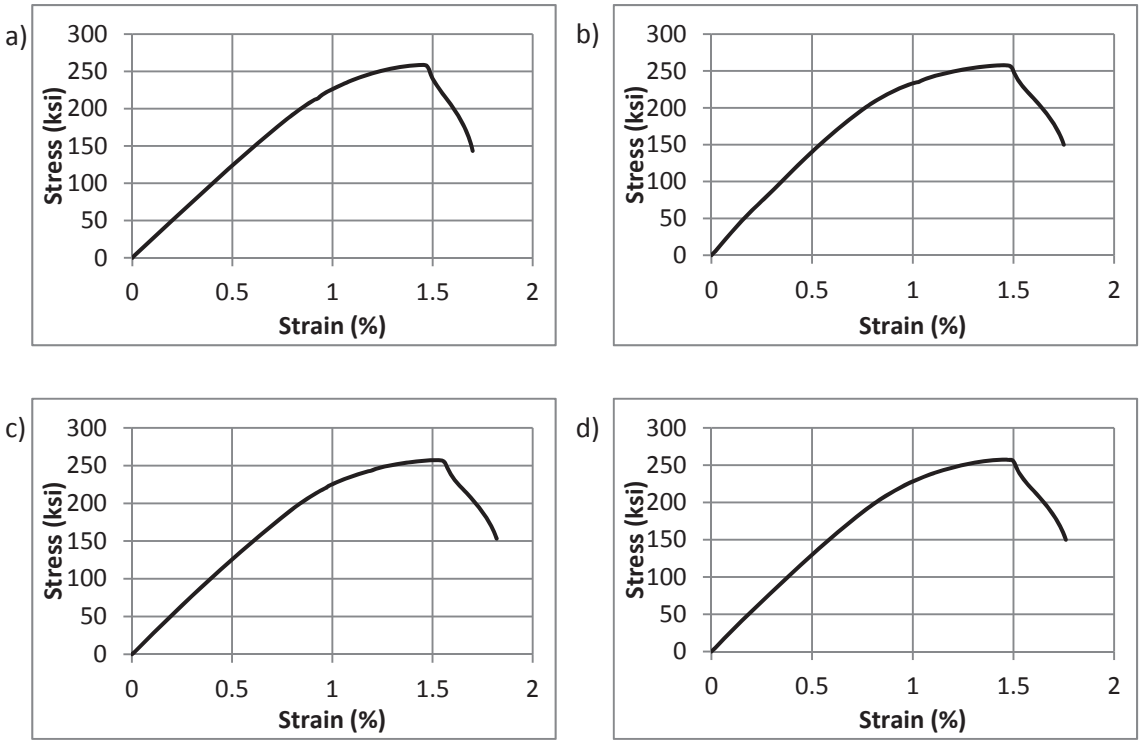

Figure C.7 2205 #7 HW wire stress-strain curves for a) test 1, b) test 2, c) test 3, and d) average

Table C.7 Mechanical properties of 2205 #7 HW wire

Test	f_y - 0.2% Offset (ksi)	UTS (ksi)	Ultimate Strain (%)	E (ksi)
1	248.0	258.7	1.7	24700
2	243.1	257.8	1.76	26800
3	241.5	257.4	1.83	25000
Average	244.2	258.0	1.76	25500

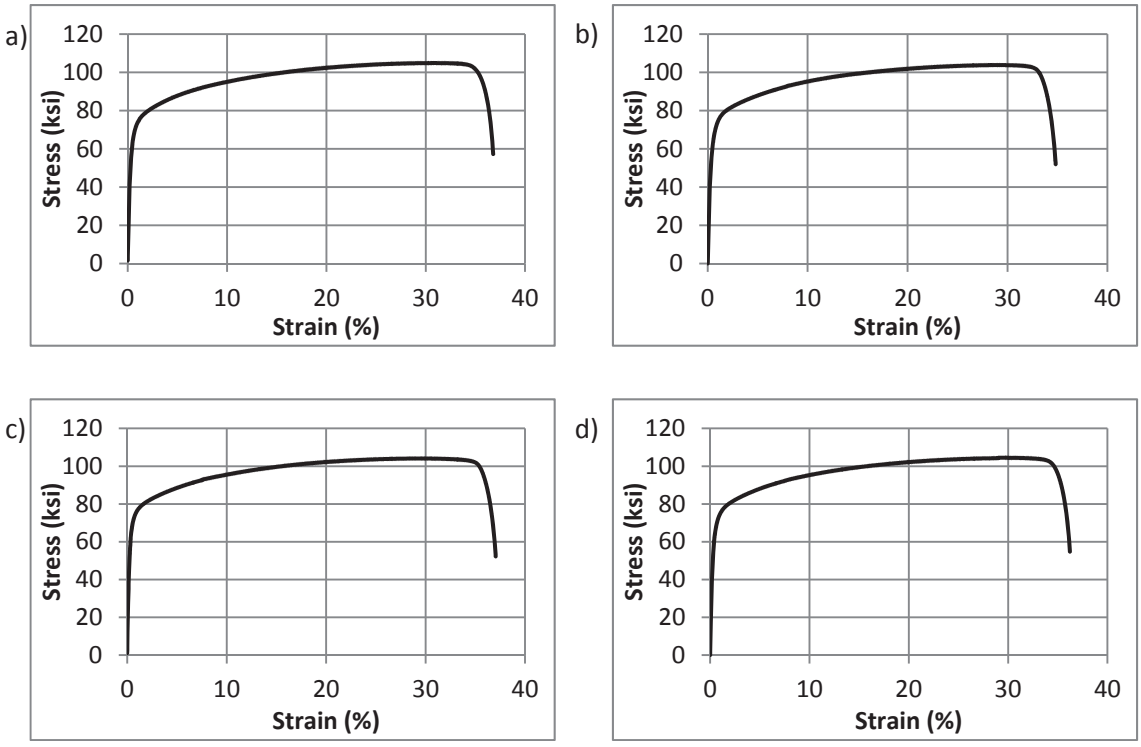

Figure C.8 2304 rod stress-strain curves for a) test 1, b) test 2, c) test 3, and d) average

Table C.8 Mechanical properties of 2304 rod

Test	f_y - 0.2% Offset (ksi)	UTS (ksi)	Ultimate Strain (%)	E (ksi)
1	66.0	104.9	36.8	18000
2	65.9	103.8	34.8	16300
3	69.9	104.1	37.1	20000
Average	67.3	104.3	36.2	18100

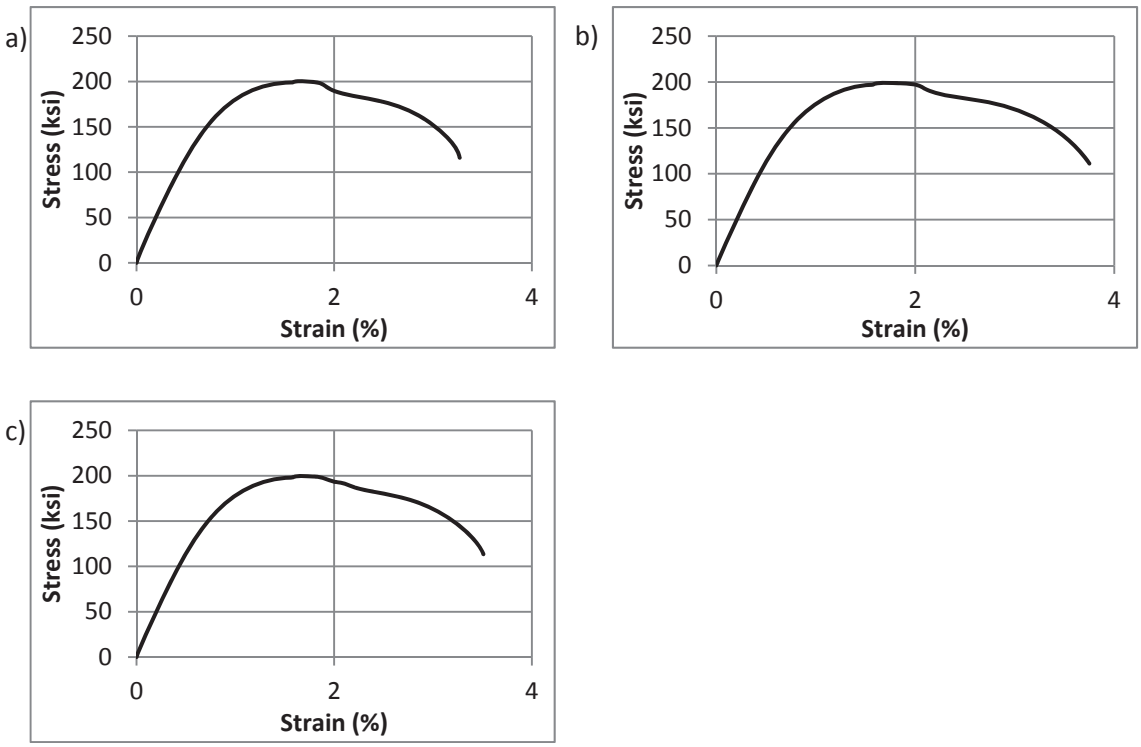

Figure C.9 2304 #3 wire stress-strain curves for a) test 1, b) test 2, c) test 3, and d) average

Table C.9 Mechanical properties of 2304 #3 wire

Test	f_y - 0.2% Offset (ksi)	UTS (ksi)	Ultimate Strain (%)	E (ksi)
1	179.7	200.4	3.27	22700
2	173.7	199.1	3.75	22600
Average	176.7	199.7	3.51	22700

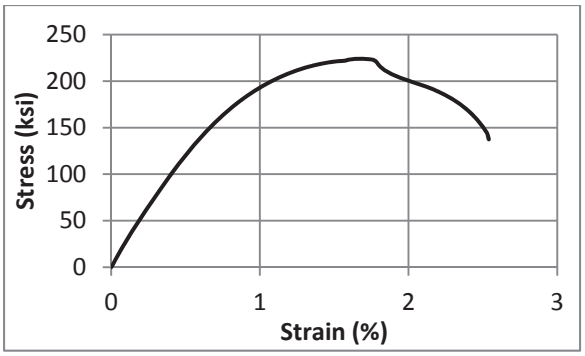

Figure C.10 2304 #5 wire stress-strain curve

Table C.10 Mechanical properties of 2304 #5 wire

Test	f_y - 0.2% Offset (ksi)	UTS (ksi)	Ultimate Strain (%)	E (ksi)
1	198.9	224.0	2.54	23000

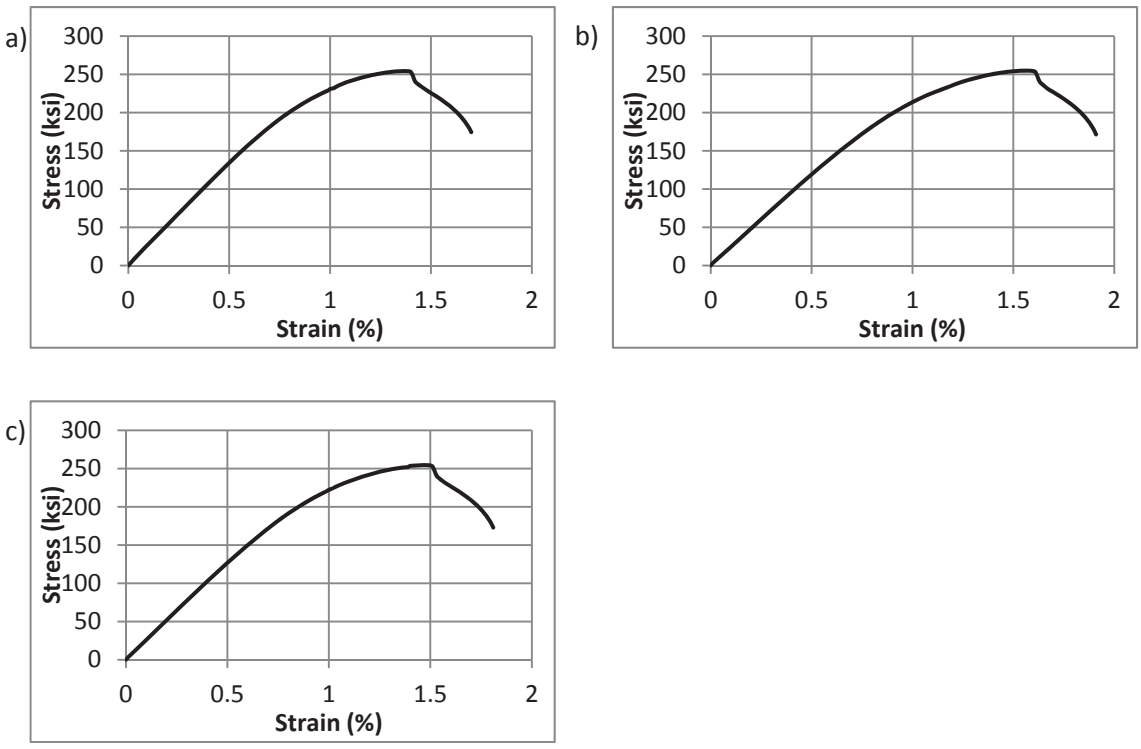

Figure C.11 2304 #7 UW wire stress-strain curves for a) test 1, b) test 2, and c) average

Table C.11 Mechanical properties of 2304 #7 UW wire

Test	f_y - 0.2% Offset (ksi)	UTS (ksi)	Ultimate Strain (%)	E (ksi)
1	241.9	254.4	1.71	26700
2	234.6	255.0	1.91	23700
Average	238.3	254.7	1.81	25200

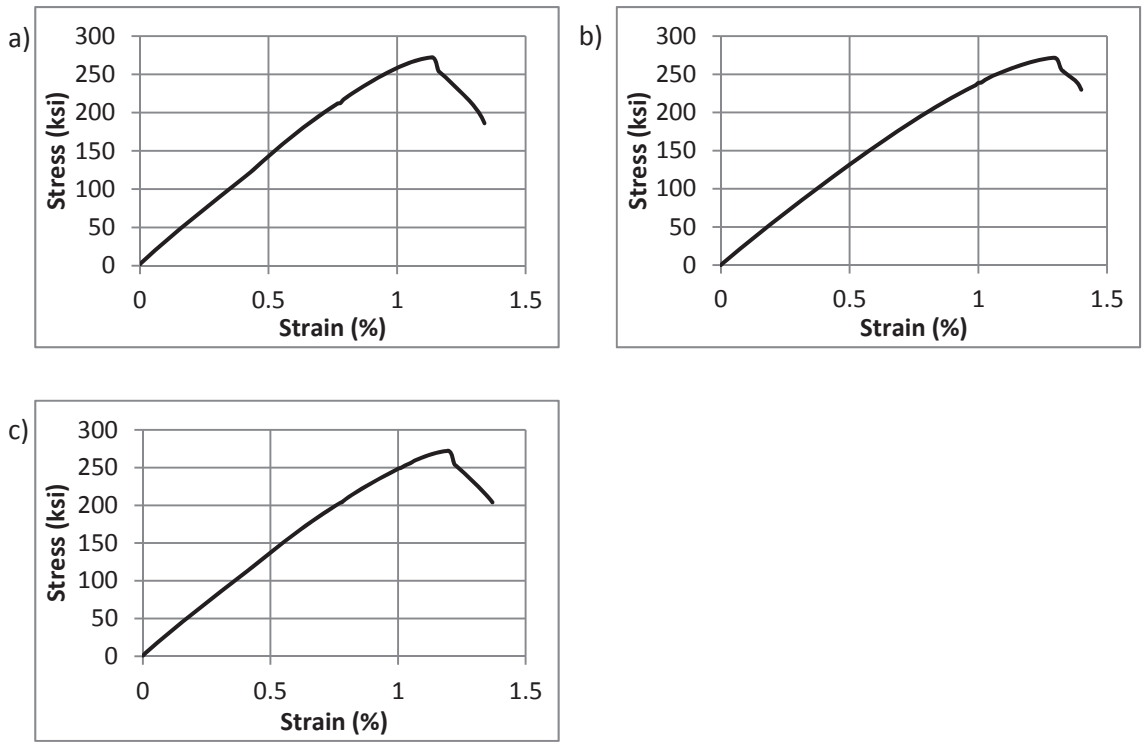

Figure C.12 2304 #7 HW wire stress-strain curves for a) test 1, b) test 2, and c) average

Table C.12 Mechanical properties of 2304 #7 UW wire

Test	fy - 0.2% Offset (ksi)	UTS (ksi)	Ultimate Strain (%)	E (ksi)
1	256	272.1	1.35	26700
2	270.8	271.6	1.41	24500
Average	263.4	271.8	1.38	25600

APPENDIX D

STRESS RELAXATION RESULTS

D.1 Strand Results

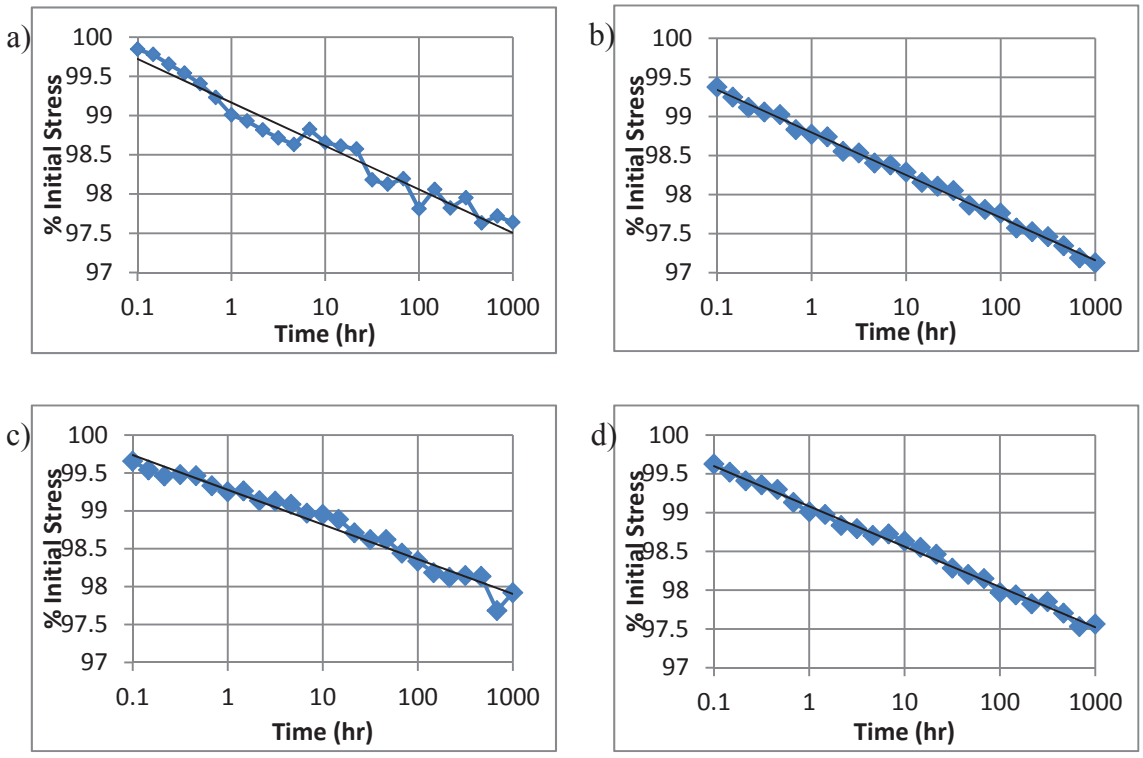

Figure D.1 2205 strand stress relaxation, 70% UTS initial Stress, 1000 hr duration, a) test 1, b) test 2, c) test 3, and d) average

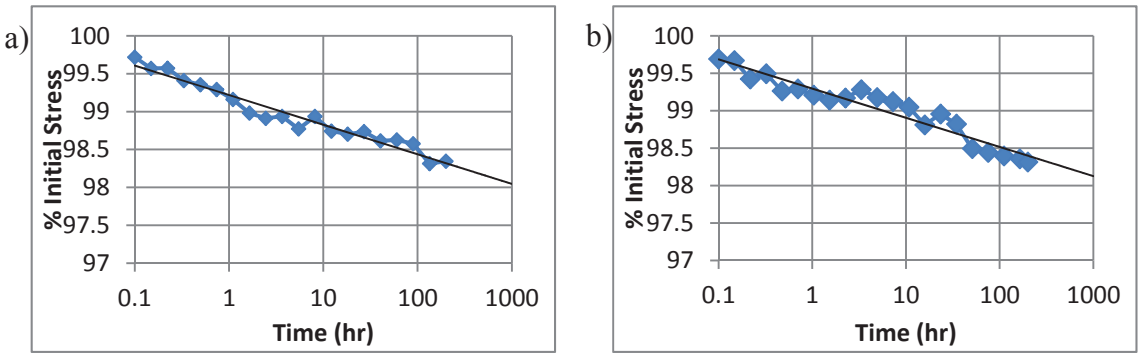

Figure D.2 2205 strand stress relaxation, 200 hr duration, a) 50% initial Stress, and b) 80% initial stress

Table D.1: Stress relaxation losses at 1000 hr for 2205 tests

Test	1000 hr Stress (% Initial)	1000 hr Loss (%)
70% UTS 1000 hr Test 1	97.57	2.43
70% UTS 1000 hr Test 2	97.19	2.81
70% UTS 1000 hr Test 3	97.78	2.22
70% UTS 1000 hr Average	97.51	2.49
50% UTS 200 hr Test 1 (Projected)	98.05	1.95
80% UTS 200 hr Test 1 (Projected)	98.09	1.91

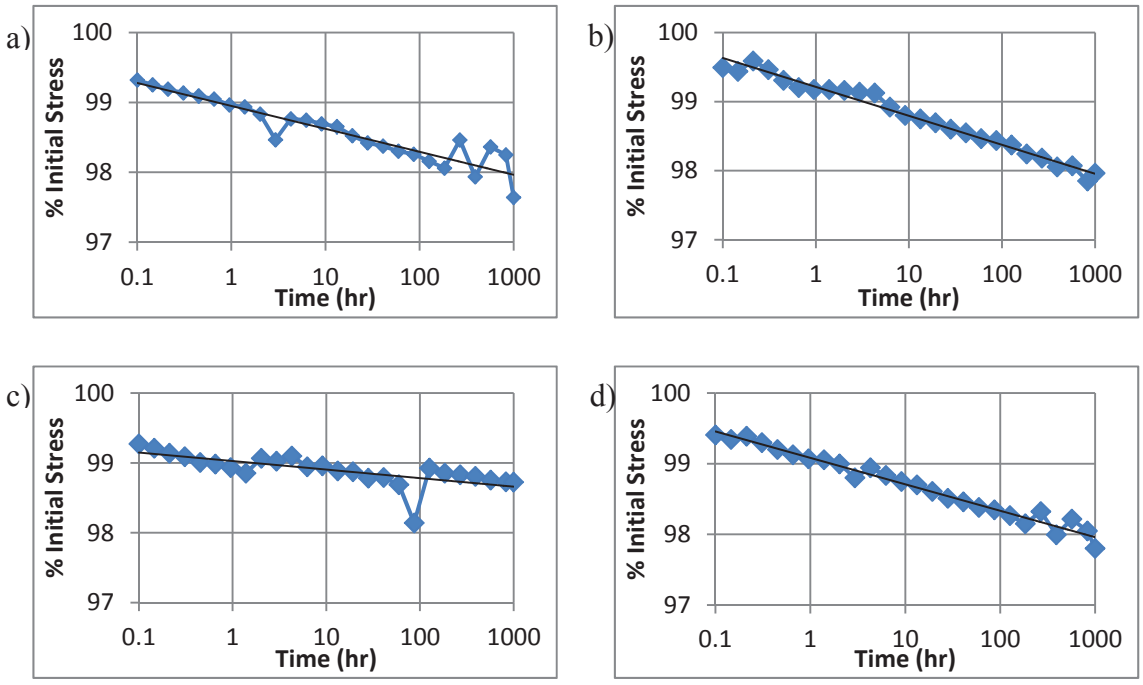

Figure D.3 2304 strand stress relaxation, 40% UTS initial stress, 1000 hr duration, a) test 1, b) test 2, c) test 3, and d) average

Table D.2 Stress relaxation losses at 1000 hr for 2304 strand tests

Test	1000 hr Stress (% Initial)	1000 hr Loss (%)
40% UTS 1000 hr Test 1	97.96	2.04
40% UTS 1000 hr Test 2	97.96	2.04
40% UTS 1000 hr Test 3*	98.66	1.34
40% UTS 1000 hr Average	97.96	2.04

*Not included in average calculations

D.2 Wire Results

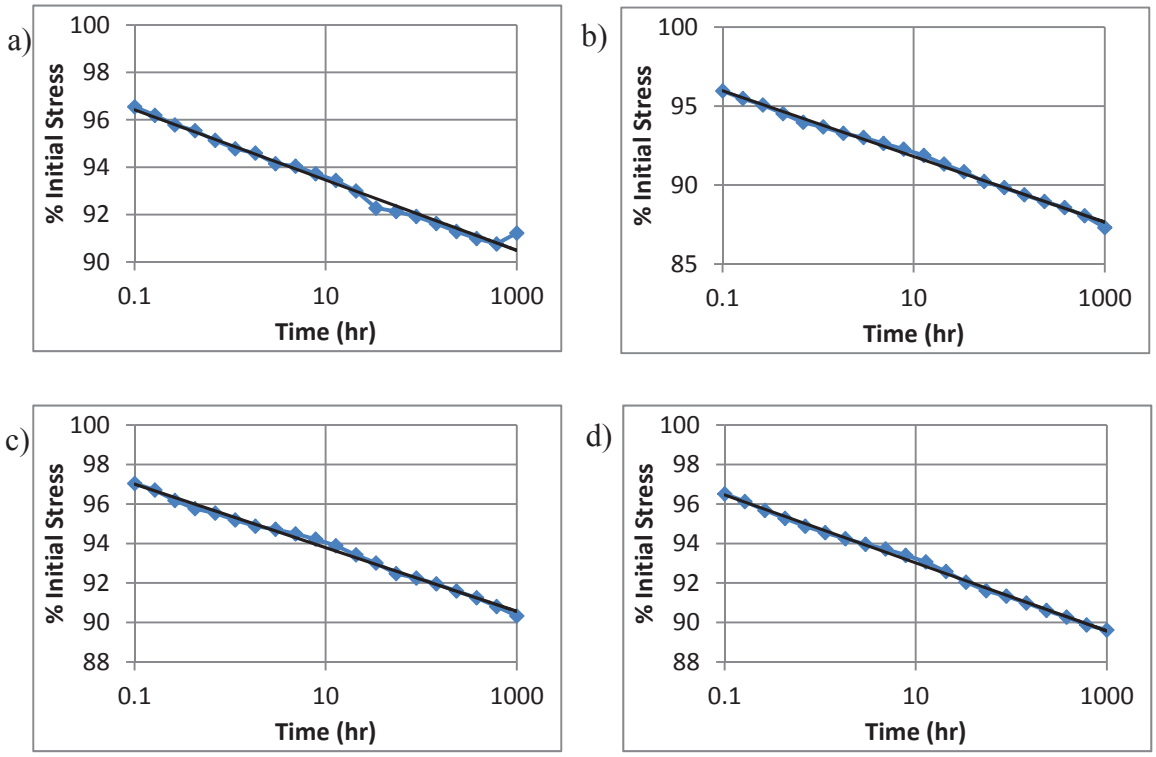

Figure D.4 2205 UW wire relaxation results for a) test 1, b) test 2, c) test 3, and d) average

Table D.3 Stress relaxation losses at 1000 hr for 2205 UW wire tests

Test	1000 hr Stress (% Initial)	1000 hr Loss (%)
70% UTS 1000 hr Test 1	90.45	9.55
70% UTS 1000 hr Test 2	87.64	12.36
70% UTS 1000 hr Test 3	90.56	9.44
70% UTS 1000 hr Average	89.56	10.44

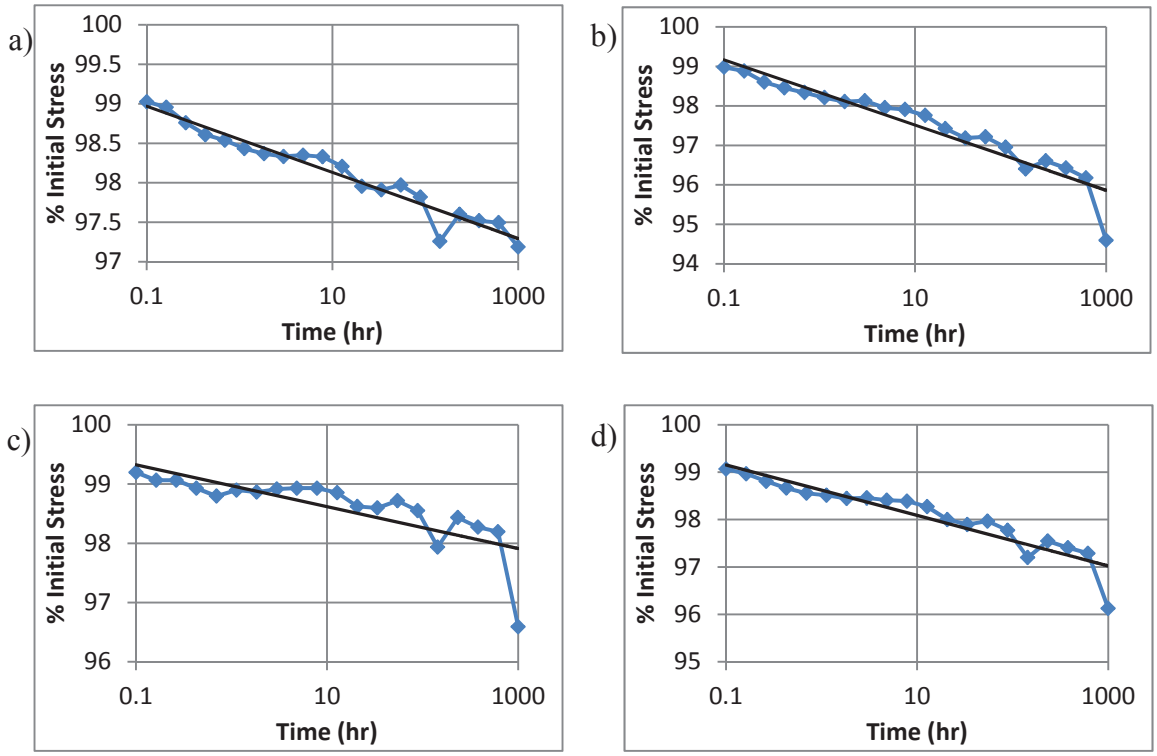

Figure D.5 2205 HW wire relaxation results for a) test 1, b) test 2, c) test 3, and d) average

Table D.4 Stress relaxation losses at 1000 hr for 2205 HW wire tests

Test	1000 hr Stress (% Initial)	1000 hr Loss (%)
70% UTS 1000 hr Test 1	97.21	2.79
70% UTS 1000 hr Test 2	96.53	3.47
70% UTS 1000 hr Test 3	98.26	1.74
70% UTS 1000 hr Average	97.33	2.67

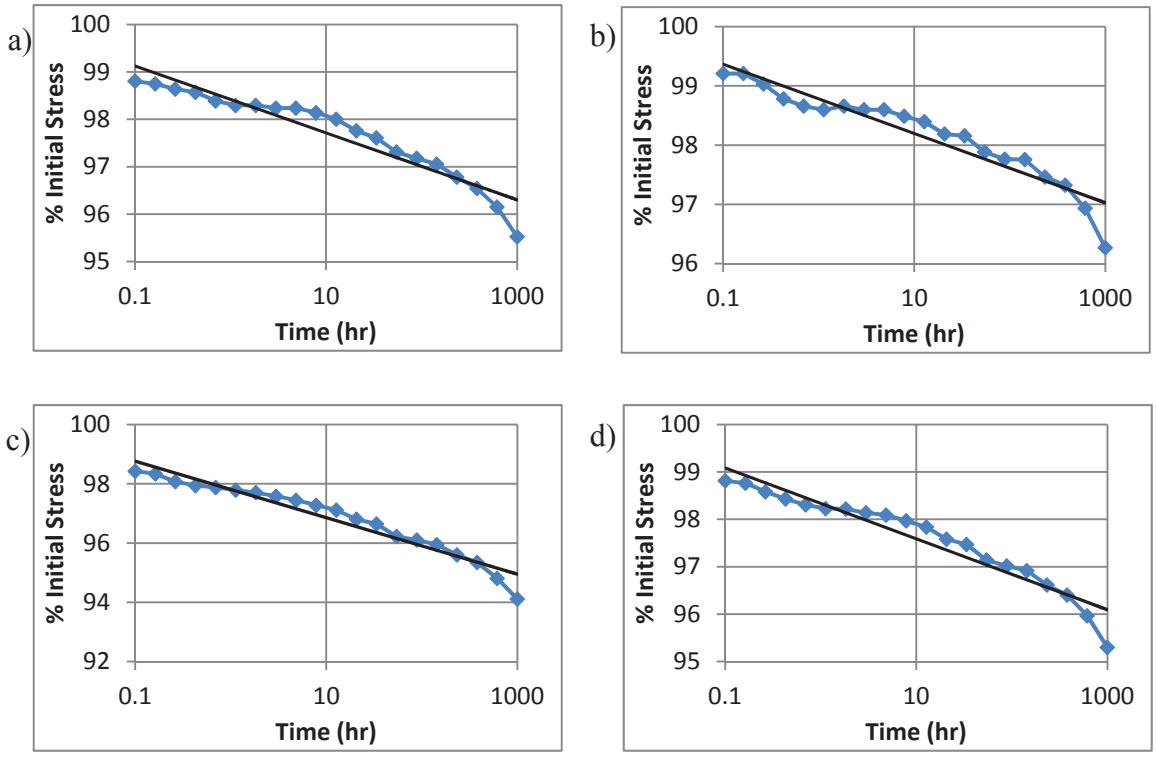

Figure D.6 2304 UW wire relaxation results for a) test 1, b) test 2, c) test 3, and d) average

Table D.5 Stress relaxation losses at 1000 hr for 2304 UW wire tests

Test	1000 hr Stress (% Initial)	1000 hr Loss (%)
70% UTS 1000 hr Test 1	96.33	3.67
70% UTS 1000 hr Test 2	97.07	2.93
70% UTS 1000 hr Test 3	94.98	5.02
70% UTS 1000 hr Average	96.12	3.88

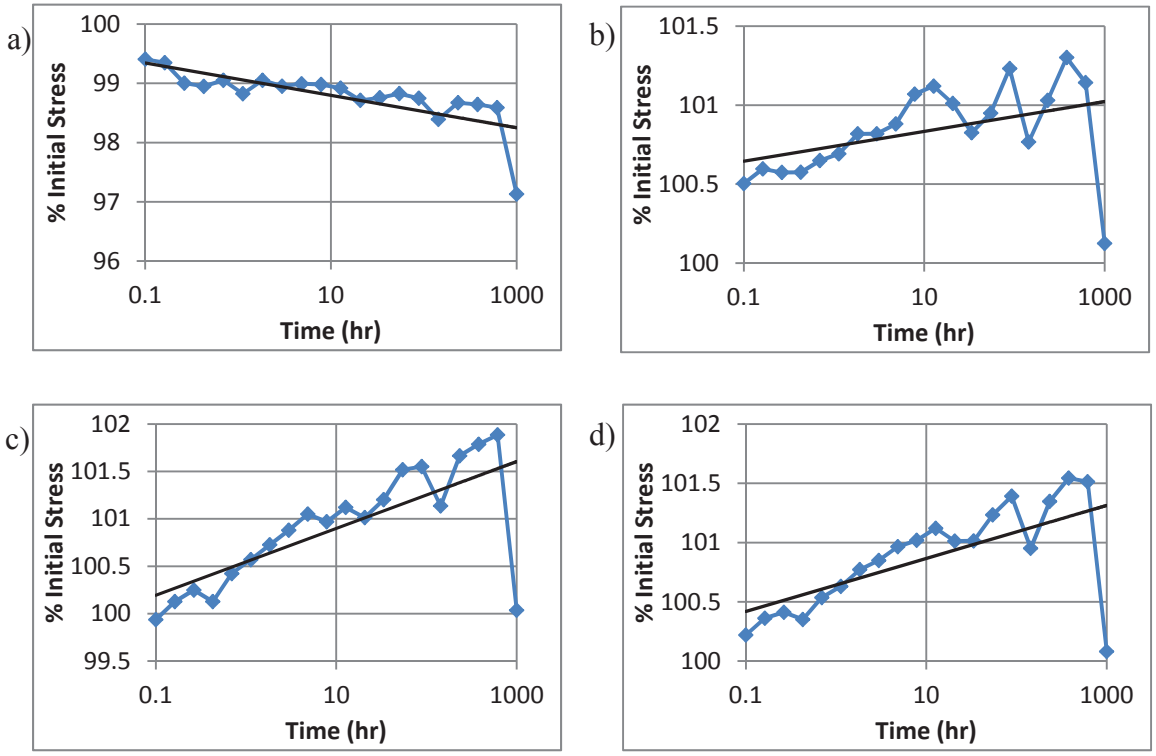

Figure D.7 2304 HW wire relaxation results for a) test 1, b) test 2, c) test 3, and d) average

Table D.6 Stress relaxation losses at 1000 hr for 2304 HW wire tests

Test	1000 hr Stress (% Initial)	1000 hr Loss (%)
70% UTS 1000 hr Test 1*	98.21	1.79
70% UTS 1000 hr Test 2	101.71	-1.71
70% UTS 1000 hr Test 3	101.86	-1.86
70% UTS 1000 hr Average	101.79	-1.79

*Not included in average calculations

APPENDIX E

MOMENT-CURVATURE AND LOAD-DEFLECTION CALCULATIONS

E.1 Moment-Curvature Calculations

Moment-curvature calculations are included in the remainder of this section. The test piles are analyzed for concrete strengths of 5 and 10 ksi.

1080 12x12 Pile, 5 ksi concrete

Pile properties:

$f'_{cp} := 5ksi \qquad b := 12in \qquad h := 12in$

$A_p := b \cdot h = 144 \cdot in^2 \qquad I_p := \frac{1}{12} \cdot b \cdot h^3 = 1.728 \times 10^3 \cdot in^4$

$f_{rp} := 7.5 \cdot \sqrt{(f'_{cp} \cdot psi)} = 0.53 \cdot ksi \qquad E_p := 57000 \cdot \sqrt{f'_{cp} \cdot psi} = 4.031 \times 10^3 \cdot ksi$

Strand Propeties:

$f_u := 270ksi \qquad f_{se} := .7 \cdot f_u = 189 \cdot ksi \qquad A_{strand} := .115in^2 \qquad cover := 3.25in$

$E_{ps} := 29500ksi$

Strand Layout, arranged by rows:

$$num := \begin{pmatrix} 3 \\ 2 \\ 3 \end{pmatrix} \qquad e_p := \begin{pmatrix} \frac{h}{2} - cover \\ 0 \\ cover - \frac{h}{2} \end{pmatrix} = \begin{pmatrix} 2.75 \\ 0 \\ -2.75 \end{pmatrix} \cdot in \qquad d_p := -e_p + \frac{h}{2} = \begin{pmatrix} 3.25 \\ 6 \\ 8.75 \end{pmatrix} \cdot in$$

$$P_i := f_{se} \cdot num \cdot A_{strand} = \begin{pmatrix} 65.205 \\ 43.47 \\ 65.205 \end{pmatrix} \cdot kip \qquad P_{tot} := \sum P_i = 173.88 \cdot kip$$

Cracking Moment:

$y_t := \frac{h}{2} \qquad y_b := \frac{-h}{2}$

$$M_{cr} := -\left(\frac{P_{tot}}{A_p} + f_{rp}\right) \cdot \frac{I_p}{y_b} = 500.495 \cdot kip \cdot in$$

$f_b := f_{rp} \qquad f_t := \frac{-P_{tot}}{A_p} - \frac{M_{cr} \cdot y_t}{I_p} = -2.945 \cdot ksi$

$\varepsilon_b := \frac{f_b}{E_p} = 1.316 \times 10^{-4} \qquad \varepsilon_t := \frac{f_t}{E_p} = -7.308 \times 10^{-4}$

$$\phi_{cr} := \frac{\varepsilon_b - \varepsilon_t}{h} = 7.186 \times 10^{-5} \cdot \frac{rad}{in}$$

Ultimate Moment Capacity:

using Todeschini stress block:

$f''_c := .9 \cdot f'_{cp} = 4.5 \cdot ksi$ $\quad e_0 := 1.71 \cdot \frac{f'_{cp}}{E_p} = 2.121 \times 10^{-3}$ $\quad e_u := .003$

$e_{tf} := .003$ specified strain in top fiber

$$\beta_1 := \frac{\ln\left[1 + \left(\frac{e_{tf}}{e_0}\right)^2\right]}{\frac{e_{tf}}{e_0}} = 0.777 \qquad k_2 := 1 - 2 \cdot \frac{\left(\frac{e_{tf}}{e_0} - \operatorname{atan}\left(\frac{e_{tf}}{e_0}\right)\right)}{\left(\frac{e_{tf}}{e_0}\right)^2 \cdot \beta_1} = 0.409$$

$e_{se} := \frac{f_{se}}{E_{ps}} = 6.407 \times 10^{-3}$ $\quad e_{ce} := \frac{-P_{tot}}{E_p \cdot A_p} = -2.996 \times 10^{-4}$

$c := 4.38in$ manual adjust

$C := \beta_1 \cdot f''_c \cdot c \cdot b = 183.737 \cdot kip$

$$e_c := \frac{e_{tf}}{c} \cdot (d_p - c) = \begin{pmatrix} -7.74 \times 10^{-4} \\ 1.11 \times 10^{-3} \\ 2.993 \times 10^{-3} \end{pmatrix} \qquad e_s := e_c + e_{se} + e_{ce} = \begin{pmatrix} 5.333 \times 10^{-3} \\ 7.217 \times 10^{-3} \\ 9.1 \times 10^{-3} \end{pmatrix}$$

note: <.06

$$index := \operatorname{round}(e_s \cdot 10000) - 1 = \begin{pmatrix} 52 \\ 71 \\ 90 \end{pmatrix}$$

SS: stresses on stress-strain curve at 0.01% strain

$$f_s := \begin{bmatrix} SS(index_0) \\ SS(index_1) \\ SS(index_2) \end{bmatrix} = \begin{pmatrix} 153.724 \\ 210.396 \\ 238.537 \end{pmatrix} \cdot ksi$$

$i := 0..2$

$$P_i := f_{s_i} \cdot num_i \cdot A_{strand} \qquad P = \begin{pmatrix} 53.035 \\ 48.391 \\ 82.295 \end{pmatrix} \cdot kip$$

$T := f_s \cdot num \cdot A_{strand} = 183.721 \cdot kip$ $\quad C = 183.737 \cdot kip$ adjust c until T=C

$M_u := -C \cdot k_2 \cdot c + P \cdot d_p = 853.42 \cdot kip \cdot in$

$$\phi_u := \frac{\left(e_{s_2} - e_{s_0}\right)}{d_{p_2} - d_{p_0}} = 6.849 \times 10^{-4} \cdot \frac{rad}{in}$$

1080 12-in. Pile, 10 ksi concrete

Pile properties:

$f'_{cp} := 10ksi \qquad b := 12in \qquad h := 12in$

$A_p := b \cdot h = 144 \cdot in^2 \qquad I_p := \frac{1}{12} \cdot b \cdot h^3 = 1.728 \times 10^3 \cdot in^4$

$f_{rp} := 7.5 \cdot \sqrt{(f'_{cp} \cdot psi)} = 0.75 \cdot ksi \qquad E_p := 57000 \cdot \sqrt{f'_{cp} \cdot psi} = 5.7 \times 10^3 \cdot ksi$

Strand Propeties:

$f_u := 270ksi \qquad f_{se} := .7 \cdot f_u = 189 \cdot ksi \qquad A_{strand} := .115in^2 \qquad cover := 3.25in$

$E_{ps} := 29500ksi$

Strand Layout, arranged by rows:

$$num := \begin{pmatrix} 3 \\ 2 \\ 3 \end{pmatrix} \qquad e_p := \begin{pmatrix} \frac{h}{2} - cover \\ 0 \\ cover - \frac{h}{2} \end{pmatrix} = \begin{pmatrix} 2.75 \\ 0 \\ -2.75 \end{pmatrix} \cdot in \qquad d_p := -e_p + \frac{h}{2} = \begin{pmatrix} 3.25 \\ 6 \\ 8.75 \end{pmatrix} \cdot in$$

$$P_i := f_{se} \cdot num \cdot A_{strand} = \begin{pmatrix} 65.205 \\ 43.47 \\ 65.205 \end{pmatrix} \cdot kip \qquad P_{tot} := \sum P_i = 173.88 \cdot kip$$

Cracking Moment:

$y_t := \frac{h}{2} \qquad y_b := \frac{-h}{2}$

$$M_{cr} := -\left(\frac{P_{tot}}{A_p} + f_{rp}\right) \cdot \frac{I_p}{y_b} = 563.76 \cdot kip \cdot in$$

$f_b := f_{rp} \qquad f_t := \frac{-P_{tot}}{A_p} - \frac{M_{cr} \cdot y_t}{I_p} = -3.165 \cdot ksi$

$\varepsilon_b := \frac{f_b}{E_p} = 1.316 \times 10^{-4} \qquad \varepsilon_t := \frac{f_t}{E_p} = -5.553 \times 10^{-4}$

$$\phi_{cr} := \frac{\varepsilon_b - \varepsilon_t}{h} = 5.724 \times 10^{-5} \cdot \frac{rad}{in}$$

Ultimate Moment Capacity:

using Todeschini stress block:

$f'_c := .9 \cdot f'_{cp} = 9 \cdot ksi$ $\quad e_0 := 1.71 \cdot \frac{f'_{cp}}{E_p} = 3 \times 10^{-3}$ $\quad e_u := .003$

$e_{tf} := .003$ specified strain in top fiber

$$\beta_1 := \frac{\ln\left[1 + \left(\frac{e_{tf}}{e_0}\right)^2\right]}{\frac{e_{tf}}{e_0}} = 0.693 \qquad k_2 := 1 - 2 \cdot \frac{\left(\frac{e_{tf}}{e_0} - \operatorname{atan}\left(\frac{e_{tf}}{e_0}\right)\right)}{\left(\frac{e_{tf}}{e_0}\right)^2 \cdot \beta_1} = 0.381$$

$$e_{se} := \frac{f_{se}}{E_{ps}} = 6.407 \times 10^{-3} \qquad e_{ce} := \frac{-P_{tot}}{E_p \cdot A_p} = -2.118 \times 10^{-4}$$

$c := 2.83in$ manual adjust

$C := \beta_1 \cdot f'_c \cdot c \cdot b = 211.854 \cdot kip$

$$e_c := \frac{e_{tf}}{c} \cdot (d_p - c) = \begin{pmatrix} 4.452 \times 10^{-4} \\ 3.36 \times 10^{-3} \\ 6.276 \times 10^{-3} \end{pmatrix} \qquad e_s := e_c + e_{se} + e_{ce} = \begin{pmatrix} 6.64 \times 10^{-3} \\ 9.555 \times 10^{-3} \\ 0.012 \end{pmatrix}$$

note: <.06

$$index := round(e_s \cdot 10000) - 1 = \begin{pmatrix} 65 \\ 95 \\ 124 \end{pmatrix}$$

SS: stresses on stress-strain curve at 0.01% strain

$$f_s := \begin{bmatrix} SS(index_0) \\ SS(index_1) \\ SS(index_2) \end{bmatrix} = \begin{pmatrix} 193.092 \\ 248.226 \\ 255.836 \end{pmatrix} \cdot ksi$$

$i := 0..2$

$P_i := f_{s_i} \cdot num_i \cdot A_{strand}$ $\quad P = \begin{pmatrix} 66.617 \\ 57.092 \\ 88.263 \end{pmatrix} \cdot kip$

$T := f_s \cdot num \cdot A_{strand} = 211.972 \cdot kip$ $\quad C = 211.854 \cdot kip$ adjust c until T=C

$M_u := -C \cdot k_2 \cdot c + P \cdot d_p = 1.103 \times 10^3 \cdot kip \cdot in$

$$\phi_u := \frac{\left(e_{s_2} - e_{s_0}\right)}{d_{p_2} - d_{p_0}} = 1.06 \times 10^{-3} \cdot \frac{rad}{in}$$

At yield point (1.0% strain)

$f'_c := .9 \cdot f'_{cp} = \quad \cdot \text{ksi}$ $\qquad e_0 := 1.71 \cdot \frac{f'_{cp}}{E_p} = \qquad e_u := .003$

$e_{tf} := .00222$ specified strain in top fiber

$$\beta_1 := \frac{\ln\left[1 + \left(\frac{e_{tf}}{e_0}\right)^2\right]}{\frac{e_{tf}}{e_0}} = \qquad k_2 := 1 - 2 \cdot \frac{\left(\frac{e_{tf}}{e_0} - \operatorname{atan}\left(\frac{e_{tf}}{e_0}\right)\right)}{\left(\frac{e_{tf}}{e_0}\right)^2 \cdot \beta_1} =$$

$$e_{se} := \frac{f_{se}}{E_{ps}} = \qquad e_{ce} := \frac{-P_{tot}}{E_p \cdot A_p} =$$

$c := 3.18\text{in}$ manual adjust

$C := \beta_1 \cdot f'_c \cdot c \cdot b = \quad \cdot \text{kip}$

$$e_c := \frac{e_{tf}}{c} \cdot (d_p - c) = \qquad e_s := e_c + e_{se} + e_{ce} =$$

$\text{index} := \text{round}(e_s \cdot 10000) - 1 =$

$$f_s := \begin{bmatrix} SS(\text{index}_0) \\ SS(\text{index}_1) \\ SS(\text{index}_2) \end{bmatrix} = \quad \cdot \text{ksi}$$

$i := 0..2$

$P_i := f_{s_i} \cdot \text{num}_i \cdot A_{strand} \qquad P = \quad \cdot \text{kip}$

$T := f_s \cdot \text{num} \cdot A_{strand} = \quad \cdot \text{kip} \qquad C = \quad \cdot \text{kip}$ adjust c until T=C

$M_y := -C \cdot k_2 \cdot c + P \cdot d_p = \quad \cdot \text{kip} \cdot \text{in}$

$$\phi_y := \frac{\left(e_{s_2} - e_{s_0}\right)}{d_{p_2} - d_{p_0}} = \quad \cdot \frac{\text{rad}}{\text{in}}$$

2304 12x12 Pile, 5 ksi concrete

Pile properties:

$f'_{cp} := 5ksi \qquad b := 12in \qquad h := 12in$

$A_p := b \cdot h = 144 \cdot in^2 \qquad I_p := \frac{1}{12} \cdot b \cdot h^3 = 1.728 \times 10^3 \cdot in^4$

$f_{rp} := 7.5 \cdot \sqrt{(f'_{cp} \cdot psi)} = 0.53 \cdot ksi \qquad E_p := 57000 \cdot \sqrt{f'_{cp} \cdot psi} = 4.031 \times 10^3 \cdot ksi$

Strand Propeties:

$f_u := 242ksi \qquad f_{se} := .4 \cdot f_u = 96.8 \cdot ksi \qquad A_{strand} := .153in^2 \qquad cover := 3.25in$

$E_{ps} := 24100ksi$

Strand Layout, arranged by rows:

$$e_{mid} := \frac{h - 2 \cdot cover}{6} = 0.917 \cdot in$$

$$num := \begin{pmatrix} 4 \\ 2 \\ 2 \\ 4 \end{pmatrix} \qquad e_p := \begin{pmatrix} \frac{h}{2} - cover \\ e_{mid} \\ -e_{mid} \\ cover - \frac{h}{2} \end{pmatrix} = \begin{pmatrix} 2.75 \\ 0.917 \\ -0.917 \\ -2.75 \end{pmatrix} \cdot in \qquad d_p := -e_p + \frac{h}{2} = \begin{pmatrix} 3.25 \\ 5.083 \\ 6.917 \\ 8.75 \end{pmatrix} \cdot in$$

$$P_i := f_{se} \cdot num \cdot A_{strand} = \begin{pmatrix} 59.242 \\ 29.621 \\ 29.621 \\ 59.242 \end{pmatrix} \cdot kip \qquad P_{tot} := \sum P_i = 177.725 \cdot kip$$

Cracking Moment:

$y_t := \frac{h}{2} \qquad y_b := \frac{-h}{2}$

$$M_{cr} := -\left(\frac{P_{tot}}{A_p} + f_{rp}\right) \cdot \frac{I_p}{y_b} = 508.185 \cdot kip \cdot in$$

$f_b := f_{rp} \qquad f_t := \frac{-P_{tot}}{A_p} - \frac{M_{cr} \cdot y_t}{I_p} = -2.999 \cdot ksi$

$\varepsilon_b := \frac{f_b}{E_p} = 1.316 \times 10^{-4} \qquad \varepsilon_t := \frac{f_t}{E_p} = -7.44 \times 10^{-4}$

$$\phi_{cr} := \frac{\varepsilon_b - \varepsilon_t}{h} = 7.297 \times 10^{-5} \cdot \frac{rad}{in}$$

Ultimate Moment Capacity:

using Todeschini stress block:

$f'_c := .9 \cdot f'_{cp} = 4.5 \cdot ksi$ $\quad e_0 := 1.71 \cdot \frac{f'_{cp}}{E_p} = 2.121 \times 10^{-3}$ $\quad e_u := .003$

$e_{tf} := .003$ specified strain in top fiber

$$\beta_1 := \frac{\ln\left[1 + \left(\frac{e_{tf}}{e_0}\right)^2\right]}{\frac{e_{tf}}{e_0}} = 0.777 \qquad k_2 := 1 - 2 \cdot \frac{\left(\frac{e_{tf}}{e_0} - \operatorname{atan}\left(\frac{e_{tf}}{e_0}\right)\right)}{\left(\frac{e_{tf}}{e_0}\right)^2 \cdot \beta_1} = 0.409$$

$e_{se} := \frac{f_{se}}{E_{ps}} = 4.017 \times 10^{-3}$ $\quad e_{ce} := \frac{-P_{tot}}{E_p \cdot A_p} = -3.062 \times 10^{-4}$

$c := 4.75in$ manual adjust

$C := \beta_1 \cdot f'_c \cdot c \cdot b = 199.258 \cdot kip$

$$e_c := \frac{e_{tf}}{c} \cdot (d_p - c) = \begin{pmatrix} -9.474 \times 10^{-4} \\ 2.105 \times 10^{-4} \\ 1.368 \times 10^{-3} \\ 2.526 \times 10^{-3} \end{pmatrix} \qquad e_s := e_c + e_{se} + e_{ce} = \begin{pmatrix} 2.763 \times 10^{-3} \\ 3.921 \times 10^{-3} \\ 5.079 \times 10^{-3} \\ 6.237 \times 10^{-3} \end{pmatrix}$$

note: <.0187 strain

$$index := round(e_s \cdot 10000) - 1 = \begin{pmatrix} 27 \\ 38 \\ 50 \\ 61 \end{pmatrix}$$

SS: stresses on stress-strain curve at 0.01% strain

$$f_s := \begin{bmatrix} SS(index_0) \\ SS(index_1) \\ SS(index_2) \\ SS(index_3) \end{bmatrix} = \begin{pmatrix} 67.291 \\ 94.227 \\ 122.957 \\ 149.608 \end{pmatrix} \cdot ksi$$

$i := 0..3$

$P_i := f_{s_i} \cdot num_i \cdot A_{strand}$ $\quad P = \begin{pmatrix} 41.182 \\ 28.833 \\ 37.625 \\ 91.56 \end{pmatrix} \cdot kip$

$T := f_s \cdot num \cdot A_{strand} = 199.2 \cdot kip$ $\quad C = 199.258 \cdot kip$ adjust c until T=C

$M_u := -C \cdot k_2 \cdot c + P \cdot d_p = 954.432 \cdot kip \cdot in$

$\phi_u := \frac{(e_{s_2} - e_{s_0})}{d_{p_2} - d_{p_0}} = 6.316 \times 10^{-4} \cdot \frac{rad}{in}$

2304 12x12 Pile, 10 ksi concrete

Pile properties:

$f'_{cp} := 10ksi \qquad b := 12in \qquad h := 12in$

$A_p := b \cdot h = 144 \cdot in^2 \qquad I_p := \frac{1}{12} \cdot b \cdot h^3 = 1.728 \times 10^3 \cdot in^4$

$f_{rp} := 7.5 \cdot \sqrt{(f'_{cp} \cdot psi)} = 0.75 \cdot ksi \qquad E_p := 57000 \cdot \sqrt{f'_{cp} \cdot psi} = 5.7 \times 10^3 \cdot ksi$

Strand Propeties:

$f_u := 242ksi \qquad f_{se} := .4 \cdot f_u = 96.8 \cdot ksi \qquad A_{strand} := .153in^2 \qquad cover := 3.25in$

$E_{ps} := 24100ksi$

Strand Layout, arranged by rows:

$$e_{mid} := \frac{h - 2 \cdot cover}{6} = 0.917 \cdot in$$

$$num := \begin{pmatrix} 4 \\ 2 \\ 2 \\ 4 \end{pmatrix} \qquad e_p := \begin{pmatrix} \frac{h}{2} - cover \\ e_{mid} \\ -e_{mid} \\ cover - \frac{h}{2} \end{pmatrix} = \begin{pmatrix} 2.75 \\ 0.917 \\ -0.917 \\ -2.75 \end{pmatrix} \cdot in \qquad d_p := -e_p + \frac{h}{2} = \begin{pmatrix} 3.25 \\ 5.083 \\ 6.917 \\ 8.75 \end{pmatrix} \cdot in$$

$$P_i := f_{se} \cdot num \cdot A_{strand} = \begin{pmatrix} 59.242 \\ 29.621 \\ 29.621 \\ 59.242 \end{pmatrix} \cdot kip \qquad P_{tot} := \sum P_i = 177.725 \cdot kip$$

Cracking Moment:

$y_t := \frac{h}{2} \qquad y_b := \frac{-h}{2}$

$$M_{cr} := -\left(\frac{P_{tot}}{A_p} + f_{rp}\right) \cdot \frac{I_p}{y_b} = 571.45 \cdot kip \cdot in$$

$f_b := f_{rp} \qquad f_t := \frac{-P_{tot}}{A_p} - \frac{M_{cr} \cdot y_t}{I_p} = -3.218 \cdot ksi$

$\varepsilon_b := \frac{f_b}{E_p} = 1.316 \times 10^{-4} \qquad \varepsilon_t := \frac{f_t}{E_p} = -5.646 \times 10^{-4}$

$$\phi_{cr} := \frac{\varepsilon_b - \varepsilon_t}{h} = 5.802 \times 10^{-5} \cdot \frac{rad}{in}$$

Ultimate Moment Capacity:

using Todeschini stress block:

$f'_c := .9 \cdot f'_{cp} = 9 \cdot ksi$ $\quad e_0 := 1.71 \cdot \frac{f'_{cp}}{E_p} = 3 \times 10^{-3}$ $\quad e_u := .003$

$e_{tf} := .003$ specified strain in top fiber

$$\beta_1 := \frac{\ln\left[1 + \left(\frac{e_{tf}}{e_0}\right)^2\right]}{\frac{e_{tf}}{e_0}} = 0.693 \qquad k_2 := 1 - 2 \cdot \frac{\left(\frac{e_{tf}}{e_0} - \operatorname{atan}\left(\frac{e_{tf}}{e_0}\right)\right)}{\left(\frac{e_{tf}}{e_0}\right)^2 \cdot \beta_1} = 0.381$$

$e_{se} := \frac{f_{se}}{E_{ps}} = 4.017 \times 10^{-3}$ $\quad e_{ce} := \frac{-P_{tot}}{E_p \cdot A_p} = -2.165 \times 10^{-4}$

$c := 3.48in$ manual adjust

$C := \beta_1 \cdot f'_c \cdot c \cdot b = 260.512 \cdot kip$

$$e_c := \frac{e_{tf}}{c} \cdot (d_p - c) = \begin{pmatrix} -1.983 \times 10^{-4} \\ 1.382 \times 10^{-3} \\ 2.963 \times 10^{-3} \\ 4.543 \times 10^{-3} \end{pmatrix} \qquad e_s := e_c + e_{se} + e_{ce} = \begin{pmatrix} 3.602 \times 10^{-3} \\ 5.182 \times 10^{-3} \\ 6.763 \times 10^{-3} \\ 8.343 \times 10^{-3} \end{pmatrix}$$

note: <.0187 strain

$$index := round(e_s \cdot 10000) - 1 = \begin{pmatrix} 35 \\ 51 \\ 67 \\ 82 \end{pmatrix}$$ SS: stresses on stress-strain curve at 0.01% strai

$$f_s := \begin{bmatrix} SS(index_0) \\ SS(index_1) \\ SS(index_2) \\ SS(index_3) \end{bmatrix} = \begin{pmatrix} 86.97 \\ 125.331 \\ 163.043 \\ 194.655 \end{pmatrix} \cdot ksi$$

$i := 0..3$

$$P_i := f_{s_i} \cdot num_i \cdot A_{strand} \qquad P = \begin{pmatrix} 53.226 \\ 38.351 \\ 49.891 \\ 119.129 \end{pmatrix} \cdot kip$$

$T := f_s \cdot num \cdot A_{strand} = 260.597 \cdot kip$ $\quad C = 260.512 \cdot kip$ adjust c until T=C

$M_u := -C \cdot k_2 \cdot c + P \cdot d_p = 1.41 \times 10^3 \cdot kip \cdot in$

$$\phi_u := \frac{\left(e_{s_2} - e_{s_0}\right)}{d_{p_2} - d_{p_0}} = 8.621 \times 10^{-4} \cdot \frac{rad}{in}$$

1080 18x18 Pile, 5 ksi concrete

Pile properties:

$f'_{cp} := 5ksi \qquad b := 18in \qquad h := 18in$

$A_p := b \cdot h = 324 \cdot in^2 \qquad I_p := \frac{1}{12} \cdot b \cdot h^3 = 8.748 \times 10^3 \cdot in^4$

$f_{rp} := 7.5 \cdot \sqrt{(f'_{cp} \cdot psi)} = 0.53 \cdot ksi \qquad E_p := 57000 \cdot \sqrt{f'_{cp} \cdot psi} = 4.031 \times 10^3 \cdot ksi$

Strand Propeties:

$f_u := 270ksi \qquad f_{se} := .7 \cdot f_u = 189 \cdot ksi \qquad A_{strand} := .115in^2 \qquad cover := 3.25in$

$E_{ps} := 29500ksi$

Strand Layout, arranged by rows:

$$e_{mid} := \frac{h - 2 \cdot cover}{6} = 1.917 \cdot in$$

$$num := \begin{pmatrix} 4 \\ 2 \\ 2 \\ 4 \end{pmatrix} \qquad e_p := \begin{pmatrix} \frac{h}{2} - cover \\ e_{mid} \\ -e_{mid} \\ cover - \frac{h}{2} \end{pmatrix} = \begin{pmatrix} 5.75 \\ 1.917 \\ -1.917 \\ -5.75 \end{pmatrix} \cdot in \qquad d_p := -e_p + \frac{h}{2} = \begin{pmatrix} 3.25 \\ 7.083 \\ 10.917 \\ 14.75 \end{pmatrix} \cdot in$$

$$P_i := f_{se} \cdot num \cdot A_{strand} = \begin{pmatrix} 86.94 \\ 43.47 \\ 43.47 \\ 86.94 \end{pmatrix} \cdot kip \qquad P_{tot} := \sum P_i = 260.82 \cdot kip$$

Cracking Moment:

$y_t := \frac{h}{2} \qquad y_b := \frac{-h}{2}$

$$M_{cr} := -\left(\frac{P_{tot}}{A_p} + f_{rp}\right) \cdot \frac{I_p}{y_b} = 1.298 \times 10^3 \cdot kip \cdot in$$

$f_b := f_{rp} \qquad f_t := \frac{-P_{tot}}{A_p} - \frac{M_{cr} \cdot y_t}{I_p} = -2.14 \cdot ksi$

$\varepsilon_b := \frac{f_b}{E_p} = 1.316 \times 10^{-4} \qquad \varepsilon_t := \frac{f_t}{E_p} = -5.31 \times 10^{-4}$

$$\phi_{cr} := \frac{\varepsilon_b - \varepsilon_t}{h} = 3.681 \times 10^{-5} \cdot \frac{rad}{in}$$

Ultimate Moment Capacity:

using Todeschini stress block:

$f'_c := .9 \cdot f'_{cp} = 4.5 \cdot ksi$ $\quad e_0 := 1.71 \cdot \frac{f'_{cp}}{E_p} = 2.121 \times 10^{-3}$ $\quad e_u := .003$

$e_{tf} := .003$ specified strain in top fiber

$$\beta_1 := \frac{\ln\left[1 + \left(\frac{e_{tf}}{e_0}\right)^2\right]}{\frac{e_{tf}}{e_0}} = 0.777 \qquad k_2 := 1 - 2 \cdot \frac{\left(\frac{e_{tf}}{e_0} - \operatorname{atan}\left(\frac{e_{tf}}{e_0}\right)\right)}{\left(\frac{e_{tf}}{e_0}\right)^2 \cdot \beta_1} = 0.409$$

$e_{se} := \frac{f_{se}}{E_{ps}} = 6.407 \times 10^{-3}$ $\quad e_{ce} := \frac{-P_{tot}}{E_p \cdot A_p} = -1.997 \times 10^{-4}$

$c := 4.73in$ manual adjust

$C := \beta_1 \cdot f'_c \cdot c \cdot b = 297.629 \cdot kip$

$$e_c := \frac{e_{tf}}{c} \cdot (d_p - c) = \begin{pmatrix} -9.387 \times 10^{-4} \\ 1.493 \times 10^{-3} \\ 3.924 \times 10^{-3} \\ 6.355 \times 10^{-3} \end{pmatrix} \qquad e_s := e_c + e_{se} + e_{ce} = \begin{pmatrix} 5.268 \times 10^{-3} \\ 7.7 \times 10^{-3} \\ 0.01 \\ 0.013 \end{pmatrix}$$

note: <.06 strain

$$index := round(e_s \cdot 10000) - 1 = \begin{pmatrix} 52 \\ 76 \\ 100 \\ 125 \end{pmatrix}$$ SS: stresses on stress-strain curve at 0.01% str

$$f_s := \begin{bmatrix} SS(index_0) \\ SS(index_1) \\ SS(index_2) \\ SS(index_3) \end{bmatrix} = \begin{pmatrix} 153.724 \\ 223.703 \\ 251.701 \\ 255.945 \end{pmatrix} \cdot ksi \qquad i := 0..3 \qquad P_i := f_{s_i} \cdot num_i \cdot A_{strand} \qquad P = \begin{pmatrix} 70.713 \\ 51.452 \\ 57.891 \\ 117.735 \end{pmatrix} \cdot kip$$

$T := f_s \cdot num \cdot A_{strand} = 297.791 \cdot kip$ $\quad C = 297.629 \cdot kip$ adjust c until T=C

$M_u := -C \cdot k_2 \cdot c + P \cdot d_p = 2.387 \times 10^3 \cdot kip \cdot in$

$$\phi_u := \frac{\left(e_{s_2} - e_{s_0}\right)}{d_{p_2} - d_{p_0}} = 6.342 \times 10^{-4} \cdot \frac{rad}{in}$$

Yield Point (1.0% strain)

using Todeschini stress block:

$f''_c := .9 \cdot f'_{cp} = 4.5 \cdot ksi$ $\quad e_0 := 1.71 \cdot \frac{f'_{cp}}{E_p} = 2.121 \times 10^{-3}$ $\quad e_u := .003$

$e_{tf} := .0021$ specified strain in top fiber

$$\beta_1 := \frac{\ln\left[1 + \left(\frac{e_{tf}}{e_0}\right)^2\right]}{\frac{e_{tf}}{e_0}} = 0.69 \qquad k_2 := 1 - 2 \cdot \frac{\left(\frac{e_{tf}}{e_0} - \operatorname{atan}\left(\frac{e_{tf}}{e_0}\right)\right)}{\left(\frac{e_{tf}}{e_0}\right)^2 \cdot \beta_1} = 0.38$$

$e_{se} := \frac{f_{se}}{E_{ps}} = 6.407 \times 10^{-3}$ $\quad e_{ce} := \frac{-P_{tot}}{E_p \cdot A_p} = -1.997 \times 10^{-4}$

$c := 5.2in$ manual adjust

$C := \beta_1 \cdot f''_c \cdot c \cdot b = 290.641 \cdot kip$

$$e_c := \frac{e_{tf}}{c} \cdot (d_p - c) = \begin{pmatrix} -7.875 \times 10^{-4} \\ 7.606 \times 10^{-4} \\ 2.309 \times 10^{-3} \\ 3.857 \times 10^{-3} \end{pmatrix} \qquad e_s := e_c + e_{se} + e_{ce} = \begin{pmatrix} 5.42 \times 10^{-3} \\ 6.968 \times 10^{-3} \\ 8.516 \times 10^{-3} \\ 0.01 \end{pmatrix}$$

$$index := round(e_s \cdot 10000) - 1 = \begin{pmatrix} 53 \\ 69 \\ 84 \\ 100 \end{pmatrix}$$

$$f_s := \begin{bmatrix} SS(index_0) \\ SS(index_1) \\ SS(index_2) \\ SS(index_3) \end{bmatrix} = \begin{pmatrix} 156.973 \\ 204.877 \\ 239.406 \\ 251.701 \end{pmatrix} \cdot ksi \qquad i := 0..3 \qquad P_i := f_{s_i} \cdot num_i \cdot A_{strand} \qquad P = \begin{pmatrix} 72.207 \\ 47.122 \\ 55.063 \\ 115.783 \end{pmatrix} \cdot kip$$

$T := f_s \cdot num \cdot A_{strand} = 290.175 \cdot kip$ $\quad C = 290.641 \cdot kip$ adjust c until T=C

$M_y := -C \cdot k_2 \cdot c + P \cdot d_p = 2.303 \times 10^3 \cdot kip \cdot in$

$\phi_y := \frac{(e_{s_2} - e_{s_0})}{d_{p_2} - d_{p_0}} = 4.038 \times 10^{-4} \cdot \frac{rad}{in}$

1080 18x18 Pile, 10 ksi concrete

Pile properties:

$f'_{cp} := 10ksi \qquad b := 18in \qquad h := 18in$

$A_p := b \cdot h = 324 \cdot in^2 \qquad I_p := \frac{1}{12} \cdot b \cdot h^3 = 8.748 \times 10^3 \cdot in^4$

$f_{rp} := 7.5 \cdot \sqrt{(f'_{cp} \cdot psi)} = 0.75 \cdot ksi \qquad E_p := 57000 \cdot \sqrt{f'_{cp} \cdot psi} = 5.7 \times 10^3 \cdot ksi$

Strand Propeties:

$f_u := 270ksi \qquad f_{se} := .7 \cdot f_u = 189 \cdot ksi \qquad A_{strand} := .115in^2 \qquad cover := 3.25in$

$E_{ps} := 29500ksi$

Strand Layout, arranged by rows:

$$e_{mid} := \frac{h - 2 \cdot cover}{6} = 1.917 \cdot in$$

$$num := \begin{pmatrix} 4 \\ 2 \\ 2 \\ 4 \end{pmatrix} \qquad e_p := \begin{pmatrix} \frac{h}{2} - cover \\ e_{mid} \\ -e_{mid} \\ cover - \frac{h}{2} \end{pmatrix} = \begin{pmatrix} 5.75 \\ 1.917 \\ -1.917 \\ -5.75 \end{pmatrix} \cdot in \qquad d_p := -e_p + \frac{h}{2} = \begin{pmatrix} 3.25 \\ 7.083 \\ 10.917 \\ 14.75 \end{pmatrix} \cdot in$$

$$P_i := f_{se} \cdot num \cdot A_{strand} = \begin{pmatrix} 86.94 \\ 43.47 \\ 43.47 \\ 86.94 \end{pmatrix} \cdot kip \qquad P_{tot} := \sum P_i = 260.82 \cdot kip$$

Cracking Moment:

$y_t := \frac{h}{2} \qquad y_b := \frac{-h}{2}$

$$M_{cr} := -\left(\frac{P_{tot}}{A_p} + f_{rp}\right) \cdot \frac{I_p}{y_b} = 1.511 \times 10^3 \cdot kip \cdot in$$

$f_b := f_{rp} \qquad f_t := \frac{-P_{tot}}{A_p} - \frac{M_{cr} \cdot y_t}{I_p} = -2.36 \cdot ksi$

$\varepsilon_b := \frac{f_b}{E_p} = 1.316 \times 10^{-4} \qquad \varepsilon_t := \frac{f_t}{E_p} = -4.14 \times 10^{-4}$

$$\phi_{cr} := \frac{\varepsilon_b - \varepsilon_t}{h} = 3.031 \times 10^{-5} \cdot \frac{rad}{in}$$

Ultimate Moment Capacity:

using Todeschini stress block:

$f'_c := .9 \cdot f'_{cp} = 9 \cdot ksi$ $\quad e_0 := 1.71 \cdot \frac{f'_{cp}}{E_p} = 3 \times 10^{-3}$ $\quad e_u := .003$

$e_{tf} := .003$ specified strain in top fiber

$$\beta_1 := \frac{\ln\left[1 + \left(\frac{e_{tf}}{e_0}\right)^2\right]}{\frac{e_{tf}}{e_0}} = 0.693 \qquad k_2 := 1 - 2 \cdot \frac{\left(\frac{e_{tf}}{e_0} - \operatorname{atan}\left(\frac{e_{tf}}{e_0}\right)\right)}{\left(\frac{e_{tf}}{e_0}\right)^2 \cdot \beta_1} = 0.381$$

$e_{se} := \frac{f_{se}}{E_{ps}} = 6.407 \times 10^{-3}$ $\quad e_{ce} := \frac{-P_{tot}}{E_p \cdot A_p} = -1.412 \times 10^{-4}$

$c := 2.9in$ manual adjust

$C := \beta_1 \cdot f'_c \cdot c \cdot b = 325.641 \cdot kip$

$$e_c := \frac{e_{tf}}{c} \cdot (d_p - c) = \begin{pmatrix} 3.621 \times 10^{-4} \\ 4.328 \times 10^{-3} \\ 8.293 \times 10^{-3} \\ 0.012 \end{pmatrix} \qquad e_s := e_c + e_{se} + e_{ce} = \begin{pmatrix} 6.628 \times 10^{-3} \\ 0.011 \\ 0.015 \\ 0.019 \end{pmatrix}$$

note: <.06 strain

$$index := round(e_s \cdot 10000) - 1 = \begin{pmatrix} 65 \\ 105 \\ 145 \\ 184 \end{pmatrix}$$

SS: stresses on stress-strain curve at 0.01% strain

$$f_s := \begin{bmatrix} SS(index_0) \\ SS(index_1) \\ SS(index_2) \\ SS(index_3) \end{bmatrix} = \begin{pmatrix} 193.092 \\ 253.086 \\ 256.92 \\ 258.741 \end{pmatrix} \cdot ksi$$

$i := 0..3$

$P_i := f_{s_i} \cdot num_i \cdot A_{strand}$ $\quad P = \begin{pmatrix} 88.822 \\ 58.21 \\ 59.092 \\ 119.021 \end{pmatrix} \cdot kip$

$T := f_s \cdot num \cdot A_{strand} = 325.145 \cdot kip$ $\quad C = 325.641 \cdot kip$ adjust c until T=C

$M_u := -C \cdot k_2 \cdot c + P \cdot d_p = 2.742 \times 10^3 \cdot kip \cdot in$

$\phi_u := \frac{(e_{s_2} - e_{s_0})}{d_{p_2} - d_{p_0}} = 1.034 \times 10^{-3} \cdot \frac{rad}{in}$

Yield Point (1.0% strain)

using Todeschini stress block:

$f'_c := .9 \cdot f'_{cp} = 9 \cdot ksi$ $\quad e_0 := 1.71 \cdot \frac{f'_{cp}}{E_p} = 3 \times 10^{-3}$ $\quad e_u := .003$

$e_{tf} := .0015$ specified strain in top fiber

$\beta_1 := \frac{\ln\left[1 + \left(\frac{e_{tf}}{e_0}\right)^2\right]}{\frac{e_{tf}}{e_0}} = 0.446$ $\quad k_2 := 1 - 2 \cdot \frac{\left(\frac{e_{tf}}{e_0} - \operatorname{atan}\left(\frac{e_{tf}}{e_0}\right)\right)}{\left(\frac{e_{tf}}{e_0}\right)^2 \cdot \beta_1} = 0.348$

$e_{se} := \frac{f_{se}}{E_{ps}} = 6.407 \times 10^{-3}$ $\quad e_{ce} := \frac{-P_{tot}}{E_p \cdot A_p} = -1.412 \times 10^{-4}$

$c := 4.15in$ manual adjust

$C := \beta_1 \cdot f'_c \cdot c \cdot b = 300.039 \cdot kip$

$e_c := \frac{e_{tf}}{c} \cdot (d_p - c) = \begin{pmatrix} -3.253 \times 10^{-4} \\ 1.06 \times 10^{-3} \\ 2.446 \times 10^{-3} \\ 3.831 \times 10^{-3} \end{pmatrix}$ $\quad e_s := e_c + e_{se} + e_{ce} = \begin{pmatrix} 5.94 \times 10^{-3} \\ 7.326 \times 10^{-3} \\ 8.711 \times 10^{-3} \\ 0.01 \end{pmatrix}$

$index := round(e_s \cdot 10000) - 1 = \begin{pmatrix} 58 \\ 72 \\ 86 \\ 100 \end{pmatrix}$

$f_s := \begin{bmatrix} SS(index_0) \\ SS(index_1) \\ SS(index_2) \\ SS(index_3) \end{bmatrix} = \begin{pmatrix} 172.004 \\ 213.154 \\ 242.047 \\ 251.701 \end{pmatrix} \cdot ksi$ $\quad i := 0..3$ $\quad P_i := f_{s_i} \cdot num_i \cdot A_{strand}$ $\quad P = \begin{pmatrix} 79.122 \\ 49.026 \\ 55.671 \\ 115.783 \end{pmatrix} \cdot kip$

$T := f_s \cdot num \cdot A_{strand} = 299.601 \cdot kip$ $\quad C = 300.039 \cdot kip$ adjust c until T=C

$M_y := -C \cdot k_2 \cdot c + P \cdot d_p = 2.486 \times 10^3 \cdot kip \cdot in$

$\phi_y := \frac{(e_{s_2} - e_{s_0})}{d_{p_2} - d_{p_0}} = 3.614 \times 10^{-4} \cdot \frac{rad}{in}$

2205 18x18 Pile, 5 ksi concrete

Pile properties:

$f'_{cp} := 5ksi \qquad b := 18in \qquad h := 18in$

$A_p := b \cdot h = 324 \cdot in^2 \qquad I_p := \frac{1}{12} \cdot b \cdot h^3 = 8.748 \times 10^3 \cdot in^4$

$f_{rp} := 7.5 \cdot \sqrt{(f'_{cp} \cdot psi)} = 0.53 \cdot ksi \qquad E_p := 57000 \cdot \sqrt{f'_{cp} \cdot psi} = 4.031 \times 10^3 \cdot ksi$

Strand Propeties:

$f_u := 242ksi \qquad f_{se} := .7 \cdot f_u = 169.4 \cdot ksi \qquad A_{strand} := .153in^2 \qquad cover := 3.25in$

$E_{ps} := 23500ksi$

Strand Layout, arranged by rows:

$$e_{mid} := \frac{h - 2 \cdot cover}{6} = 1.917 \cdot in$$

$$num := \begin{pmatrix} 4 \\ 2 \\ 2 \\ 4 \end{pmatrix} \qquad e_p := \begin{pmatrix} \frac{h}{2} - cover \\ e_{mid} \\ -e_{mid} \\ cover - \frac{h}{2} \end{pmatrix} = \begin{pmatrix} 5.75 \\ 1.917 \\ -1.917 \\ -5.75 \end{pmatrix} \cdot in \qquad d_p := -e_p + \frac{h}{2} = \begin{pmatrix} 3.25 \\ 7.083 \\ 10.917 \\ 14.75 \end{pmatrix} \cdot in$$

$$P_i := f_{se} \cdot num \cdot A_{strand} = \begin{pmatrix} 103.673 \\ 51.836 \\ 51.836 \\ 103.673 \end{pmatrix} \cdot kip \qquad P_{tot} := \sum P_i = 311.018 \cdot kip$$

Cracking Moment:

$y_t := \frac{h}{2} \qquad y_b := \frac{-h}{2}$

$$M_{cr} := -\left(\frac{P_{tot}}{A_p} + f_{rp}\right) \cdot \frac{I_p}{y_b} = 1.449 \times 10^3 \cdot kip \cdot in$$

$f_b := f_{rp} \qquad f_t := \frac{-P_{tot}}{A_p} - \frac{M_{cr} \cdot y_t}{I_p} = -2.45 \cdot ksi$

$\varepsilon_b := \frac{f_b}{E_p} = 1.316 \times 10^{-4} \qquad \varepsilon_t := \frac{f_t}{E_p} = -6.079 \times 10^{-4}$

$$\phi_{cr} := \frac{\varepsilon_b - \varepsilon_t}{h} = 4.108 \times 10^{-5} \cdot \frac{rad}{in}$$

Ultimate Moment Capacity:

using Todeschini stress block:

$f'_c := .9 \cdot f'_{cp} = 4.5 \cdot ksi$ $\quad e_0 := 1.71 \cdot \frac{f'_{cp}}{E_p} = 2.121 \times 10^{-3}$ $\quad e_u := .003$

$e_{tf} := .003$ specified strain in top fiber

$$\beta_1 := \frac{\ln\left[1 + \left(\frac{e_{tf}}{e_0}\right)^2\right]}{\frac{e_{tf}}{e_0}} = 0.777 \qquad k_2 := 1 - 2 \cdot \frac{\left(\frac{e_{tf}}{e_0} - \operatorname{atan}\left(\frac{e_{tf}}{e_0}\right)\right)}{\left(\frac{e_{tf}}{e_0}\right)^2 \cdot \beta_1} = 0.409$$

$e_{se} := \frac{f_{se}}{E_{ps}} = 7.209 \times 10^{-3}$ $\quad e_{ce} := \frac{-P_{tot}}{E_p \cdot A_p} = -2.382 \times 10^{-4}$

$c := 5.48in$ manual adjust

$C := \beta_1 \cdot f'_c \cdot c \cdot b = 344.822 \cdot kip$

$$e_c := \frac{e_{tf}}{c} \cdot (d_p - c) = \begin{pmatrix} -1.221 \times 10^{-3} \\ 8.777 \times 10^{-4} \\ 2.976 \times 10^{-3} \\ 5.075 \times 10^{-3} \end{pmatrix} \qquad e_s := e_c + e_{se} + e_{ce} = \begin{pmatrix} 5.75 \times 10^{-3} \\ 7.848 \times 10^{-3} \\ 9.947 \times 10^{-3} \\ 0.012 \end{pmatrix}$$

note: <.0160 strain

$$index := round(e_s \cdot 10000) - 1 = \begin{pmatrix} 56 \\ 77 \\ 98 \\ 119 \end{pmatrix}$$

SS: stresses on stress-strain curve at 0.01% strain

$$f_s := \begin{bmatrix} SS(index_0) \\ SS(index_1) \\ SS(index_2) \\ SS(index_3) \end{bmatrix} = \begin{pmatrix} 134.885 \\ 179.682 \\ 212.76 \\ 230.634 \end{pmatrix} \cdot ksi \qquad i := 0..3 \qquad P_i := f_{s_i} \cdot num_i \cdot A_{strand} \qquad P = \begin{pmatrix} 82.55 \\ 54.983 \\ 65.105 \\ 141.148 \end{pmatrix} \cdot kip$$

$T := f_s \cdot num \cdot A_{strand} = 343.785 \cdot kip$ $\quad C = 344.822 \cdot kip$ adjust c until T=C

$M_u := -C \cdot k_2 \cdot c + P \cdot d_p = 2.677 \times 10^3 \cdot kip \cdot in$

$\phi_u := \frac{(e_{s_2} - e_{s_0})}{d_{p_2} - d_{p_0}} = 5.474 \times 10^{-4} \cdot \frac{rad}{in}$

2205 18x18 Pile, 10 ksi concrete

Pile properties:

$f'_{cp} := 10ksi \qquad b := 18in \qquad h := 18in$

$A_p := b \cdot h = 324 \cdot in^2 \qquad I_p := \frac{1}{12} \cdot b \cdot h^3 = 8.748 \times 10^3 \cdot in^4$

$f_{rp} := 7.5 \cdot \sqrt{(f'_{cp} \cdot psi)} = 0.75 \cdot ksi \qquad E_p := 57000 \cdot \sqrt{f'_{cp} \cdot psi} = 5.7 \times 10^3 \cdot ksi$

Strand Propeties:

$f_u := 242ksi \qquad f_{se} := .7 \cdot f_u = 169.4 \cdot ksi \qquad A_{strand} := .153in^2 \qquad cover := 3.25in$

$E_{ps} := 23500ksi$

Strand Layout, arranged by rows:

$$e_{mid} := \frac{h - 2 \cdot cover}{6} = 1.917 \cdot in$$

$$num := \begin{pmatrix} 4 \\ 2 \\ 2 \\ 4 \end{pmatrix} \qquad e_p := \begin{pmatrix} \frac{h}{2} - cover \\ e_{mid} \\ -e_{mid} \\ cover - \frac{h}{2} \end{pmatrix} = \begin{pmatrix} 5.75 \\ 1.917 \\ -1.917 \\ -5.75 \end{pmatrix} \cdot in \qquad d_p := -e_p + \frac{h}{2} = \begin{pmatrix} 3.25 \\ 7.083 \\ 10.917 \\ 14.75 \end{pmatrix} \cdot in$$

$$P_i := f_{se} \cdot num \cdot A_{strand} = \begin{pmatrix} 103.673 \\ 51.836 \\ 51.836 \\ 103.673 \end{pmatrix} \cdot kip \qquad P_{tot} := \sum P_i = 311.018 \cdot kip$$

Cracking Moment:

$y_t := \frac{h}{2} \qquad y_b := \frac{-h}{2}$

$$M_{cr} := -\left(\frac{P_{tot}}{A_p} + f_{rp}\right) \cdot \frac{I_p}{y_b} = 1.662 \times 10^3 \cdot kip \cdot in$$

$f_b := f_{rp} \qquad f_t := \frac{-P_{tot}}{A_p} - \frac{M_{cr} \cdot y_t}{I_p} = -2.67 \cdot ksi$

$\varepsilon_b := \frac{f_b}{E_p} = 1.316 \times 10^{-4} \qquad \varepsilon_t := \frac{f_t}{E_p} = -4.684 \times 10^{-4}$

$$\phi_{cr} := \frac{\varepsilon_b - \varepsilon_t}{h} = 3.333 \times 10^{-5} \cdot \frac{rad}{in}$$

Ultimate Moment Capacity:

using Todeschini stress block:

$f'_c := .9 \cdot f'_{cp} = 9 \cdot ksi$ $\quad e_0 := 1.71 \cdot \frac{f'_{cp}}{E_p} = 3 \times 10^{-3}$ $\quad e_u := .003$

$e_{tf} := .0028$ specified strain in top fiber

$$\beta_1 := \frac{\ln\left[1 + \left(\frac{e_{tf}}{e_0}\right)^2\right]}{\frac{e_{tf}}{e_0}} = 0.671 \qquad k_2 := 1 - 2 \cdot \frac{\left(\frac{e_{tf}}{e_0} - \operatorname{atan}\left(\frac{e_{tf}}{e_0}\right)\right)}{\left(\frac{e_{tf}}{e_0}\right)^2 \cdot \beta_1} = 0.376$$

$e_{se} := \frac{f_{se}}{E_{ps}} = 7.209 \times 10^{-3}$ $\quad e_{ce} := \frac{-P_{tot}}{E_p \cdot A_p} = -1.684 \times 10^{-4}$

$c := 3.5\,lin$ manual adjust

$C := \beta_1 \cdot f'_c \cdot c \cdot b = 381.706 \cdot kip$

$$e_c := \frac{e_{tf}}{c} \cdot (d_p - c) = \begin{pmatrix} -2.074 \times 10^{-4} \\ 2.851 \times 10^{-3} \\ 5.908 \times 10^{-3} \\ 8.966 \times 10^{-3} \end{pmatrix} \qquad e_s := e_c + e_{se} + e_{ce} = \begin{pmatrix} 6.833 \times 10^{-3} \\ 9.891 \times 10^{-3} \\ 0.013 \\ 0.016 \end{pmatrix}$$

note: <.0160 strain

$$index := round(e_s \cdot 10000) - 1 = \begin{pmatrix} 67 \\ 98 \\ 128 \\ 159 \end{pmatrix}$$

SS: stresses on stress-strain curve at 0.01% strain

$$f_s := \begin{bmatrix} SS(index_0) \\ SS(index_1) \\ SS(index_2) \\ SS(index_3) \end{bmatrix} = \begin{pmatrix} 158.696 \\ 212.76 \\ 235.434 \\ 239.513 \end{pmatrix} \cdot ksi \qquad i := 0..3 \qquad P_i := f_{s_i} \cdot num_i \cdot A_{strand} \qquad P = \begin{pmatrix} 97.122 \\ 65.105 \\ 72.043 \\ 146.582 \end{pmatrix} \cdot kip$$

$T := f_s \cdot num \cdot A_{strand} = 380.851 \cdot kip$ $\quad C = 381.706 \cdot kip$ adjust c until T=C

$M_u := -C \cdot k_2 \cdot c + P \cdot d_p = 3.221 \times 10^3 \cdot kip \cdot in$

$$\phi_u := \frac{\left(e_{s_2} - e_{s_0}\right)}{d_{p_2} - d_{p_0}} = 7.977 \times 10^{-4} \cdot \frac{rad}{in}$$

At Yield:

using Todeschini stress block:

$f'_c := .9 \cdot f'_{cp} = 9 \cdot ksi$ $\quad e_0 := 1.71 \cdot \frac{f'_{cp}}{E_p} = 3 \times 10^{-3}$ $\quad e_u := .003$

$e_{tf} := .00195$ specified strain in top fiber

$$\beta_1 := \frac{\ln\left[1 + \left(\frac{e_{tf}}{e_0}\right)^2\right]}{\frac{e_{tf}}{e_0}} = 0.542 \qquad k_2 := 1 - 2 \cdot \frac{\left(\frac{e_{tf}}{e_0} - \operatorname{atan}\left(\frac{e_{tf}}{e_0}\right)\right)}{\left(\frac{e_{tf}}{e_0}\right)^2 \cdot \beta_1} = 0.357$$

$e_{se} := \frac{f_{se}}{E_{ps}} = 7.209 \times 10^{-3}$ $\quad e_{ce} := \frac{-P_{tot}}{E_p \cdot A_p} = -1.684 \times 10^{-4}$

$c := 4.1in$ manual adjust

$C := \beta_1 \cdot f'_c \cdot c \cdot b = 360.115 \cdot kip$

$$e_c := \frac{e_{tf}}{c} \cdot (d_p - c) = \begin{pmatrix} -4.043 \times 10^{-4} \\ 1.419 \times 10^{-3} \\ 3.242 \times 10^{-3} \\ 5.065 \times 10^{-3} \end{pmatrix} \qquad e_s := e_c + e_{se} + e_{ce} = \begin{pmatrix} 6.636 \times 10^{-3} \\ 8.459 \times 10^{-3} \\ 0.01 \\ 0.012 \end{pmatrix}$$

note: <.0160 strain

$$index := round(e_s \cdot 10000) - 1 = \begin{pmatrix} 65 \\ 84 \\ 102 \\ 120 \end{pmatrix}$$

$$f_s := \begin{bmatrix} SS(index_0) \\ SS(index_1) \\ SS(index_2) \\ SS(index_3) \end{bmatrix} = \begin{pmatrix} 154.728 \\ 191.745 \\ 217.626 \\ 230.738 \end{pmatrix} \cdot ksi \qquad i := 0..3 \qquad P_i := f_{s_i} \cdot num_i \cdot A_{strand} \qquad P = \begin{pmatrix} 94.694 \\ 58.674 \\ 66.594 \\ 141.212 \end{pmatrix} \cdot kip$$

$T := f_s \cdot num \cdot A_{strand} = 361.173 \cdot kip$ $\quad C = 360.115 \cdot kip$ adjust c until T=C

$M_y := -C \cdot k_2 \cdot c + P \cdot d_p = 3.006 \times 10^3 \cdot kip \cdot in$

$\phi_y := \frac{(e_{s_2} - e_{s_0})}{d_{p_2} - d_{p_0}} = 4.756 \times 10^{-4} \cdot \frac{rad}{in}$

E.2 Load-Deflection Calculations

Load-deflection calculations were performed utilizing the results from moment-curvature analysis. At each point where moment-curvature was calculated, a corresponding load and deflection were calculated for the 4-point bending test setup. As outlined in Figures E.1 to E.4, moment diagrams were calculated along with corresponding curvature diagrams for the simply supported beam. Midspan deflection was calculated using the moment-area method about the pin support for the discrete sections shown in figure E.1 to E.4. The contributions from each of these sections were added together to calculate total deflection. These calculations are given in the appended tables.

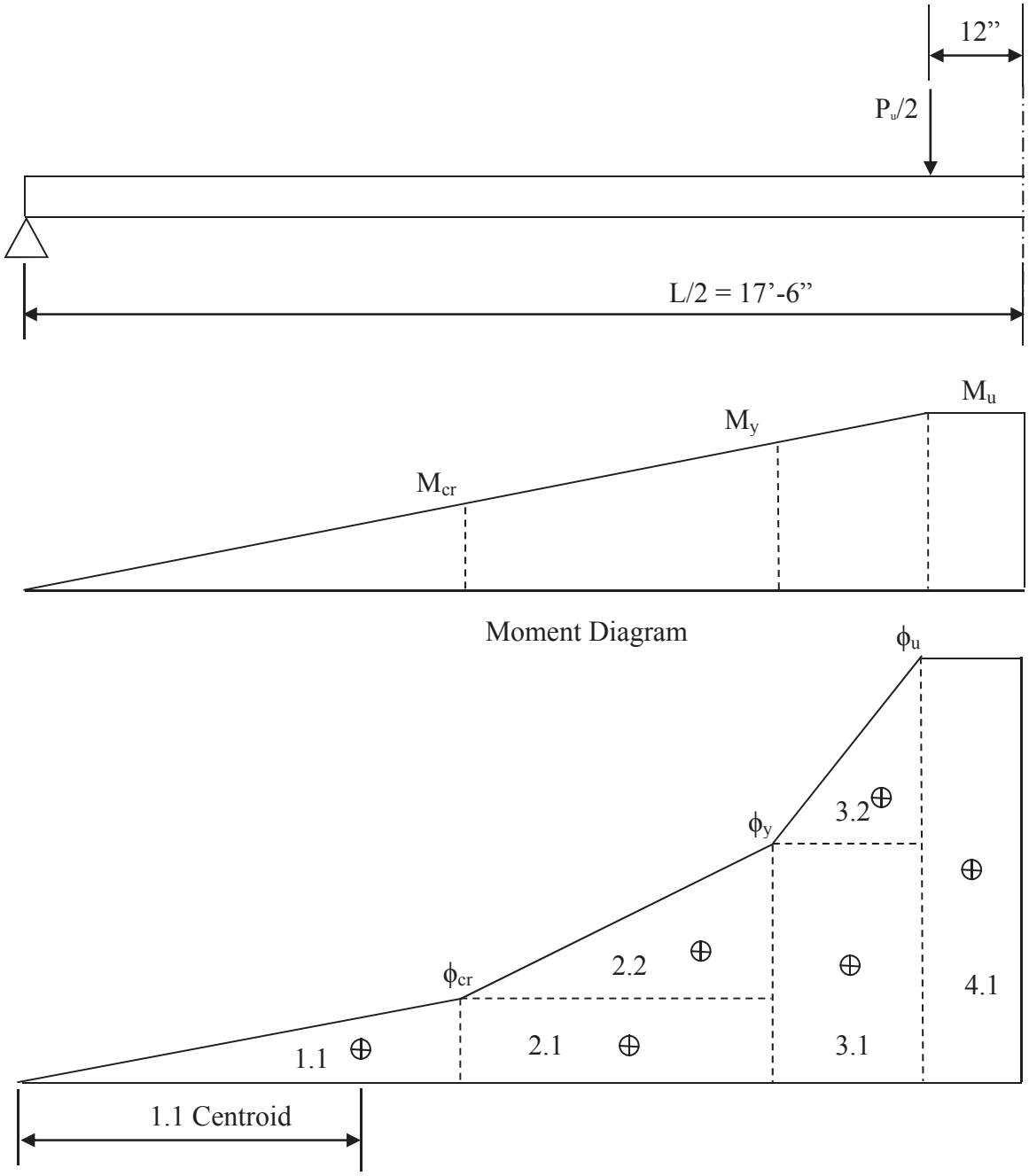

Figure E.1 Load-deflection calculation methodology for ultimate condition with yield point

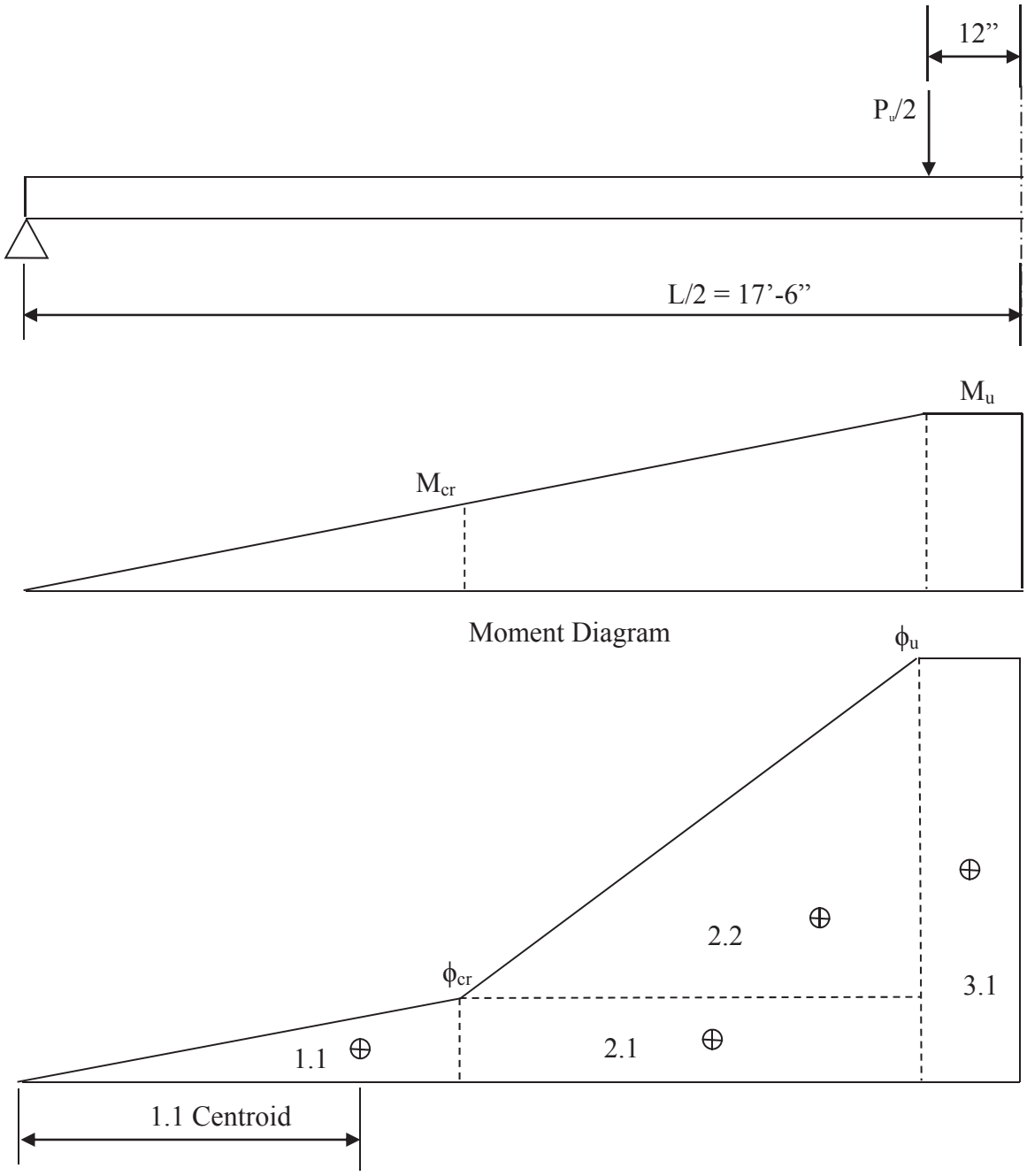

Figure E.2 Load-deflection calculation methodology for ultimate condition without yield point

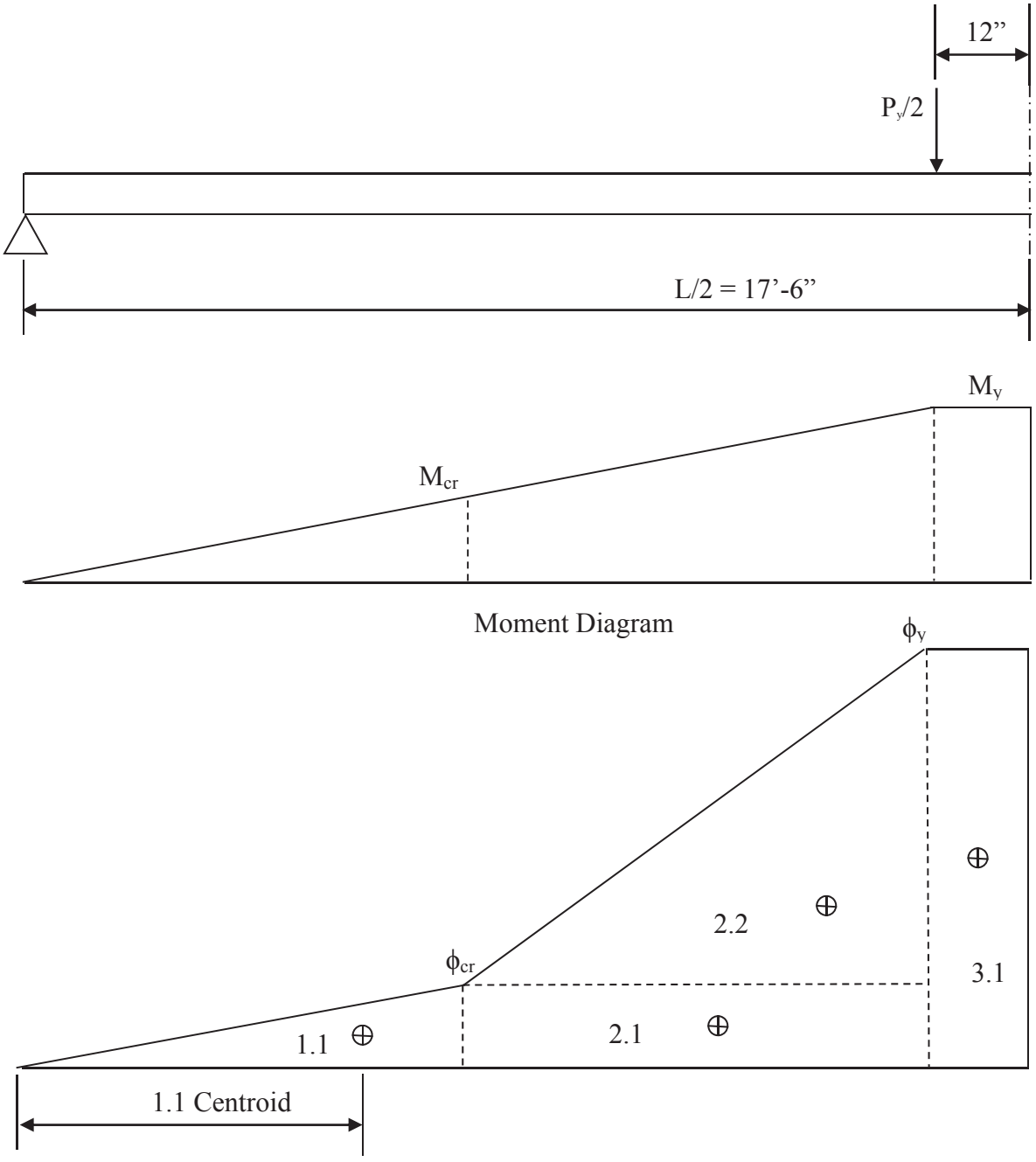

Figure E.3 Load-deflection calculation methodology for yield condition

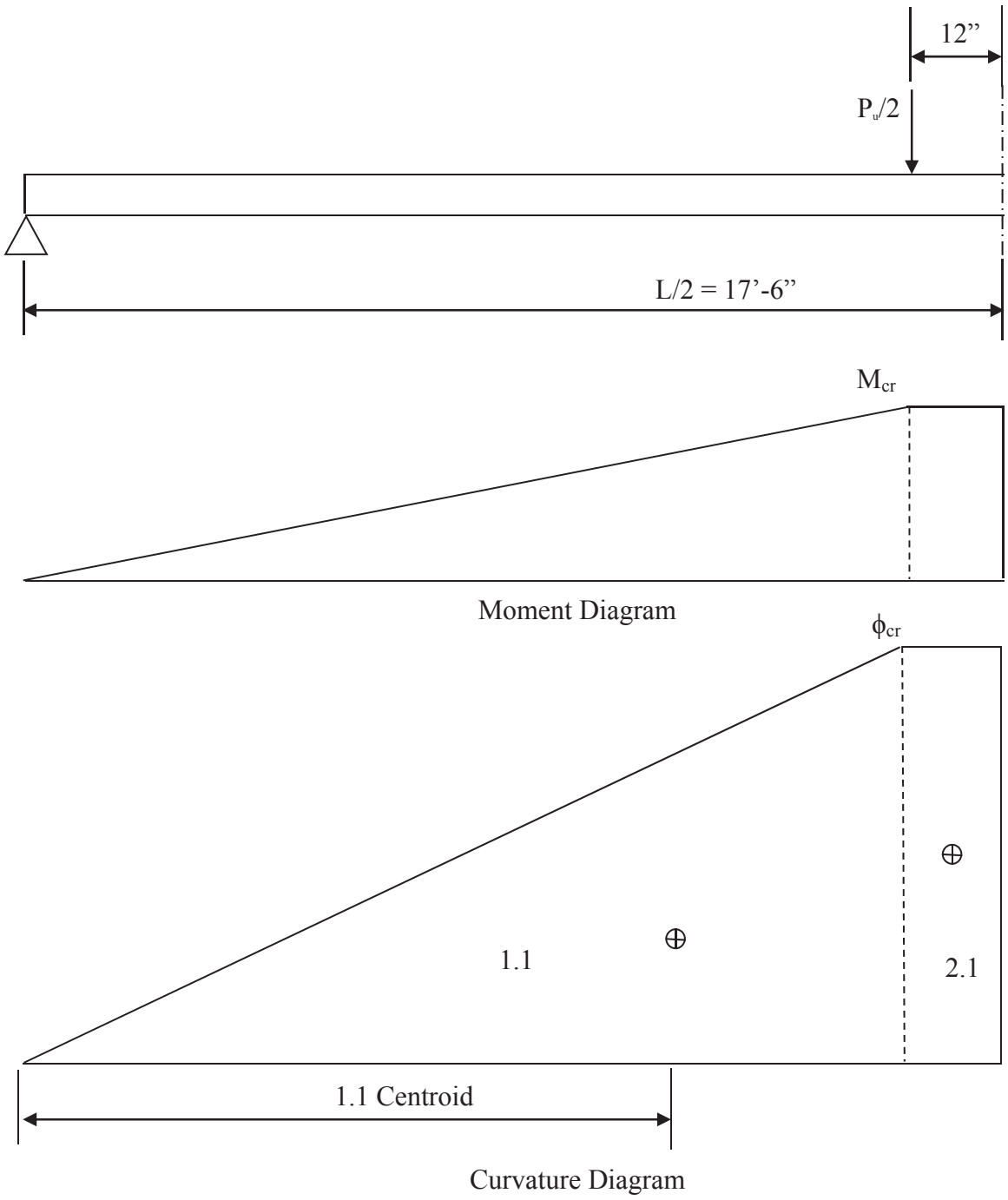

Figure E.4 Load-deflection calculation methodology for cracking condition

Table E.1 Load-deflection calculations for 12-in. sq. piles with 1080 strand, f_c' = 5 ksi

	Crack	Ultimate
Moment (kip*in)	500	853
Phi (rad/in)	7.2E-05	0.00068
Hinge Location (in)	-	-
Yield Location (in)	-	198.0
Crack Location (in)	7.21087	116.1
Delta Contrib. (in)		
1.1	0.000	0.323
2.1	0.000	0.925
2.2	-	4.287
3.1	-	1.677
Delta (in)	132.000	0.000
P (kip)	0.000	0.000

Table E.2 Load-deflection calculations for 12-in. sq. piles with 1080 strand, f_c' = 10 ksi

	Crack	Yield	Ultimate
Moment (kip*in)	563	1052	1103
Phi (rad/in)	5.7E-05	0.0006981	0.00106
Hinge Location (in)	-	-	198
Yield Location (in)	-	198.0	188.845
Crack Location (in)	198	106.0	101.064
Delta Contrib. (in)			
1.1	0.748	0.214	0.195
2.1	0.140	0.801	0.728
2.2	-	4.934	4.489
3.1	-	1.709	1.236
3.2	-	-	0.646
4.1	-	-	2.595
Delta (in)	0.888	7.658	9.889
P (kip)	5.687	10.626	11.141

Table E.3 Load-deflection calculations for 12-in. sq. piles with 2304 strand, f_c' = 5 ksi

	Crack	Ultimate
Moment (kip*in)	508	954
Phi (rad/in)	7.297E-05	0.00063
Hinge Location (in)	-	-
Yield Location (in)	-	198.0
Crack Location (in)	198	105.4
Delta Contrib. (in)		
1.1	0.954	0.270
2.1	0.179	1.025
2.2	-	4.322
3.1	-	1.546
Delta (in)	1.132	7.163
P (kip)	5.131	9.636

Table E.4 Load-deflection calculations for 12-in. sq. piles with 2304 strand, f_c' = 10 ksi

	Crack	Ultimate
Moment (kip*in)	571	1410
Phi (rad/in)	5.8E-05	0.0008621
Hinge Location (in)	-	-
Yield Location (in)	-	198.0
Crack Location (in)	198	80.2
Delta Contrib. (in)		
1.1	0.758	0.124
2.1	0.142	0.951
2.2	-	7.518
3.1	-	2.110
Delta (in)	0.900	10.704
P (kip)	5.768	14.242

Table E.5 Load-deflection calculations for 18-in. sq. piles with 1080 strand, f_c' = 5 ksi

	Crack	Yield	Ultimate
Moment (kip*in)	1298	2303	2387
Phi (rad/in)	3.7E-05	0.0004	0.00063
Hinge Location (in)	-	-	198
Yield Location (in)	-	198.0	191.032
Crack Location (in)	198	111.6	107.668
Delta Contrib. (in)			
1.1	0.481	0.153	0.142
2.1	0.090	0.492	0.458
2.2	-	2.683	2.497
3.1	-	0.989	0.547
3.2	-	-	0.314
4.1	-	-	1.553
Delta (in)	0.571	4.316	5.512
P (kip)	13.111	23.263	24.111

Table E.6 Load-deflection calculations for 18-in. sq. piles with 1080 strand, f_c' = 10 ksi

	Crack	Yield	Ultimate
Moment (kip*in)	1511	2486	2742
Phi (rad/in)	3E-05	0.0003614	0.00103
Hinge Location (in)	-	-	198
Yield Location (in)	-	198.0	179.514
Crack Location (in)	198	120.3	109.109
Delta Contrib. (in)			
1.1	0.396	0.146	0.120
2.1	0.074	0.375	0.308
2.2	-	2.213	1.819
3.1	-	0.885	1.261
3.2	-	-	2.385
4.1	-	-	2.531
Delta (in)	0.470	3.618	8.424
P (kip)	15.263	25.111	27.697

Table E.7 Load-deflection calculations for 18-in. sq. piles with 2205 strand, f_c' = 5 ksi

	Crack	Ultimate
Moment (kip*in)	1316	2677
Phi (rad/in)	4.108E-05	0.00055
Hinge Location (in)	-	-
Yield Location (in)	-	198.0
Crack Location (in)	198	97.3
Delta Contrib. (in)		
1.1	0.537	0.130
2.1	0.101	0.611
2.2	-	4.191
3.1	-	1.340
Delta (in)	0.637	6.271
P (kip)	13.293	27.040

Table E.8 Load-deflection calculations for 18-in. sq. piles with 2205 strand, f_c' = 10 ksi

	Crack	Yield	Ultimate
Moment (kip*in)	1662	3006	3221
Phi (rad/in)	3.333E-05	0.0004756	0.0008
Hinge Location (in)	-	-	198
Yield Location (in)	-	198.0	184.784
Crack Location (in)	198	109.5	102.166
Delta Contrib. (in)			
1.1	0.436	0.133	0.116
2.1	0.082	0.454	0.395
2.2	-	3.298	2.873
3.1	-	1.164	1.203
3.2	-	-	0.824
4.1	-	-	1.953
Delta (in)	0.517	5.049	7.364
P (kip)	16.788	30.364	32.535

APPENDIX F

DEVELOPMENT LENGTH TESTING CALCULATIONS

The calculations for determining the setup for development length testing are included in this section.

1080 Pile with Topping for Development and Transfer Length Testing

Pile properties:

$f'_{cp} := 5ksi \qquad b := 12in \qquad h := 12in$

$A_p := b \cdot h = 144 \cdot in^2 \qquad I_p := \frac{1}{12} \cdot b \cdot h^3 = 1.728 \times 10^3 \cdot in^4$

$f_{rp} := 7.5 \cdot \sqrt{(f'_{cp} \cdot psi)} = 0.53 \cdot ksi \qquad E_p := 57000 \cdot \sqrt{f'_{cp} \cdot psi} = 4.031 \times 10^3 \cdot ksi$

Topping Properties:

$f'_{ct} := 6ksi \qquad h_{tot} := 42in \qquad h_t := h_{tot} - h = 30 \cdot in \qquad b_2 := 24in$

$f_{rt} := 7.5 \cdot \sqrt{(f'_{ct} \cdot psi)} = 0.581 \cdot ksi \qquad E_t := 57000 \cdot \sqrt{f'_{ct} \cdot psi} = 4.415 \times 10^3 \cdot ksi$

Strand Propeties:

$f_u := 281.7ksi \qquad f_{se} := .7 \cdot f_u = 197.19 \cdot ksi \qquad A_{strand} := .115in^2 \qquad cover := 3.25in$

$E_{ps} := 28500ksi$

Strand Layout, arranged by rows:

$$num := \begin{pmatrix} 3 \\ 2 \\ 3 \end{pmatrix} \qquad e_p := \begin{pmatrix} \frac{h}{2} - cover \\ 0 \\ cover - \frac{h}{2} \end{pmatrix} = \begin{pmatrix} 2.75 \\ 0 \\ -2.75 \end{pmatrix} \cdot in \qquad d_{pt} := -e_p + h_{tot} - \frac{h}{2} = \begin{pmatrix} 33.25 \\ 36 \\ 38.75 \end{pmatrix} \cdot in$$

$$P_i := f_{se} \cdot num \cdot A_{strand} = \begin{pmatrix} 68.031 \\ 45.354 \\ 68.031 \end{pmatrix} \cdot kip \qquad P_{itot} := \sum P_i = 181.415 \cdot kip$$

Shear Friction:

$$P_{max} := \sum\left(f_u \cdot num \cdot A_{strand}\right) = 259.164 \cdot kip$$

$a := 7ft$ shear span $\mu := 1.0$

Rebar:

$f_y := 60ksi$ $A_4 := .31in^2$ $A_5 := .44in^2$

$$A_{vtot} := \frac{\mu \cdot P_{max}}{f_y} = 4.319 \cdot in^2$$

$$s_4 := \frac{a \cdot A_4}{A_{vtot}} = 6.029 \cdot in \qquad s_5 := \frac{a \cdot A_5}{A_{vtot}} = 8.557 \cdot in$$

minimum req. spacing for #4 and #5 bars

Ultimate Moment Capacity of Composite Section:

using Todeschini stress block:

$$f'_c := .9 \cdot f'_{ct} = 5.4 \cdot ksi \qquad e_0 := 1.71 \cdot \frac{f'_{ct}}{E_t} = 2.324 \times 10^{-3} \qquad e_u := .003$$

$e_{tf} := .003$ specified strain in top fiber

$$\beta_1 := \frac{\ln\left[1 + \left(\frac{e_{tf}}{e_0}\right)^2\right]}{\frac{e_{tf}}{e_0}} = 0.76 \qquad k_2 := 1 - 2 \cdot \frac{\left(\frac{e_{tf}}{e_0} - \operatorname{atan}\left(\frac{e_{tf}}{e_0}\right)\right)}{\left(\frac{e_{tf}}{e_0}\right)^2 \cdot \beta_1} = 0.401$$

$$e_{se} := \frac{f_{se}}{E_{ps}} = 6.919 \times 10^{-3} \qquad e_{ce} := \frac{-P_{itot}}{E_t \cdot A_p} = -2.853 \times 10^{-4}$$

$c := 2.55in$ manual adjust

$C := \beta_1 \cdot f'_c \cdot c \cdot b_2 = 251.081 \cdot kip$

$$e_c := \frac{e_{tf}}{c} \cdot \left(d_{pt} - c\right) = \begin{pmatrix} 0.036 \\ 0.039 \\ 0.043 \end{pmatrix} \qquad e_s := e_c + e_{se} + e_{ce} = \begin{pmatrix} 0.043 \\ 0.046 \\ 0.049 \end{pmatrix}$$

note: bottom strand >.02 strain

$$\text{index} := \text{round}\left(e_s \cdot 10000\right) - 1 = \begin{pmatrix} 427 \\ 459 \\ 491 \end{pmatrix}$$

$$f_s := \begin{bmatrix} SS_{(\text{index}_0)} \\ SS_{(\text{index}_1)} \\ SS_{(\text{index}_2)} \end{bmatrix} = \begin{pmatrix} 271.846 \\ 273.572 \\ 275.297 \end{pmatrix} \cdot \text{ksi} \qquad i := 0..2 \qquad P_i := f_{s_i} \cdot \text{num}_i \cdot A_{\text{strand}} \qquad P = \begin{pmatrix} 93.787 \\ 62.921 \\ 94.978 \end{pmatrix} \cdot \text{kip}$$

$T := f_s \cdot \text{num} \cdot A_{\text{strand}} = 251.686 \cdot \text{kip} \qquad C = 251.081 \cdot \text{kip}$ adjust c until T=C

$$M_u := -C \cdot k_2 \cdot c + P \cdot d_{pt} = 8.807 \times 10^3 \cdot \text{kip} \cdot \text{in} \qquad \phi_u := \frac{\left(e_{s_2} - e_{s_0}\right)}{d_{pt_2} - d_{pt_0}} = 1.176 \times 10^{-3} \cdot \frac{1}{\text{in}}$$

2304 Pile with Topping for Development and Transfer Length Testing

Pile properties:

$f'_{cp} := 5ksi \qquad b := 12in \qquad h := 12in$

$A_p := b \cdot h = 144 \cdot in^2 \qquad I_p := \frac{1}{12} \cdot b \cdot h^3 = 1.728 \times 10^3 \cdot in^4$

$f_{rp} := 7.5 \cdot \sqrt{(f'_{cp} \cdot psi)} = 0.53 \cdot ksi \qquad E_p := 57000 \cdot \sqrt{f'_{cp} \cdot psi} = 4.031 \times 10^3 \cdot ksi$

Topping Properties:

$f'_{ct} := 6ksi \qquad h_{tot} := 42in \qquad h_t := h_{tot} - h = 30 \cdot in \qquad b_2 := 24in$

$f_{rt} := 7.5 \cdot \sqrt{(f'_{ct} \cdot psi)} = 0.581 \cdot ksi \qquad E_t := 57000 \cdot \sqrt{f'_{ct} \cdot psi} = 4.415 \times 10^3 \cdot ksi$

$f_u := 260.6ksi \qquad f_{se} := .4 \cdot f_u = 104.24 \cdot ksi \qquad A_{strand} := .153in^2 \qquad cover := 3.25in$

$E_{ps} := 24100ksi$

Strand Propeties:

Strand Layout, arranged by rows:

$$e_{mid} := \frac{h - 2 \cdot cover}{6} = 0.917 \cdot in$$

$$num := \begin{pmatrix} 4 \\ 2 \\ 2 \\ 4 \end{pmatrix} \qquad e_p := \begin{pmatrix} \frac{h}{2} - cover \\ e_{mid} \\ -e_{mid} \\ cover - \frac{h}{2} \end{pmatrix} = \begin{pmatrix} 2.75 \\ 0.917 \\ -0.917 \\ -2.75 \end{pmatrix} \cdot in \qquad d_{pt} := -e_p + \frac{h}{2} + h_t = \begin{pmatrix} 33.25 \\ 35.083 \\ 36.917 \\ 38.75 \end{pmatrix} \cdot$$

$$P_i := f_{se} \cdot num \cdot A_{strand} = \begin{pmatrix} 63.795 \\ 31.897 \\ 31.897 \\ 63.795 \end{pmatrix} \cdot kip \qquad P_{itot} := \sum P_i = 191.385 \cdot kip$$

Shear Friction:

$$P_{max} := \sum\left(f_u \cdot num \cdot A_{strand}\right) = 478.462 \cdot kip$$

$a := 7ft$ shear span $\mu := 1.0$

Shear Rebar:

$f_y := 60ksi$ $A_4 := .4in^2$ $A_5 := .62in^2$

$$A_{vtot} := \frac{\mu \cdot P_{max}}{f_y} = 7.974 \cdot in^2$$

$$s_4 := \frac{a \cdot A_4}{A_{vtot}} = 4.214 \cdot in \qquad s_5 := \frac{a \cdot A_5}{A_{vtot}} = 6.531 \cdot in$$

minimum req. spacing for #4 and #5 bars

Ultimate Moment Capacity of Composite Section:

using Todeschini stress block:

$$f'_c := .9 \cdot f'_{ct} = 5.4 \cdot ksi \qquad e_0 := 1.71 \cdot \frac{f'_{ct}}{E_t} = 2.324 \times 10^{-3} \qquad e_u := .003$$

$e_{tf} := .00235$ specified strain in top fiber Note: <.003

$$\beta_1 := \frac{\ln\left[1 + \left(\frac{e_{tf}}{e_0}\right)^2\right]}{\frac{e_{tf}}{e_0}} = 0.697 \qquad k_2 := 1 - 2 \cdot \frac{\left(\frac{e_{tf}}{e_0} - \operatorname{atan}\left(\frac{e_{tf}}{e_0}\right)\right)}{\left(\frac{e_{tf}}{e_0}\right)^2 \cdot \beta_1} = 0.382$$

$$e_{se} := \frac{f_{se}}{E_{ps}} = 4.325 \times 10^{-3} \qquad e_{ce} := \frac{-P_{itot}}{E_t \cdot A_p} = -3.01 \times 10^{-4}$$

$c := 5.33in$ manual adjust require 6" depth of flange

$C := \beta_1 \cdot f'_c \cdot c \cdot b_2 = 481.168 \cdot kip$

$$e_c := \frac{e_{tf}}{c} \cdot \left(d_{pt} - c\right) = \begin{pmatrix} 0.012 \\ 0.013 \\ 0.014 \\ 0.015 \end{pmatrix} \qquad e_s := e_c + e_{se} + e_{ce} = \begin{pmatrix} 0.016 \\ 0.017 \\ 0.018 \\ 0.019 \end{pmatrix}$$

$$\text{index} := \text{round}\left(e_s \cdot 10000\right) - 1 = \begin{pmatrix} 162 \\ 170 \\ 179 \\ 187 \end{pmatrix}$$ strand break at index=187

$$f_s := \begin{bmatrix} SS\left(\text{index}_0\right) \\ SS\left(\text{index}_1\right) \\ SS\left(\text{index}_2\right) \\ SS\left(\text{index}_3\right) \end{bmatrix} = \begin{pmatrix} 258.529 \\ 259.762 \\ 260.468 \\ 260.732 \end{pmatrix} \cdot \text{ksi} \qquad i := 0..3 \qquad P_i := f_{s_i} \cdot \text{num}_i \cdot A_{\text{strand}} \qquad P = \begin{pmatrix} 158.22 \\ 79.487 \\ 79.703 \\ 159.568 \end{pmatrix} \cdot \text{kip}$$

$T := f_s \cdot \text{num} \cdot A_{\text{strand}} = 476.978 \cdot \text{kip}$ $\quad C = 481.168 \cdot \text{kip}$ C is slightly greater than T, therefore strand breaks at top fiber strain =0.00235

$$M_u := -C \cdot k_2 \cdot c + P \cdot d_{pt} = 1.62 \times 10^{4} \cdot \text{kip} \cdot \text{in} \qquad \phi_u := \frac{\left(e_{s_2} - e_{s_0}\right)}{d_{pt_2} - d_{pt_0}} = 4.409 \times 10^{-4} \cdot \frac{\text{rad}}{\text{in}}$$

REFERENCES

AASHTO LRFD (2008), “Bridge Design Specifications,” American Association of State Highway and Transportation Officials, Washington, DC.

ACI 222.2 (2001), "Corrosion of Prestressing Steels," American Concrete Institute, Farmington Hills, MI.

ACI 318 (2008), "Building Code Requirement for Structural Concrete and Commentary," American Concrete Institute, Farmington Hills, MI.

Allegheny Technologies, Inc. (2010), "ATI 2003 Duplex Stainless Steel Datasheet." Allegheny Ludlum Technologies Inc., Brackenridge, PA.

ASTM A416 (2006), "Standard Specification for Steel Strand, Uncoated Seven-Wire for Prestressed Concrete," American Society for Testing and Materials, West Conshohoken, PA.

ASTM E328 (2008), "Standard Test Methods for Stress Relaxation Tests for Materials and Structures," American Society for Testing and Materials, West Conshohoken, PA.

Atienza, J. M., and Elices, M. (2007), "Role of Residual Stresses in Stress Relaxation of Prestressed Concrete Wires," Journal of Materials in Civil Engineering, V. 19 (8), pp. 703-708.

Conference Proceedings 693-756 edited R. A. Lula

DeLong, W. T., Ostrom, G. A., and Szumachowski, E. R. (1956), "Measurement and calculation of ferrite in stainless steel weld metal," Journal of Welding, V. 35 (11), pp. 521-528.

Elices, M., Cabllero, L., Valiente, A., Ruiz, J., and Martin, A. (2008), "Hydrogen Embrittlement of Steel for Prestressing Concrete: The FIP and DIBt Tests," CORROSION V. 64 (2), pp. 164-174.

Gardner, L. (2005), "The Use of Stainless Steel in Structures," Progress in Structural Engineering and Materials, V. 7 (2), pp. 45-55.

Griggs, R. D. (1987), "Structural Concrete in the Georgia Coastal Environment." Georgia Department of Transportation, Atlanta, GA.

Hamilton III, H. R. (2007), "St. George Island Bridge Pile Testing," Florida Department of Transportation, Tallahassee, FL.

Holland, R. B. “Durability of Precast Prestressed Concrete Piles in Marine Environments,” Doctoral Dissertation, Georgia Institute of Technology, Atlanta, GA, 2012, 427 pp.

Insteel (2002), "1/2 inch 240ksi Stainless Steel Strand," Insteel Industries, Sanderson, FL.

Jenkins, J. F. (1987), "Validation of Nitronic 33 in Reinforced and Prestressed Concrete," Naval Facilites Engineering Command, Jacksonville, FL.

Koch, G. H., Brongers, M. P. H., Thompson, N. G., Virmani, Y. P., and Payer, J. H. (2008), "Corrosion Costs and Preventive Strategies in the United States," National Association of Corrosion Engineers, Houston, TX.

Le May, Iain. *Principles of Mechanical Metallurgy*. New York: Elsevier North-Holland, 1981.

Lee, Y. K., Shin, H. C., Leem, D. S., Choi, J. Y., Jin, W., Choi, C. S. (2003), “Reverse Transformation Mechanism of Martensite to Austenite and Amount of Retained Austenite After Reverse Transformation in Fe—3Si—13Cr—7Ni (wt%) Martensitic Stainless Steel,” Materials Science and Technology, V. 19, pp. 393-398.

Moser, Robert. “High-Strength Stainless Steels for Corrosion Mitigation in Prestressed Concrete: Development and Evaluation,” Doctoral Dissertation, Georgia Institute of Technology, Atlanta, GA, 2011, 299 pp.

NACE (2008), "How Much Can a Bridge Take," National Association of Corrosion Engineers, Houston, TX.

Padilha, A.F., Aguiar, D. J. M., Plaut, R. L. (2012), “Duplex Stainless Steels: a Dozen of Significant Phase Transformations,” Defect and Diffusion Forum, V. 322, pp. 163-174.

Reutlinger, Chris. “Direct Pull-Out Capacity and transfer Length of 0.6-inch Diameter Prestressing Strand in High-Performance Concrete,” Masters Thesis, Georgia Institute of Technology, Atlanta, GA, May 1999, 352 pp

Russell, Bruce Wayne. “Design Guidelines for Transfer, Development and Debonding of Large Diameter Seven Wire Strands in Pretensioned Concrete Girders,” Doctoral Dissertation, Georgia Institute of Technology, Atlanta, GA, 1992, 464 pp.

Schaeffler, A. L. (1949), "Constitution Diagram for Stainless Steel Weld Metal," Metals Progress, V. 56 (11), pp. 680.

Sedriks, A. J. *Corrosion of Stainless Steels*. New York: Wiley, 1979. Print.

Solomon, Harvey D., and T. M. Devine. "Duplex Stainless Steels - A Tale of Two Phases." *American Society for Metals* (1983): 63 pp.